ELECTROCHEMICAL BIOSENSING APPROACH FOR MODERN DIAGNOSTICS

A LABEL-FREE ELECTROCHEMICAL BIOSENSING APPROACH FOR MODERN DIAGNOSTICS USING SCREEN-PRINTED ELECTRODES

By REHMAT GREWAL, B.Tech.

A Thesis Submitted to the School of Graduate Studies in Partial Fulfilment of the Requirements for the Degree of a Master of Applied Science

McMaster University MASTER OF APPLIED SCIENCE (2023) Hamilton, Ontario

TITLE: A Label-Free Electrochemical Biosensing Approach for Modern Diagnostics using Screen-Printed Electrodes

AUTHOR: Rehmat Grewal, B.Tech. (McMaster University)

SUPERVISORS: Professors Amin Reza Rajabzadeh and Seshasai Srinivasan

NUMBER OF PAGES: xiv, 115

1 Lay Abstract

An electrochemical biosensor is a sensing device with the ability to detect biological species via the transduction of a specific biological event into electrochemical signals. These sensors are extremely useful for the detection of analytes in biological fluids for clinical diagnostics, to determine the presence or absence of diseases. This manuscript addresses the challenges associated with the stability, reproducibility, and the low limits of detection associated with screen-printed carbon electrodes used in electrochemical biosensing. Subsequently, due to the strong correlation between glycated hemoglobin (HbA1c) and C-reactive protein (CRP) to connote the risk of contracting coronary heart disease (CHD), the manuscript presents a novel label-free electrochemical biosensing method for the detection of HbA1c and CRP with low detection limits. Secondly, the manuscript identifies ambient storage conditions for the long-term stability of a biomolecule-free sensing device for the roadside detection of ultra-low concentrations of Δ9-tetrahydrocannabinol (THC).

2 Abstract

Electrochemical biosensors are renowned for their ability to detect a wide range of analytes in biological fluids for clinical diagnosis. The implementation of biomarkers in electrochemical biosensors for clinical diagnosis is essential for the specific and accurate diagnosis of the disease with high sensitivity and selectivity. Therefore, this thesis evaluates the challenges pertaining to the stability, reproducibility, and obtaining a low limit of detection for the internal/external biomarkers associated with two distinct electrochemical biosensors.

The first study tackles the challenge of detecting low analyte concentrations in a label-free biosensor. It introduces an innovative label-free electrochemical biosensing method for the detection of glycosylated hemoglobin (HbA1c) and C-reactive protein (CRP) to predict Coronary Heart Disease (CHD) progression using tailored redox probes, proposing a dual biomarker biosensing platform for future research. Calibration curves reveal an LOD of 5 mg/mL in PBS (8) FeCN (II) and 6 mg/mL in SB for a linear range of 0 – 30 mg/mL of HbA1c. Similarly, an LOD of 0.007 mg/mL and 0.008 mg/mL in PBS (7.4) PcA-NO_2 and SB, respectively, is reported for a linear range of 0 – 0.05 mg/mL of CRP.

The second study focuses on stabilizing a biomolecule-free sensor for the ultra-low detection of Δ9-tetrahydrocannabinol (THC) in roadside testing. Pre-depositing THC, an external biomarker for drug-impaired driving, onto the biosensor's working electrode enhances its interaction with analytes. However, THC's oxidative nature compromises sensor stability during manufacturing. Consequently, optimal electrode storage conditions were explored, indicating frozen storage as ideal for up to six months, effectively preventing THC oxidation at -18°C, while degradation occurs at 4°C. Modified electrodes stored under optimal conditions exhibit improved calibration curves when exposed to various THC samples.

3 Acknowledgements

I would like to commence by extending my sincere appreciation to my supervisor and co-supervisor, Dr. Seshasai Srinivasan and Dr. Amin Rajabzadeh, for providing me the privilege to collaborate with an exceptionally supportive and a highly knowledgeable team. This invaluable opportunity enabled me to bridge the gap between my prior undergraduate education and its practical application. Their guidance, motivation, and positivity served as inspirational qualities that propelled me to attain my academic objectives. I would also like to express my appreciation to Dr. Fei Geng for his contribution as a committee member, by providing insightful suggestions.

I wish to extend my gratitude to Dr. Greter Amelia Ortega for her pivotal role in accompanying me throughout this journey, which commenced with comprehensive training, introduction to fundamental concepts, and her unwavering commitment to addressing all my inquiries without judgment. Dr. Ortega's approach has consistently encouraged me to think beyond conventional boundaries i.e., instead of thinking outside the box, often prompting me to question the very existence of the 'box' and encouraging creative problem-solving in our experiments. I'd also like to thank all other members part of the BioX research group for their continual support and guidance.

Finally, I am extremely grateful to my family for serving as a steadfast pillar of support throughout my journey and playing an integral role in continually encouraging me to seek personal growth and self-improvement. In particular, I would like to acknowledge both my late grandfathers, whose legacy I strive to honor and follow, and I hope they are watching proudly as I tread in their footsteps. I extend my thanks to my parents for their unwavering wisdom and support, and to my fiancé, whose encouragement was instrumental in my decision to embark on this role to begin with.

4 Table of Contents

5 List of Figures

6 List of Tables

7 List of all Abbreviations and Symbols

EC	Electrochemical
SPCE(s)	Screen-printed carbon electrode(s)
GCE	Glassy carbon electrode
Au/AuNPs	Gold/gold nanoparticles
POC	Point-of-care
SCs	Supercapacitors
WE	Working electrode
CE	Counter electrode
RE	Reference electrode
CV	Cyclic voltammetry
IUPAC	International Union of Pure and Applied Chemistry
FET	Field-effect transistors
OF(s)	Oral fluid(s)
WHO	World Health Organization
CRP	C-reactive protein
COVID-19	Coronavirus-2019
HbA1c	Glycated hemoglobin
LPL	Low-density lipoproteins
CHD	Coronary heart disease
GO	Graphene oxide
PSA	Prostate-specific antigen
BNP	Brain natriuretic peptide
TSH	Thyroid stimulating hormones
CO	Carbon monoxide
NO_2	Nitrogen dioxide
BPA	Bisphenol A
MIP(s)	Molecularly imprinted polymers(s)
AQ	Air-quality
NO	Nitrogen oxide
O_3	Ozone
LOD	Limit of detection
SNR	Signal-to-noise
ELISA	Enzyme linked immunosorbent assay
Hs-CRP	High sensitivity C-reactive protein
Hb	Hemoglobin
PcA-NO_2	O-(4-Nitrophenylphosphoryl)choline
PBS	Phosphate buffer
SB	Simulated blood

EPIC	European Prospective Investigations into Cancer
ADA	American Diabetes Association
H_2SO_4	Sulphuric acid
KCl	Potassium chloride
$HAuCl_4$	Chloroauric acid
MUA	11-mercaptoundecanoic acid
EDC	1-Ethyl-3-(3-dimethylaminopropyl)carbodiimide
N_2	Nitrogen
BSA	Bovine serum albumin
FeCN(II)	Potassium hexacyanoferrate(II) trihydrate
DPV	Differential pulse voltammetry
$[Fe(CN)6]^{4-}$	Ferrocyanide
$[Fe(CN)6]^{3-}$	Ferricyanide
EIS	Impedance spectroscopy
CT	Charge transfer
AUC	Area under the curve
PcA	Phosphorylcholine
NH_2	Amine
T2DM	Type 2 diabetes mellitus
DWSPCE(s)	Dual working screen-printed carbon electrode(s)
AI	Artificial intelligence
THC	Δ9-tetrahydrocannabinol
MVA	Motor vehicle accident
THCi	Deposited THC molecules
SWV	Square wave voltammetry
AA	Ascorbic acid
CA	Citric acid
BHT	Butylated hydroxytoluene
THCA	Tetrahydrocannabinolic acid
THC-OAc	Δ9-Tetrahydrocannabinol Acetate
DA	Dopamine
CBD	Cannabidiol
RT	Room temperature
O_2	Oxygen
OTR	Oxygen transmission rate
CBN	Cannabinol
XPS	X-ray photoelectron spectroscopy
P-Z	Pristine screen-printed electrode

8 Declaration of Academic Achievement

I, Rehmat Grewal, would like to hereby affirm that the thesis presented is my original work, and has not been previously submitted by any other individual for any degree or professional qualifications. I further declare that the contents of this thesis are my own, except for jointly-authored publications in which I am the chief contributor. In such cases, the contributions of all authors are explicitly documented, and I affirm that due credit has been properly attributed to them within this thesis whenever references to their work have been incorporated.

Chapter 1 : Introduction

1.1. Motivation

The rationale for selecting this topic for the thesis stems from the imperative need for detection devices, particularly those based on electrochemical principles. Electrochemical-based devices offer rapid real-time results, cost-effectiveness, user-friendliness, portability, and a high degree of accuracy without necessitating extensive professional expertise. They align with the contemporary requirements of modern diagnostics. The first proposed sensor has the capacity to predict the progression of heart disease swiftly, eliminating the need for patients to endure prolonged wait times for their results and potentially contributing to life-saving interventions. On the other hand, the deployment of stable electrochemical sensors for roadside drug detection has the potential to significantly diminish drug-impaired driving incidents and subsequent collisions. Therefore, both electrochemical sensors focus on enhancing human well-being and contributing to the preservation of human life.

1.2. Objectives

The main objectives of this thesis encompass the mitigation of challenges inherent to biomolecule-free and label-free electrochemical biosensors, including issues related to stability, reproducibility, and the detection of low analyte concentrations. Consequently, both manuscripts are dedicated to the resolution of these challenges and the development of accurate and precise electrochemical detection devices. The primary focus of the first manuscript is dedicated to overcoming the challenge of detecting low analyte concentrations, specifically targeting internal biomarkers glycated hemoglobin (HbA1c) and C-reactive protein (CRP) for the assessment of heart disease maturation in clinical diagnostics. On the other hand, the role of the second manuscript is to address

the chemical instability associated with a previously reported biomolecule-free device designed for the roadside detection of the external biomarker, Δ9-tetrahydrocannabinol (THC).

1.3. Thesis Outline

A schematic flow chart illustrating the overarching concepts and the underlying key themes explored within the thesis is depicted in Figure 1- 1. The flow chart is essential in demonstrating the synergistic interrelation between the two distinct categories of biomarkers explored (i.e., internal and external) within the two publishable manuscripts presented. Both emanate from a common foundational basis and pertain to modern clinical diagnostics through the utilization of electrochemical detection methodology.

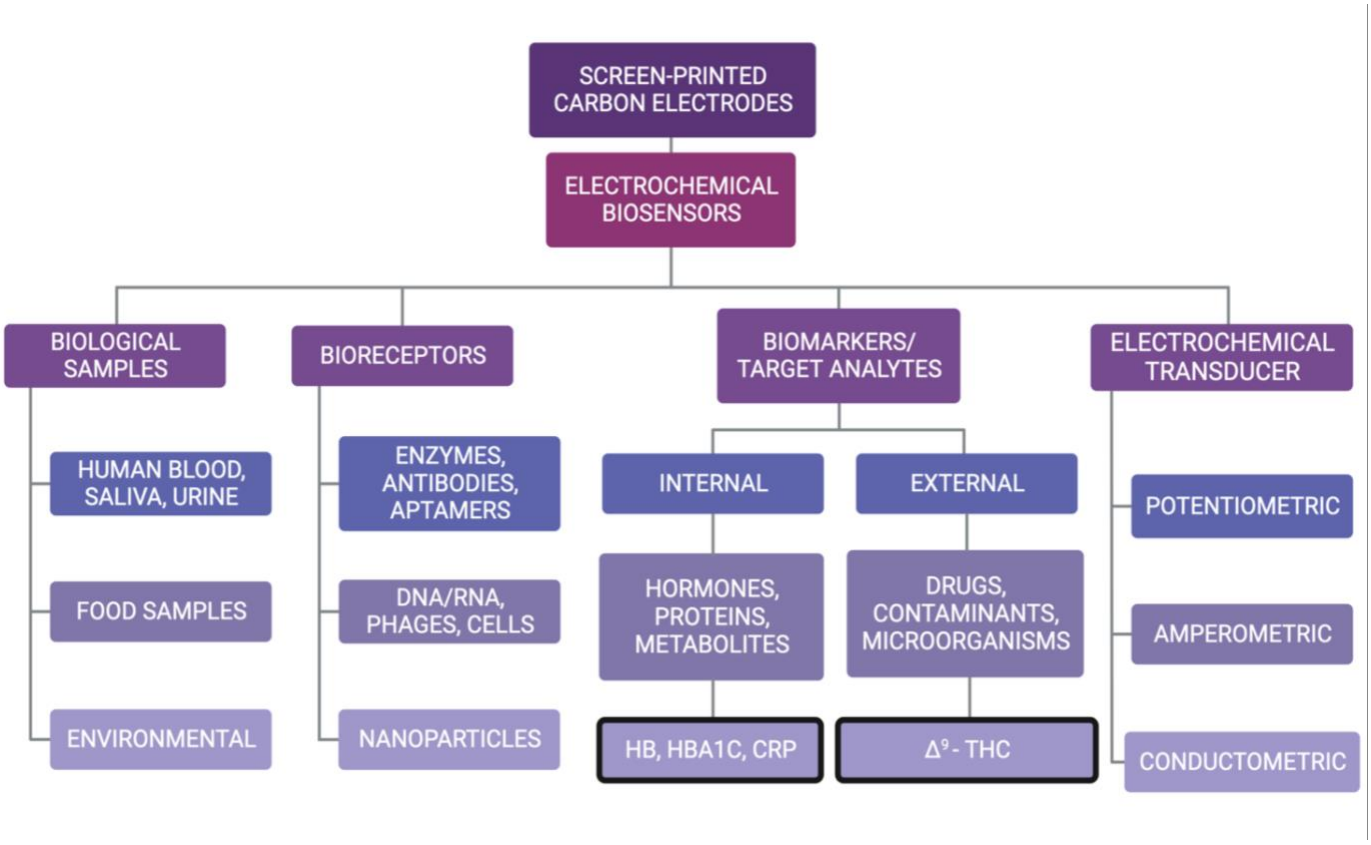

Figure 1- 1: Schematic flow chart representing the general theme of the thesis contents.

The thesis outline is as follows:

→ Chapter 2 includes the literature review on the electrochemical detection of biological fluids with prime biomarkers using different electrochemical techniques.

→ Chapter 3 outlines the challenges pertaining to label-free electrochemical sensors and provides a novel label-free electrochemical method for the quantification of low analyte concentrations for clinical diagnosis via the publishable manuscript, "*Label-Free Electrochemical Detection of Glycated Hemoglobin (HbA1c) and C-Reactive Protein (CRP) to Predict the Maturation of Coronary Heart Disease due to Diabetes*."

→ Chapter 4 focuses on the challenges associated with biomolecule-free electrochemical sensors and identifies optimal storage conditions aimed at enhancing the long-term stability of this approach via the publishable manuscript, "*Determining Optimal Storage Conditions to Enhance the Stability of Δ9-tetrahydrocannabinol (THC)-Modified Screen-Printed Carbon Electrodes (SPCEs)*."

→ Chapter 5 summarizes the key findings and associated field contributions of this thesis.

Chapter 2 : Electrochemical Detection of Biological Fluids Using Screen-Printed Carbon Electrodes

2.1 Preface

This literature review aims to explicate the electrochemical (EC) detection of biological fluids using screen-printed carbon electrodes (SPCEs). The review provides an insight on the numerous EC techniques for the measurement of SPCEs and extends to presenting an in-depth analysis on the EC detection of biological fluids with prime biomarkers relevant in the subsequent chapters of this thesis.

Rehmat Grewal is the sole author of this chapter.

2.2 Introduction to Electrochemical-based Biosensors

An EC biosensor is defined as an analytical device which functions based on the transformation of a biological response into an electronic signal [1]. EC-based biosensors have been tremendously advantageous in the field of medical diagnostics for the rapid and specific measurement of the bio-analyte, in conjunction with the high sensitivity, energy efficiency, and economic feasibility presented by the device. Hence, EC-based biosensors have been used extensively for the detection of key bio-analytes including glucose, cholesterol, uric acid, hemoglobin, neurotransmitters, biological fluids, and also pathogens such as bacteria and viruses [2].

A biosensor is primarily comprised of an EC transducer, a receptor, and a corresponding detector. The mechanism of detection for a typical EC biosensor entails: (a) the specific binding of the bioreceptor to the analyte which initiates the occurrence of a biological event in the interface, (b) the biological event resulting in generating a specific EC signal received by the transducer, (c) the EC signal amplified via a detector circuit and processed using an EC computing software by the human operator for analysis [3] (Figure 2- 1).

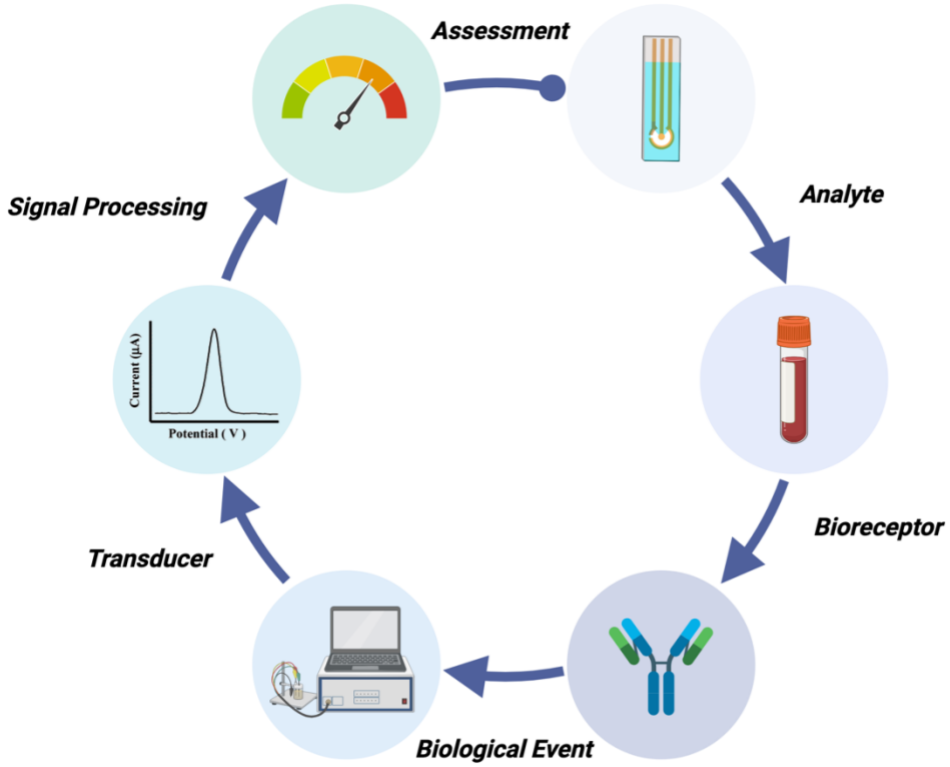

Figure 2- 1: The mechanism of detection for electrochemical biosensors for clinical diagnosis, created using BioRender.com.

The fabrication of a successful EC biosensor necessitates materializing the following conditions: the use of a highly specific biocatalyst and a biocompatible probe (if applicable), performing minimal pre-treatment of the sensor, obtaining an accurate and reproducible linear response, preferable for the biosensor to provide real-time analysis, and the overall biosensor to be small, portable, cost effective, and operable by semi-skilled operators [3]. EC-based biosensors can demonstrate high selectivity due to the prospect of immobilizing biological recognition elements such as antibodies, nucleic acids, receptors, or enzymes [4] on the sensor to induce a specific interaction between the substrate and the target analyte [5].

2.3 Screen-Printed Carbon Electrodes for Electrochemical Biosensing

The most vital constituent of an EC biosensor which influences the performance of the sensor is the electrode. The electrode material and associated surface modifications performed on the

electrode can elicit a major impact on the aptitude of the sensor to detect. Although glassy carbon electrodes (GCE), silicon electrodes, and gold (Au) based electrodes are widely used in laboratories for the purposes of standard sensing [6], these electrodes are often used as static devices and hence, lack portability [7]. With the demand for the biosensing device to be portable and offer real-time detection for the provision of point-of-care (POC) testing, screen-printed carbon electrodes (SPCEs) [8] were developed.

SPCEs are the most common type of electrodes used for EC biosensing applications due to their versatility, low cost, mass producibility, reproducibility, miniaturization, and disposability [9]. The carbon-based electrodes are widely recognized due to their exceptional thermal, chemical, electrical, mechanical, and catalytic properties [10]. This category of electrodes has been utilized in the field of electrochemistry in abundance as a biological and chemical sensor, in the conversion and storage of energy, microelectronics, and as supercapacitors (SCs) [10].

The EC biosensing for SPCEs are fulfilled via its base substrates: the working electrode (WE) or the sensing electrode, a counter electrode (CE), and a reference electrode (RE). Wherein, the WE serves as a vessel for conducting the biochemical reaction, the CE as a conductor, and the RE regulates a stable EC potential. Both, CE and RE must be chemically stable to aid in devising a connection with the electrolytic solution for current to flow through the WE [3]. The mode of measurement for biological systems in biosensing is typically electrochemical in nature, with the bio-electrochemical component as the transducer. The specific biological event engenders either a current that is measurable (amperometric), a potential that is measurable (potentiometric), or changes the conductive properties of electrode (conductometric) [5].

2.3.1 Amperometric Devices

Amperometric-based sensors operate by measuring the continuous current materialized by the oxidation or reduction of the electroactive species in use [4]. The measurement of the current at a constant potential is termed as amperometry, whereas measurement of the potential with controlled variation is termed as voltammetry. Consequently, the intensity of the measured current using a linear range of potential is directly proportional to the concentration of the analyte of interest [4, 5], mediated by the EC reaction occurring at the WE. As a result, studies [11, 12] demonstrate that amperometric-based devices present improved sensitivity to potentiometric devices.

The most common examples of voltammetric techniques include linear sweep, differential staircase, cyclic, normal pulse, reverse pulse, differential pulse, and polarography [3]. Cyclic voltammetry (CV) is considered the most powerful EC voltammetric technique to analyze the oxidation and reduction processes of the electroanalytic solution, and the corresponding EC reaction rates. Another category of amperometric techniques is chronoamperometry, which involves the application of a square-wave potential to the WE and subsequently, the steady state current is determined as a function of time [3].

2.3.2 Potentiometric Devices

Potentiometric devices are responsible for measuring the total accumulated potential of the WE in the absence of current flow at the RE [3 – 5]. Potentiometric-based EC sensors are capable of delivering knowledge pertaining to the ion activity during an EC reaction and hence, are useful in detecting low concentrations from small sample volumes [13]. However, the variety of ions available is insufficient for the possibility of low detection limits due to the lack of important analytes, including nickel, mercury, and arsenate.

As per the International Union of Pure and Applied Chemistry (IUPAC), the two major advantages presented by potentiometric biosensors are: the biological species are a vital part of the receptor, and the resultant EC produced is in the form of a potential [14]. Additionally, potentiometry has also been used to determine the specific stage in a biochemical reaction during which, contrasting solutions of equivalent amounts would reach a state of equilibrium. Potentiometric devices based on field-effect transistors (FET) have also been used extensively to quantify changes in pH, selective ion concentrations, and determining the kinetics of biocatalytic reactions associated with enzymes [15].

2.3.3 Conductometric Devices

Conductometric devices are used to measure the electrical conductivity between the electrodes or the reference nodes of an electrolytic solution. These devices are often linked with enzymes wherein, the changes in the conductivity between two electrodes in a solution observed is due to the occurrence of an enzymatic reaction. Therefore, conductometric devices have been used to analyze the fluctuations in the concentration of a charged species in an electrolytic solution [16]. However, these devices are limited for clinical biosensing applications with majority clinical samples being ionic-based, and with the need to measure conductivity in high ionic strength solutions [17].

Opposingly, multi-analyte and polymer-based conductometric devices have gained popularity due to improvements in sensor integration and semiconductor technologies in microelectronic devices, including FET-based ones [18]. This had led to the recognition of conductometric-based immunosensors fabricated with nanowires [19]. These devices have often been affiliated with the detection of drugs and contaminants, in biological fluids and environmental samples, respectively [20]. Furthermore, conductometric devices have been associated with the

use of whole cells for conducting toxicity analysis by arresting the cells to interdigitated electrodes [21].

2.4 The Electrochemical Detection of Diseases in Biological Fluids

EC biosensors can be used for the detection of a wide range of samples including biological fluids and specimens, food items, environmental samples, and cell cultures. Human body fluids or biological fluids (Figure 2- 2) are of great significance in the field of EC biosensing to provide confirmation for a clinical diagnosis, in monitoring the progression and predicting the maturation of diseases. Common biological fluids comprise of blood, saliva, nasal fluid, gastric fluid, seminal fluid, urine, vaginal secretions, amniotic fluid, and breast milk [22]. Considerable research has been conducted to identify appropriate surface modifications with specific binding affinities in biological fluids over extended periods of time [23].

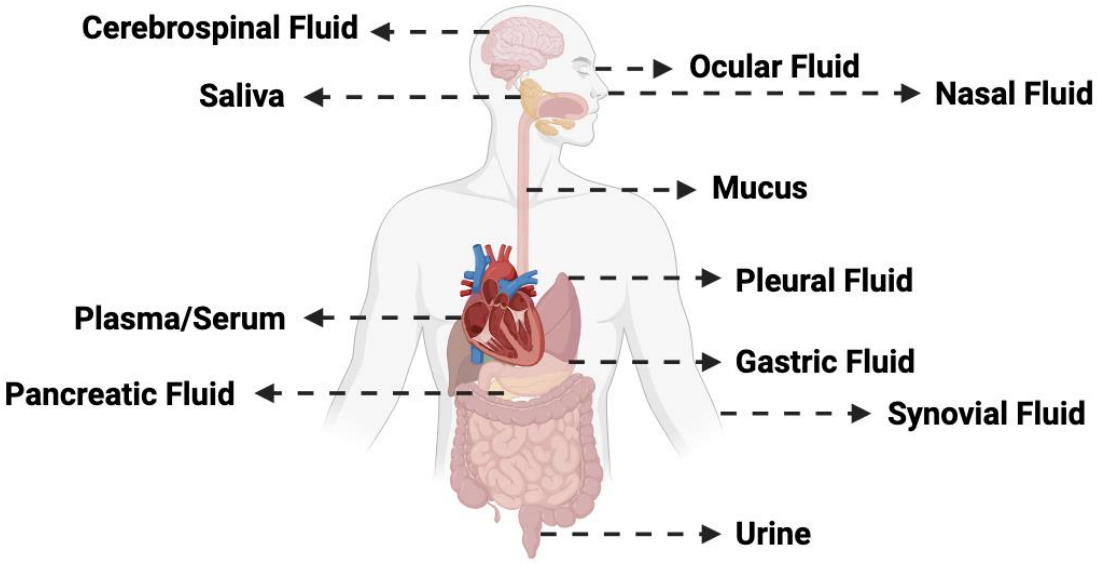

Figure 2- 2: Common human bodily fluids used for electrochemical biosensing, created using BioRender.com.

Blood has been established as the standard biological fluid for the detection of diseases and illicit substances, with the pharmacokinetic effects of biomarkers in blood validated [24]. The

correlation between blood, oral fluids (OF), and urine must be explored further for the purposes of standardizing results [25]. Recently, OF have been used for EC biosensing applications extensively due to their non-invasive collection methods. Specifically, saliva is an OF which has been used as the primary biological medium for biosensing increasingly [25], highly relevant for coronavirus (COVID-19) diagnosis. Despite the challenges associated with developing a correlation amongst biological fluids, the correlation of using biological fluids in EC biosensing has often been reported [25].

The mechanism for the EC detection of diseases in biological fluids entails: the addition of the biological fluid onto the substrate, followed by the incidence of a specific interaction between the biomarker (target material) in the biological fluid with the bioreceptor on the sensor, resulting in a unique EC signal change, indicating the presence or the absence of the disease [26]. However, the lack of surface architecture in EC biosensors with the demand for measuring high concentration ranges has resulted in decreased sensitivity, and in the inability of the biosensor to identify the distinct response associated with the biochemical event. Additionally, the immunosensor is deeply affected by the differences in the pH and ionic strength of biological fluids [20].

As per the World Health Organization (WHO), a biomarker can be defined as "any substance, structure, or process that can be measured in the body or its products and influence or predict the incidence of outcome or disease" [27]. The implementation of biomarkers as diagnostic indicators in clinically relevant samples is a necessity to provide specific and accurate assessments regarding the risk or the presence of diseases with high sensitivity and selectivity [12].

A comprehensive analysis of the biomarkers relevant to this thesis will be provided in Chapters 3 and 4 to avoid any overlap of information. For the purposes of introducing the biomarkers of interest in the subsequent chapters of this thesis, biomarkers can be grouped into

two distinct categories: internal ("found in the human body") and external ("not found in the human body") biomarkers. While the list of internal and external biomarkers is endless, the following sections present the most common ones for the EC diagnosis of diseases.

2.4.1 Internal Biomarkers

Internal biomarkers comprise of substances or molecules which exist within the human body and are indicative of physiological processes and diseases. Bodaghi and associates [28] further categorize them into cellular, molecular (chemical, protein, or genetic), and imaging biomarkers, in addition to diagnostic, prognostic, and therapeutic biomarkers for clinical applications. Recently, high levels of urea and creatinine [29], C-reactive protein (CRP) [30], lactate dehydrogenase [31], and serum amyloid A [32] have been termed as valuable biomarkers for the prognosis of the ongoing COVID-19 pandemic.

Blood glucose levels are an essential and established biomarker for the EC-POC sensing of glycemia [33]. Numerous amperometric and impedimetric EC biosensors have been developed for the detection of glycated hemoglobin (HbA1c) for diabetes with high sensitivity [34, 35]. Wu et al. [36] presented a novel β-Cyclodextrin coated EC biosensor for the selective recognition of low-density lipoproteins (LPL) to predict the accumulation of cholesterol. Balayan and colleagues [37] provide a comprehensive review on the recent EC biosensors fabricated for the measurement of CRP levels, directly linked with the development of coronary heart disease (CHD) [38, 39].

Additionally, a highly-sensitive EC biosensor comprised of graphene oxide (GO), gold nanoparticles (AuNPs), and specific antibodies for the detection of prostate-specific antigen (PSA) has been reported for prostate cancer [40]. Supraja et al. [41] present a label-free EC detection of the cardiac biomarker troponin T using $ZnSnO_3$ perovskite nanomaterials on a glassy carbon electrode (GCE). Other common biomarkers used for EC biosensing include aptamer-based

biosensors for the detection of brain natriuretic peptide (BNP) for heart failure [42], impedimetric immunosensors for the detection of thyroid stimulating hormones (TSH) [43], and the measurement of the steroid cortisol in human serum using an aptamer with an antifouling composite layer [44] .

2.4.2 External Biomarkers

Opposingly, external biomarkers consist of substances or molecules present in the environment which can influence the human body via inhalation, ingestion, or exposure to these contaminants. These consist of food samples, drugs, alcohol, metal contaminants in the water, waterborne pathogens, environmental pollutants such as pesticides and herbicides, organic pollutants, air quality pollutants including carbon monoxide (CO) and nitrogen dioxide (NO_2) gases, bacterial toxins and microorganisms, hormone disruptors like bisphenol A (BPA) present in plastics, and oil spill contaminants such as hydrocarbons in aquatic environments.

Ortega and colleagues [45] report a biomolecule-free EC sensing approach for the detection of ultra-low concentrations of Δ^9-tetrahydrocannabinol in saliva. Florea et al. [46] present a highly selective EC sensor for the detection of cocaine using molecularly imprinted polymers (MIP) arrested onto graphene-based electrodes. Costa and associates [47] published a review on the specific biomarkers for the detection of alcohol, EC biosensors for the detection of alcohol in sweat, and the correlation between blood and alcohol.

Furthermore, Riu and Giussani [48] provide a detailed review of the current EC biosensors for the detection of pathogenic bacteria in food as an alternative to traditional methods of analyses. Other examples include the EC detection of BPA using an MIP nanocomposite [49], amperometric detection for selective pesticides [50], low-cost and rapid air-quality (AQ) EC devices for the

measurements of CO, NO, NO2, and O3 [51], and microfluid-based EC biosensors for the detection of waterborne pathogens [52].

Chapter 3 : The Label-Free Electrochemical Detection of Screen-Printed Electrodes – Challenges and Perspective

3.1 Preface

This chapter introduces the challenges associated with the label-free EC detection of biomarkers in clinical diagnosis and provides a label-free EC sensing approach for detecting low analyte concentrations. Specifically, the publishable manuscript in Section 3.3 presents a label-free electrochemical detection method for HbA1c and CRP to predict the maturation of CHD. The manuscript renders a novel label-free EC sensing approach using specific redox probes with a high binding affinity to the biomarkers of interest. The contributors of the manuscript include:

1. *Ms. Rehmat Grewal*
2. *Dr. Greter A. Ortega* – divisions 2.3 and 3.1, and part of 3.2 (under the scope of section 3.3 in this chapter).

3.2 Introduction to the Challenges Associated with the Label-Free Electrochemical Detection of Biomarkers

The term “label-free” sensing approach refers to the detection of the target analyte without the use of artificial probes or labels [53], allowing clinicians to monitor the interaction between the bioreceptor and the analyte in real-time. Label-free biosensors have the ability to detect target analytes in their biological form, without the need for chemical modifications and labelling. Additionally, they present a rapid response time, are economically feasible, can detect small molecules with minimal use of organic solvents, don’t necessitate the need for highly trained personnel, and offer a simplified process for analysis with high sensitivity [54].

Despite the numerous advantages demonstrated by label-free biosensors, achieving low limits of detection (LOD) can be challenging using this approach due to a variety of reasons. With label-free sensors highly reliant on subtle changes in the physical or chemical properties of the

analyte or the biomarker, this can lead to inducing a poor signal-to-noise ratio (SNR), especially for low analyte concentrations. The detection of smaller analytes can also deem unsuccessful in generating significant changes in the electrochemical signal, resulting in the inability to detect the analyte itself. Additionally, the lack of selectivity presented by labeled methods such as ELISA can induce the cross reactivity with non-targeted molecules. Therefore, the label-free detection of biomarkers can lead to affecting the sensitivity, specificity, and the practicality of the biosensor.

The subsequent section of this chapter emanates from the challenges stated above and provides a label-free EC biosensing approach for the detection of the internal biomarkers, HbA1c and CRP, for the maturation of CHD. The label-free approach proposed uses redox probes with a specific interaction with each biomarker to significantly improve the LOD. The redox probes presented aid in amplifying the corresponding EC signals retrieved during detection and hence, can measure low analyte concentrations with ease. The use of highly-specific redox probes also results in enhancing the kinetics between the biomarker and the surface of the electrode, promoting high selectivity and sensitivity.

3.3 Label-Free Electrochemical Detection of Glycated Hemoglobin (HbA1c) and C-Reactive Protein (CRP) to Predict the Maturation of Coronary Heart Disease due to Diabetes

Diabetes presents a high risk of promoting coronary heart disease (CHD). Prevailing evidence confirms that small increases of C reactive protein (CRP) in the human body can determine the tendency of developing CHD. In addition, glycated hemoglobin (HbA1c) is a well-recognized biomarker to evaluate diabetes progression. Given the positive correlation between diabetes and CHD, this research presents a label-free electrochemical method for the dual detection of %HbA1c and hs-CRP, facilitating early CHD prediction and cost-effective point-of-care diagnostics. With only a limited number of studies reported regarding both, the association and the electrochemical detection of HbA1c and CRP, this research represents a pioneering effort in this regard. This study

also presents an innovative approach by utilizing O-(4-Nitrophenylphosphoryl)choline (PcA-NO_2) as a redox probe for the electrochemical detection of CRP, a method not documented in scientific literature before. The specific application of PcA-NO_2 adds to the uniqueness of this research, marking a significant advancement in the field of electrochemical biomarker detection. The resultant calibration curves demonstrate a limit of detection (LOD) of 5 mg/mL in PBS (pH 8) and 6 mg/mL in simulated blood (SB) for a linear range of 0 – 30 mg/mL of HbA1c. Conjointly, a LOD of 0.007 mg/mL and 0.008 mg/mL for measurement in PBS (pH 7.4) and SB are reported for a linear range of 0 – 0.05 mg/mL of CRP.

1 Introduction

Diabetes is a well-established risk element for the development of coronary heart disease (CHD) [1, 2]. National surveys conducted on the U.S. population illustrate that the occurrence of coronary heart disease was higher amongst adults with diabetes, opposed to those without diabetes. The initial extensive cohort study in diverse populations was the European Prospective Investigations into Cancer (EPIC) study, which reported a graded affiliation between the %HbA1c/Total Hb and the risk for CHD and death for both sexes [3]. Lastly, the most credible research emanates from the University of Cambridge which designed a meta-analysis to discover the reservations associated with the degree of affiliation between diabetes and fasting glycemia with the risk of developing CHD. Their findings demonstrate that the risk of contracting CHD was twice as greater in individuals with diabetes at the baseline [4].

Glycated hemoglobin (HbA1c) is a significant biomarker for the long-term detection of glycemic index with its capacity to provide a cumulative history of glycemic levels from the preceding three months. The formation of HbA1c is a natural part of the physiological cycle wherein, the average plasma glucose and the amount of HbA1c in the plasma are directly

proportional to each other [5]. The corrective treatment for diabetes is determined based on the A1c levels, expressed as a percentage representing the concentration of the total hemoglobin that was glycated [5]. Therefore, HbA1c levels can be used to monitor glycemia for individuals with diabetes since it presents less day-to-day variability than glucose levels.

According to the American Diabetes Association (ADA), diagnosis of %HbA1c/Total Hb within the 5.7 – 6.4% spectrum implies the existence of intermediate hyperglycaemia or prediabetic, and a value above the benchmark of 6.4% is defined as the high-risk range or diabetic [6]. A value below 5.7% is classified as the non-diabetic or the normal range. As a result, the development of a total hemoglobin sensor is necessitated, as the quantification of both total hemoglobin and HbA1c is imperative for assessing the proportion of hemoglobin that has undergone glycation. With %HbA1c defined as the concentration ratio of HbA1c to total hemoglobin (%HbA1c/Total Hb), the document will henceforth employ %HbA1c to represent the aforementioned measure.

Subsequently, C reactive protein (CRP) is applicable as a pathological biomarker when the levels of CRP in the blood are relative to the intensity of the pathology with CRP levels < 10 mg/L classified as normal, and CRP levels > 10 mg/L indicative of elevation [7]. However, this threshold arises from redundant and outdated point-of-care tests, which lack the sensitivity to detect pathologies associated with lower concentrations. Hence, high-sensitivity (hs-CRP) tests were implemented to detect CRP concentrations as low as 1 mg/L to predict the maturation of CHD in individuals with no history of heart disease. The clinical range established for hs-CRP tests includes CRP < 0.1 mg/mL defined as low risk, 0.1 mg/mL < CRP < 0.3 mg/mL defined as moderate risk, and CRP > 0.3 mg/mL defined as high risk for developing CHD [8].

Several studies indicate that both biomarkers, HbA1c and CRP, can be used interchangeably for the detection of diabetes and CHD [9–13]. Researchers at John Hopkins University state that every 1%-point increase in HbA1c levels resulted in a 14% increase in risk of contracting a heart disease [14]. Although numerous clinical testing methods including immunoassays [15, 16], electrophoresis [17], spectroscopy [18, 19], and chromatography [20, 21] have been established for the detection of HbA1c and CRP in commercial devices (S1, Table S1-1), the ease-of-use of these methods and equipment are often questionable. Contrastingly, the use of electrochemical (EC) methods offers a simple, feasible, and rapid detection for a wide range of analytes [22, 23]. Furthermore, no studies associated with the binary electrochemical detection of %HbA1c and CRP have been reported yet.

Herein, a label-free voltammetric method to detect %HbA1c and hs-CRP to predict the maturation of CHD is reported using specific redox probes with high sensitivity and selectivity. The study aims to present a biosensing platform for the dual detection of both these biomarkers connoted with the development of CHD. By providing reliable results instantaneously, the implementation of EC methods in point-of-care (POC) diagnostics can also aid in the detection of CHD at an early stage and save treatment costs [24]. This can be tremendously advantageous in making firm clinical decisions and improving patient diagnosis.

2 Materials and Methods

2.1 Experimental Protocol for the Detection of HbA1c & CRP

2.1.1 Pre-treatment of the Electrodes

Screen-printed carbon electrodes (SPCEs) purchased from Zensor R&D were used for the purposes of this research. The TE-100 Zensor electrodes were first washed with milliQ water and then dried in the fumehood using hot air flow.

The electrochemical (EC) pre-treatment was carried out using the PalmSens4 potentiostat, driven by the PS Trace 5-PalmSens software. The electrodes were subjected to cyclic voltammetry (CV) using 100 µL of 1M H_2SO_4 using the following conditions: an equilibration time of 3 s, an initial potential of -0.5V, a voltametric potential scan from -0.5 to 1 V, a step potential of 0.01 V, a scan rate of 0.05 V/s for a total of 3 scans. The H_2SO_4 solution was rinsed off from the electrodes using milliQ water and the process of pre-treatment was continued with 100 µL of 0.1 M KCl using the following CV conditions: an equilibration time of 3 s, an initial potential of -0.5V, a voltametric potential scan from -0.5 to 1 V, a step potential of 0.01 V, a scan rate of 0.1 V/s for a total of 3 scans.

2.1.2 Electrochemical Deposition of Gold Nanoparticles (AuNPs)

A concentration of 5 mM of chloroauric acid ($HAuCl_4$) was dissolved in 0.1 M of KCl in a glass beaker on a hot plate subjected to magnetic stirring. Next, 0.1 M of 11-Mercaptoundecanoic acid (MUA) was first dissolved in ethanol, and then added to the solution stated above. The solution was then subjected to continuous magnetic stirring in the dark for 10 minutes, while simultaneously being purged with N_2 gas. A volume of 100 µL was then added onto each individual pre-treated electrode and scanned using the following conditions of CV: an equilibration time of 5 s, an initial potential of 0 V, a voltammetric potential scan from 0 to -1 V, a step potential of 0.01 V, a scan rate of 0.05 V/s for a total of 5 scans. Finally, the solution was rinsed off from the electrodes using milliQ water and dried.

2.1.3 Electrode Modification: Antibody Conjugation

The electrodes were then divided into two distinct groups, for HbA1c and CRP detection. The antibody conjugation was performed using antibodies specific to both analytes in conjunction with

1-Ethyl-3-(3-dimethylaminopropyl)carbodiimide (EDC). Both antibodies, anti-HbA1c (1 mg/mL) and anti-CRP (1 mg/mL) were purchased from MyBioSource.

The antibody solution was created using 10 µL of the anti-HbA1c/anti-CRP with 0.0022 g of EDC in 100 µL of H_2O. The first group of electrodes was modified using 5 µL of anti-HbA1c solution (AuNP/anti-HbA1c-SPCE) and the second group using 5 µL of anti-CRP solution onto the working electrode (WE) (AuNP/anti-CRP- SPCE). The modified electrodes were then stored inside of a wet chamber at room temperature for a period of 5 hours. The electrodes were rinsed with milliQ water and dried post incubation, followed by storage at 4°C.

The free area of the modified working electrodes was blocked by using bovine serum albumin (BSA). In this sense, a concentration of 0.014 mg/mL of BSA was prepared in 10 mM of PBS (pH 8). A volume of 5 µL of the BSA solution was deposited onto the WE of both groups of electrodes prepared in this section, after which the electrodes were incubated at 37°C for 1 hour. Lastly, the BSA solution was washed from the electrodes using milliQ water and dried. **Error! Reference source not found.**

2.1.4 Detection

2.1.4.1 The Detection of Total Hb

The detection of total Hb was performed using the pristine TE-100 Zensor electrodes, untreated and unmodified. The total Hb detection solutions constituted of Hb sample concentrations of 0, 50, 70, 100, 120, 150, and 170 mg/mL dissolved in phosphate buffer solution (PBS) (pH 8) and/or with simulated blood (SB), diluted by a factor of 10x. 10 mM of potassium hexacyanoferrate(II) trihydrate (FeCN(II)) was added to the sample to serve as a redox probe. A volume of 50 µL from the total Hb detection solution was then added onto three electrode array (i.e., the working, counter, and reference electrode), and scanned using the following conditions of differential pulse

voltammetry (DPV): an equilibration time of 60 s, a voltammetric potential scan from -0.5 to 1.0 V, a voltammetric step of 0.01 V, a potential pulse of 0.2 V, a time pulse of 0.02 s and a scan rate of 0.05 V/s.

2.1.4.2 The Detection of HbA1c

The detection of HbA1c was performed using the hemoglobin A1c protein (human erythrocytes) (1 mg/mL) procured from MyBioSource. The HbA1c detection sample comprised of HbA1c concentrations 0, 6, 9.7, 15, and 30 mg/mL dissolved in PBS (pH 8) and/or with SB, diluted by a factor of 10x. A concentration of 10 mM of FeCN(II) was added to the samples to serve as the redox probe. A volume of 50 µL from the HbA1c detection solution was then added to the AuNP/anti-HbA1c-modified WE SPCE array and incubated at room temperature (RT) for 30 minutes prior to detection. The electrodes were then scanned using the following conditions of DPV: an equilibration time of 60 s, a voltammetric potential scan from -0.5 to 1.0 V, a voltammetric step of 0.01 V, a potential pulse of 0.2 V, a time pulse of 0.02 s and a scan rate of 0.05 V/s.

2.1.4.3 The Detection of CRP

The detection of CRP was achieved with the human C-reactive protein (1 mg/mL) purchased from MyBioSource. The CRP detection solution consisted of CRP concentrations 0, 0.05, 0.1, 0.3, and 0.5 mg/mL dissolved in PBS (pH 7.4) and/or with SB, diluted by a factor of 10x. A concentration of 0.1 mM of O-(4-Nitrophenylphosphoryl)choline (PcA-NO_2) was added to serve as the redox probe. A volume of 50 µL from the CRP detection solution was then added to AuNP/anti-CRP-modified WE SPCE array and scanned (SCAN 1) using the following conditions of DPV: an equilibration time of 60 s, a voltametric potential scan from 0 to -1.5 V, a voltametric step of 0.01 V, a potential pulse of 0.2 V, a time pulse of 0.02 s and a scan rate of 0.05 V/s. The electrodes

were then maintained at RT for 10 mins before undergoing a second scan (SCAN 2), using the same DPV parameters as above. A detailed graphical abstract illustrating the experimental procedure is provided in Figure 3- 1 below.

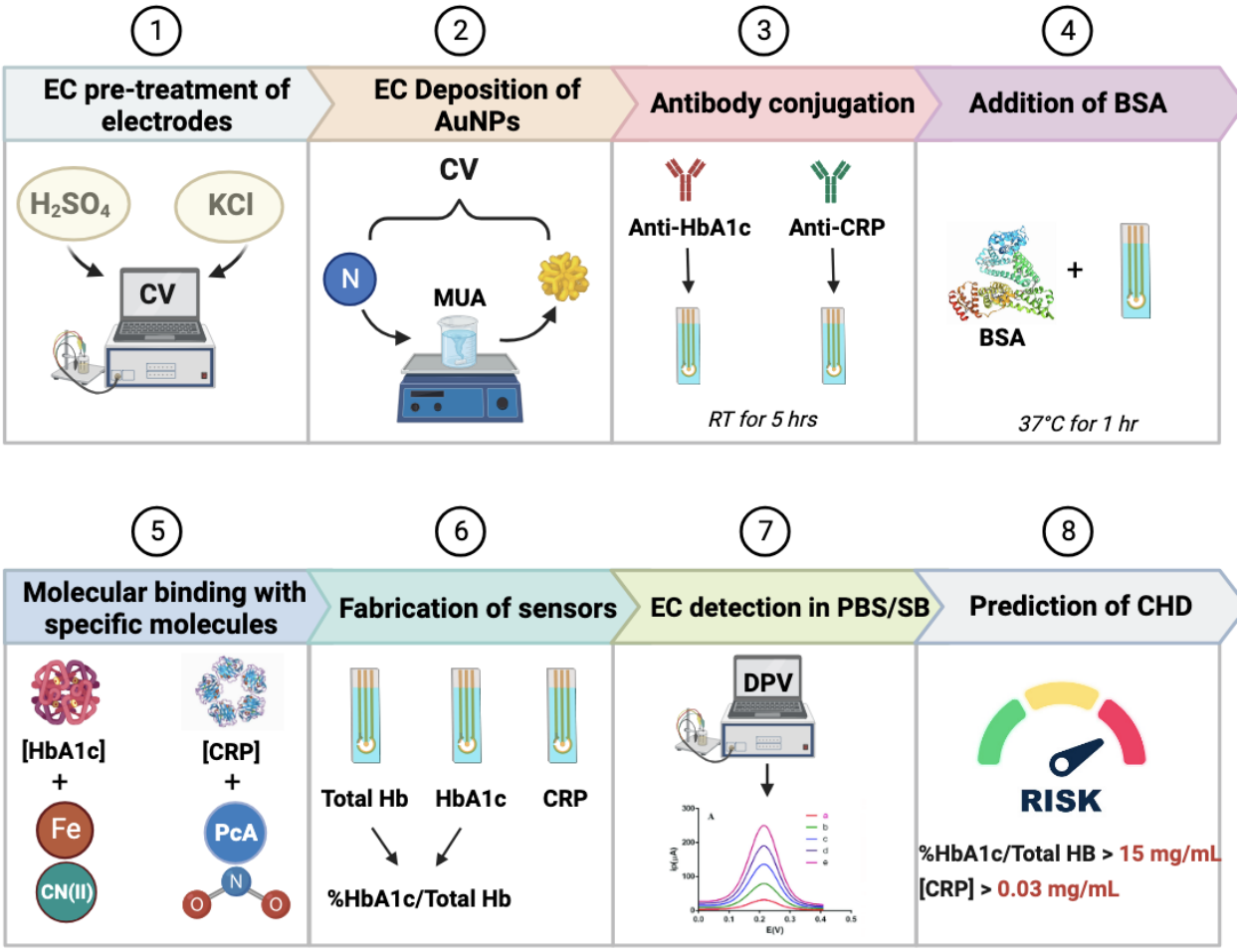

Figure 3- 1: Graphical procedure overview for preparing the electrodes for the detection of HbA1c and CRP levels, created via BioRender.com.

2.2 Percent Recovery Analysis

The percent recovery analysis was conducted by adding 10 µL of 5% chicken red blood cells (i.e., manufactured from whole blood, and procured from Innovative Research) to certain concentrations of Total Hb, HbA1c, and CRP.

2.3 Characterization

The modified WE of the Zensor-T100 SPCE by electrochemical deposition of AUNP@MUA were characterized by scanning electron microscopy (SEM JSM 7000F) working at 5.0 kV with a LED detector and EDS analysis. Raman spectrum was performed with Renishaw InVia Raman Spectrometer with a laser at 635 nm (50% of power) and 20 accumulations scans.

3 Results & Discussion

3.1 Functionalization and Characterization of the WE in the Zensor-T100 Array

The SPCE Zensor-T100 electrodes were first pretreated under acidic conditions and then modified with gold particles functionalized working electrodes. In this case, 11-Mercaptoundecanoic acid (MUA) is a fatty acid bifunctional group comprised of both carboxylic and thiol groups. Hence, this molecule was used during this process to act as a stabilizer in the process of generating AuNP's and to create carboxylic moieties to initiate antibody (Anti-HbA1c and Anti-CRP) covalent attachment.

Figure 3- 2(a) shows the cyclic voltammograms during the gold deposition and presents a comparison of CV signals in $[Fe(CN)6]^{3-}$/$[Fe(CN)6]^{4-}$ and 0.1 mol/L KCl electrolyte solution corresponding with the pretreated electrodes before and after modification. The EC deposition of gold nanoparticles (AuNPs) is known to increase the electroactive surface area, and the conductivity of the electrochemical biosensor [25].

Furthermore, electrochemical impedance spectroscopy (EIS) was used to characterize the electrode modification by using the electrolyte solution mentioned above as a redox probe. The Nyquist plots of the pristine SPCE, AuNp@MUA modified SPCE, and after conjugation with antibodies (e.g., Anti-HbA1c) are shown in Figure 3- 2(b). A modified Randle's circuit model was used to extract accurate information about the circuit elements (inset in Figure 3- 2(b)).

The arcs or semicircles at relatively high frequencies in the Nyquist plots are related to the resistance (parameter R2) at the electrode|solution interface. Gold deposition improved the electrical conductivity (786 Ω) compared with the pretreated electrodes (1279 Ω). Additionally, the considerable change in the signals of the AuNp@MUA modified SPCE after the antibody coupling suggests successful conjugation while slightly increasing the resistance (991 Ω). In addition, the depressed semicircles in the Nyquist plots is attributed to non-ideal double-layer capacitances characteristic of rough surfaces (parameter Q1). The circuit adjusting resulted in Q1 parameters for SPCE of 4E-7 T and 7E-5 T for AuNp@MUA-SPCE, demonstrating the roughness increment after the gold deposition.

Scanning electron microscopies demonstrate a homogenous presence of AuNP@MUA agglomerates on the WE surface (Figure 3- 2(c) and (d)). The EDS layered image shown in Figure 2(e) confirms the gold nature of the clusters on the electrode with a high atomic weight composition of 54% (S1, Figure S1-1).

The Raman spectrum analysis in Figure 3- 2(f) compares the SPCE surface before and after modification. The assoociated pristine WE spectrum depicts two traditional bands of graphitic carbon-based materials, corresponding to D at 1331 cm^{-1} and G at 1590 cm^{-1}. On the other hand, AuNP@MUA modified electrodes present two additional bands at 1076 and 273 cm^{-1} assigned to C-C and Au-S valence vibrations. This result demonstrates the presence of MUA residues on the gold clusters.

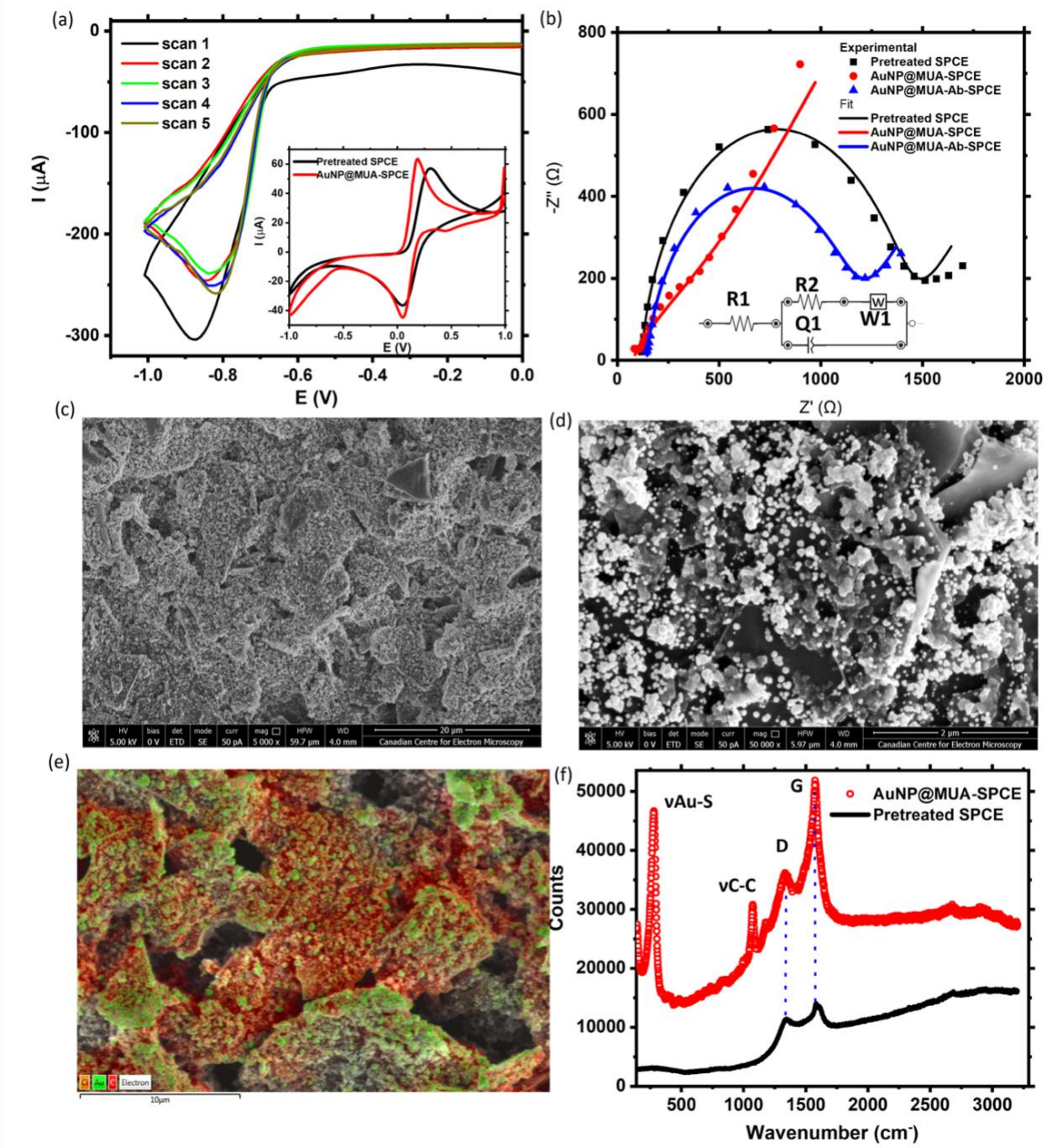

Figure 3- 2: (a) Cyclic voltammograms during the AuNP@MUA deposition on the WE, 5 scans, and inset CV of SPCE and AuNP@MUA-SPCE in $[Fe(CN)6]^{3-}$/$[Fe(CN)6]^{4-}$ and 0.1 mol/L KCl electrolyte solution. (b) Nyquist plots for SPCE, AuNP@MUA-SPCE, and conjugated AuNP@MUA-SPCEs with antibodies, (AuNP@MUA-Ab-SPCEs). EIS were recorded at 0.22 V in 10 mM Na4Fe(CN)6 (in 0.1 M KCl). The inset in (b) shows the equivalent circuit used. (c and d) SEM images of AuNP@MUA-SPCE. (e) EDS layered image of AuNP@MUA-SPCE. (f) Raman spectrum of the working electrodes after pre-treatment and gold deposition.

3.2 The Detection of Total Hb

The detection of total Hb in PBS (8) FeCN (II) was performed using the untreated and unmodified pristine TE-100 Zensor electrodes. The resultant DPV signals for total Hb concentrations 0, 50, 70, 100, 120, 150, and 170 mg/mL in PBS (pH = 8) are depicted in Figure 3- 3(a), with the oxidation of FeCN (II) into FeCN (III) observed at a potential of 0.2 V. The x-axis represents the concentration of total Hb before dilution, with the measurement performed after a dilution of 10x. The oxidation curves demonstrate a gradual decrease in the current signals with the increase in the total Hb concentration.

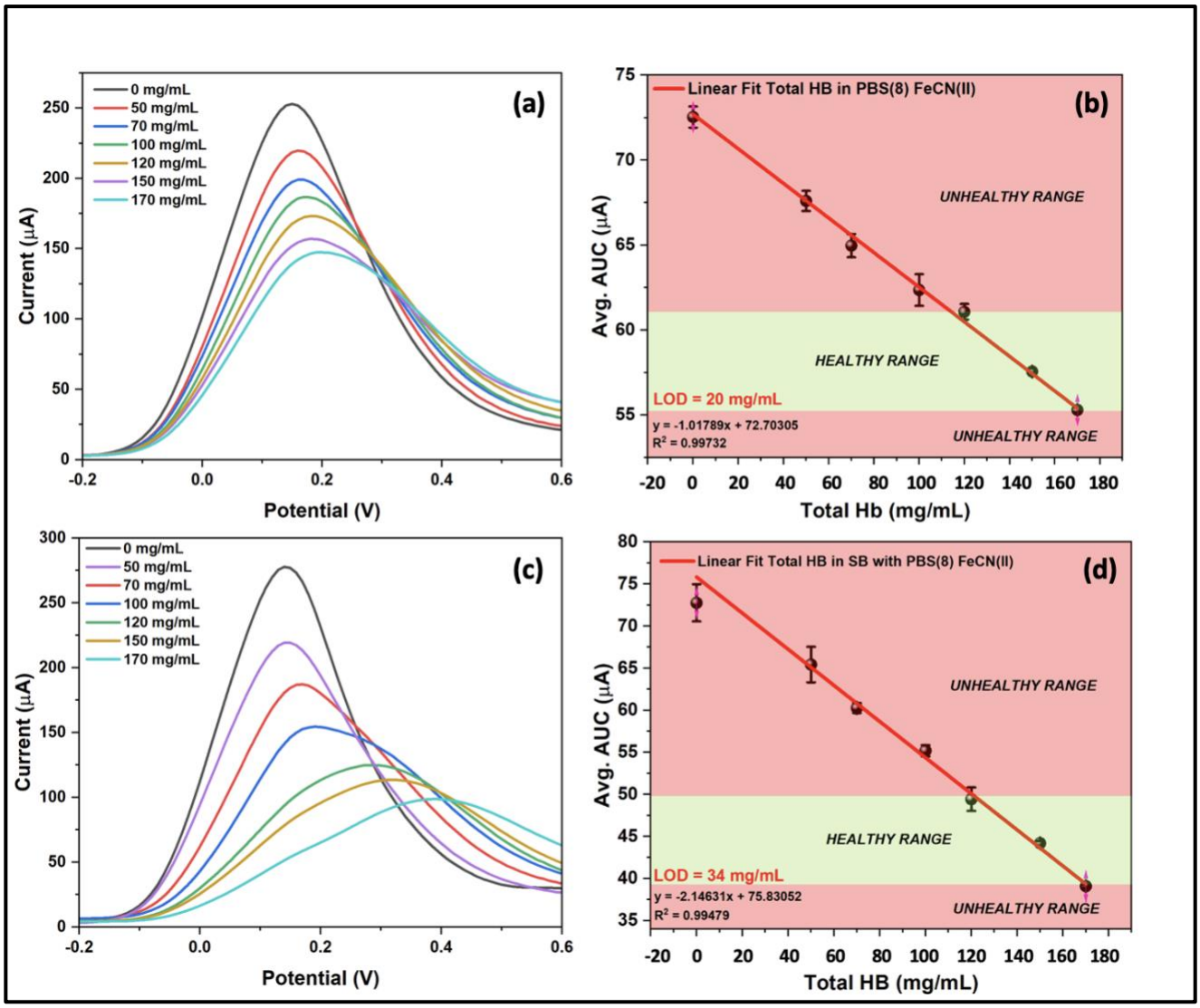

Figure 3- 3: (a) DPV signals for the clinical range of Total Hb in PBS(8) FeCN(II) and resultant (b) calibration curve for the detection of Total Hb, (c) DPV signals for the clinical range of Total HbFeCN(II) with SB and resultant (d) calibration curve for the detection of Total Hb with SB. Wherein: 120 mg/mL < [Total HB] < 170 mg/mL = a healthy range, and [Total Hb] < 120 mg/mL or [Total Hb] > 170 mg/mL = an unhealthy range [26].

FeCN(II) is a common redox probes used in numerous voltammetric and impedimetric biosensors [27]. Generally, there is no specific interaction between the FeCN(II) and the analyte. In this case, the analyte molecules hinder the electron transfer between the FeCN(II) and the electrode surface, engendering the final analytical signal [27]. However, additional consideration must be included in this work.

In this particular case, hemoglobin proteins present two α and two β chains with heme groups in hydrophobic pockets with proximal His93(F8) residues. The great majority of all human Hb in functional erythrocytes exist in ferric oxy form (oxyHb-Fe(III)) and ferrous deoxy form (deoxyHb-Fe(II)), constituting approximately up to 97–98% of all Hb forms (equation 1). FeCN(II) presents a selective pH-binding selectivity in the region of His moieties due to high positive local electrostatic potential at this region with a pocket with enough space on open conformation (equation 2). Also, FeCN(II) might present a complex reaction and or catalytic activity with oxyHb-Fe(III) determined by the concentration ratio FeCN(II)/Hb, pH, and the correct orientation inside the cavity (equation 3) [28].

$$\text{oxyHb} - \text{Fe(III)} \rightleftharpoons \text{deoxyHb} - \text{Fe(II)} \quad (1)$$

$$\text{oxyHb} - \text{Fe(III)} + \ FeCN(II) \longrightarrow \ \text{oxyHb} - \text{Fe(III)} * FeCN(II) \quad (2)$$

$$\text{oxyHb} - \text{Fe(III)} * FeCN(II) \longrightarrow \text{deoxyHb} - \text{Fe(II)} + FeCN(III) \quad (3)$$

After an optimization study (S1, Figure S1-2 and S1-3), the best electrochemical signal during Hb detection was settled by using 10 mM of FeCN(II) in phosphate buffer with pH = 8 and using DPV. In order to have an idea about the possible interaction between the Hb and the FeCN(II)

in the testing conditions, UV-Vis spectrum was recovered from isolated and combined samples of Hb 30 mg/mL and FeCN(II) 10 mM in PBS pH=8 (S1, Figure S1-4).

The spectrum of Hb resulted in the Soret band at 407 nm, and additional charge-transfer (CT) bands at 540, 575, and 631 nm, suggesting the prevalence of $\mathrm{oxyHb-Fe(III)}$ species [29]. After adding FeCN(II), the subtracted spectra with the corresponding control, resulted in a new contribution band at 420 nm in the mix of Hb and FeCN(II), indicating the presence of $FeCN(III)$ and another contribution to the CT bands at 552 nm (between 540 nm and 575 nm), indicating a possible partial transformation to $\mathrm{deoxyHb-Fe(II)}$.

In summary, both effects of sterical hindrance and specific interaction and possible redox reaction between Hb and the redox probe might decrease the local FeCN(II) concentration and availability on the electrode surface, dramatically decreasing the electrochemical oxidation DPV signal. Further studies must be carried out to demonstrate our understanding of the mechanism.

In addition, the oxidation peak potentials shift with each subsequent Hb increased concentration, and the peak seems to have more than one contribution due to collateral oxidation reactions. Considering that an increase in the Hb attracts more FeCN (II) units to the protein surface, the proximity of ferrocyanide species might induce changes in the coordinative environment and interacting iron center reactions at different potentials [28].

The corresponding calibration curve (Figure 3- 3(b)) was retrieved by using the average area under the curve (AUC) values for each concentration of total Hb. A coefficient of determination (R^2) of 99% and a LOD of 2 g/dL or 20 mg/mL was established using a linear fit model. The calibration curve is able to categorize individuals into the healthy and unhealthy ranges of total Hb using 12 – 15 g/dL (i.e., translated into 120 – 150 mg/mL) as the healthy range for females, and 13.8 – 17.2 g/dL (i.e., 138 – 172 mg/mL) for males [26]. An individual

comprised of total Hb below these benchmarks would classify as an unhealthy person in the anemic range.

The DPV signals associated with the detection of total Hb in PBS (8) FeCN (II) with simulated blood (SB) are illustrated in Figure 3- 3(c). Comparing these signals with those observed in Figure 3- 3(a), the presence of SB resulted in increased current signals due to the electrolytic composition and the ionic strength of the blood being higher than that of PBS. The calibration curve for the same is portrayed in Figure 3- 3(d), which presents an exceptional R^2 value of 99%, and a LOD of 3.4 g/dL or 34 mg/mL for the range 0 – 17 g/dL or 0 – 170 mg/mL.

3.3 The Detection of HbA1c

The DPV signals for the detection of HbA1c in both, PBS (8) FeCN(II) (Figure 3- 4(a)) and with SB (Figure 3- 4(c)) using the pre-treated and AuNP/anti-HbA1c modified TE-100 Zensor. The corresponding x-axis represents the concentration of HbA1c before dilution, with the measurement conducted after a dilution of 10x. The electrodes were retrieved after performing a sample incubation for a period of 30 minutes at room temperature allowing specific interaction. Liu et al [31]., were able to bind HbA1c to the ferrocene-boronic acid solution after an incubation for 30 minutes after which, the resultant EC signals were observed to have increased. Furthermore, Eissa and Zourob [32] reported the maximum EC signal change in the current after using a primer-based binding time of 30 mins for HbA1c. Additional electrochemical biosensors reported for the detection of HbA1c can be found in supplementary information S1, Table S1-2.

With the oxidation potential identified at 0.1 V [33, 34], the EC signals decreased with an increase in the HbA1c concentration due to the previously explained Hb-FeCN(II) interaction. Different calibration curves were recovered considering current intensities and the area under the curve (AUC) pertaining to the original peak and post-deconvolution peaks (S1, Figure S1-5).

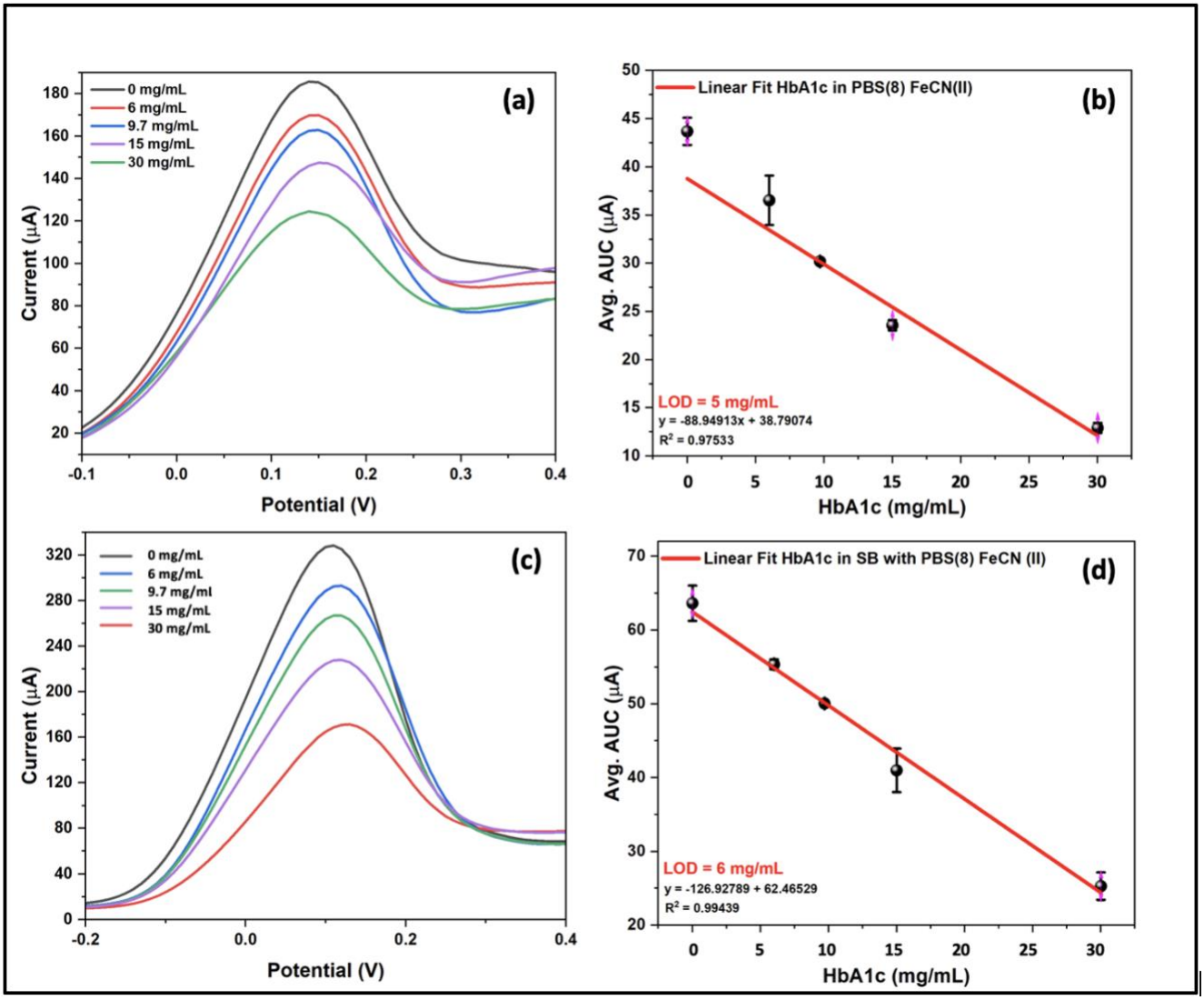

Figure 3- 4: (a) DPV signals for the clinical range of HbA1c in PBS(8) FeCN(II) and resultant (b) calibration curve for the detection of HbA1c, (c) DPV signals for the clinical range of HbA1c FeCN(II) with SB and resultant (d) calibration curve for the detection of HbA1c with SB.

The results depicted in Figure 3- 4(b) and Figure 3- 4(d) correspond to the AUC of the original DPV signal versus the analyte concentration. The associated R^2 values of 97% and 99% for HbA1c detection in PBS (8) FeCN (II), and in PBS (8) FeCN (II) with SB respectively, imply that the linear fit models demonstrate a significant relationship between the HbA1c concentrations and the resultant signal response. Additionally, the calibration curve provides a LOD of 5 mg/mL in PBS (8) FeCN (II) and 6 mg/mL in PBS (8) FeCN (II) with SB. Therefore, the calibration curves can aid in the diagnosis of HbA1c levels within the clinical range wherein, %[HbA1c]< 5.7%

classifies as non-diabetic, %[HbA1c] between the range 5.7 – 6.4% classifies as prediabetic, and %[HbA1c] > 6.4% is indicative of a diabetic patient.

3.4 The Biosensing Electrolyte for the Detection of CRP

Although PBS (8) FeCN (II) was initially used for the detection of CRP following the same approach for HbA1c (S1, Figure S1-6), ferrocyanide lacks the inherent specificity for CRP and hence was proven unsuitable for its measurement. Opposingly, phosphorylcholine (PcA) is the most abundant structural component of phospholipids found in the membranes of eukaryotic cells. It plays a major role in maintaining the physical properties of membranes and forming liquid crystalline bilayers spontaneously, with its trifling transfer rate between membranes [35]. This molecule presents a high affinity for CRP domains.

The molecular mechanism for the high affinity between CRP and PcA-containing substances has been well corroborated [36, 37]. Wherein, the hydrophobic pocket of the PcA is known to interact with each subunit of the pentamer i.e., CRP, and activate the complement system [38]. The phosphate groups bind to the PcA-binding sites of CRP and induce a conformational change in the binding cites of the protein, allowing direct interaction with PcA [36]. Several studies have also reported the use of PcA for the EC biosensing of CRP [39–42]. Therefore, O-(4-Nitrophenylphosphoryl)choline (PcA-NO_2) was employed as the biosensing electrolyte for the detection of CRP. In this case, the presence of the highly electroactive NO_2 group enables the compound to undergo the reduction process. As a result, the PcA-NO_2 presents a high affinity for the analyte while acting as a redox probe (S1, Figure S1-7).

With PcA classified as a zwitterionic compound [43], the stability of the compound is highly dependent on the pH of the solution that its dissolved in. Zwitterionic compounds demonstrate better stability and reactivity at a pH value near their isoelectric point (pI). Since the

pI of PcA is known to be approximately at 7.4 [43], using PBS with a pH of 7.4 would result in the best stability of the compound. Therefore, 0.1 M of PcA-NO_2 was dissolved in PBS (7.4) to transpire the specific and targeted detection of CRP to predict the maturation of CHD.

3.4.1 The Detection of CRP

The DPV signals associated with the detection of CRP concentrations 0, 0.005, 0.01, 0.03, and 0.05 mg/mL in PBS (7.4) PcA-NO_2 are depicted in Figure 3- 5(a). The x-axis represents the concentration of CRP prior to dilution, with the measurement performed after a dilution of 10x. Since the reduction of the nitro (NO_2) group in PcA to the amine (NH_2) group is a two-step reaction: PcA -NO_2 → PcA -NH-OH → PcA -NH_2 (S1, Figure S1-8 and S1-9) the resultant DPV signals illustrated in Figure 3- 5(a) and Figure Figure 3- 5(c) were retrieved after performing a second scan. Therefore, a second was executed after incubating the detection sample for a period of 10 minutes on the electrode after having completed the first scan. In this case, the CRP-PcA-specific interaction induces an increment of redox probe species, NH-OH after the first scan, on the electrode surface resulting in signal amplification. Hence, an increase in CRP concentration led to an increase in the corresponding area under the curve values (Figure 3- 5(a) and Figure 3- 5(c)).

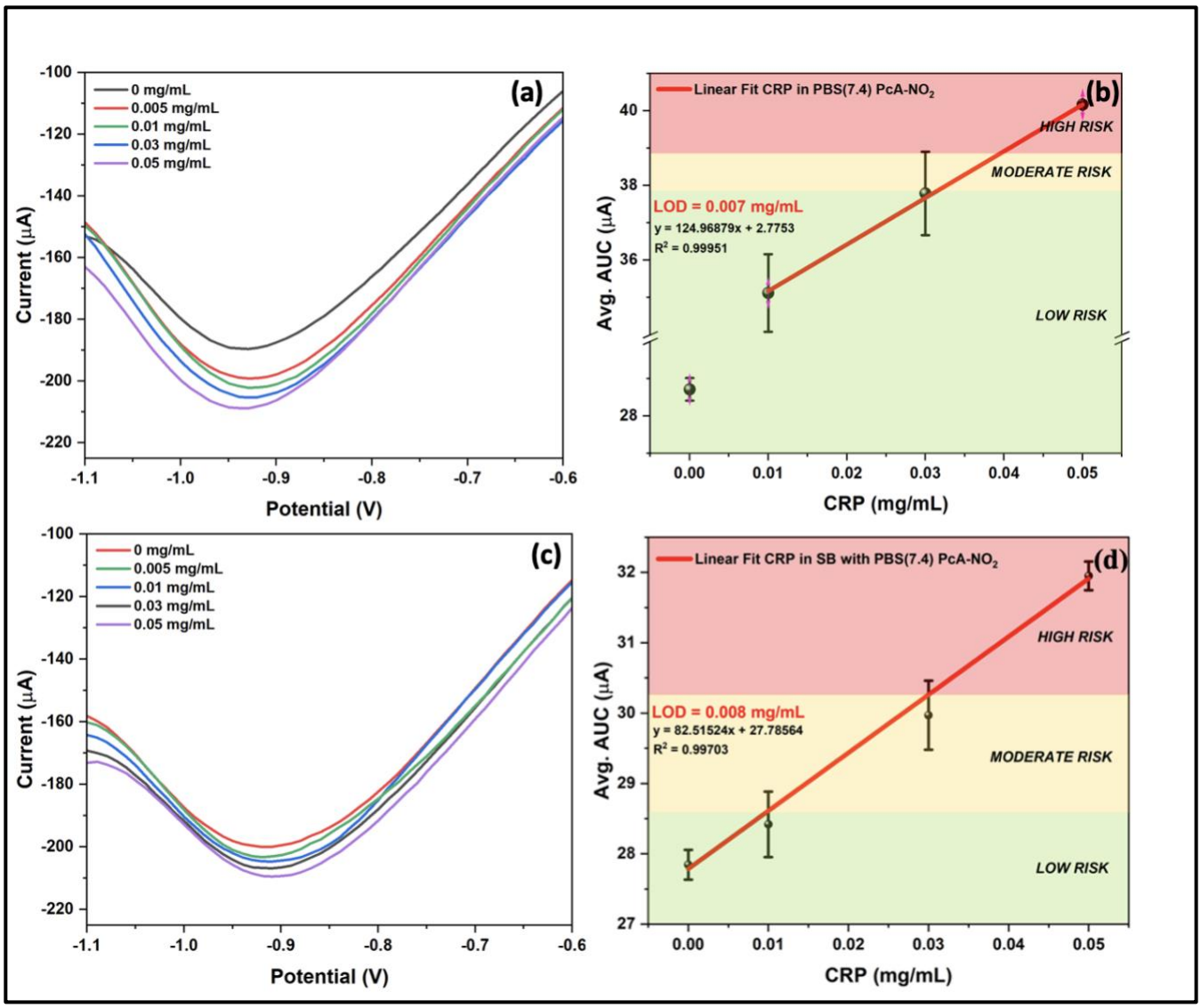

Figure 3- 5: (a) DPV signals (Scan 2) for the clinical range of CRP in PBS(7.4) PcA-NO_2 and resultant (b) calibration curve for the detection of CRP, (c) DPV signals (Scan 2) for the clinical range of CRP in PBS(7.4) PcA-NO_2 with SB and resultant (d) calibration curve for the detection of CRP with SB. Wherein: [hs-CRP] < 0.01 mg/mL = low risk, 0.01 mg/ml < [hs-CRP] < 0.03 mg/mL = moderate risk, and [hs-CRP] > 0.03 mg/mL = high risk for developing CHD.

The corresponding calibration curves for the label-free EC detection of CRP in PBS (7.4) PcA-NO_2 and in PBS (7.4) PcA-NO_2 with SB are showcased in Figure 3- 5(b) and Figure 3- 5(d). Both linear fit models present an exceptional R^2 value of 98% and 99% with an associated LOD of 0.007 mg/mL and 0.008 mg/mL for measurement in PBS (7.4) PcA-NO_2 and in SB respectively. The models are able to predict the maturation of CRP with high sensitivity (hs-CRP): [hs-CRP] <

0.01 mg/mL = low risk of developing CHD, [hs-CRP] 0.01 – 0.03 mg/mL = moderate risk of developing CHD, and [hs-CRP] > 0.03 mg/mL = high risk of developing CHD.

Additional electrochemical biosensors reported for the detection of CRP can be found in supplementary information, S1, Table S1-3. The novelty of the calibration curves presented arises from the utilization of PcA-NO2, a molecule known for its pronounced affinity to C-reactive protein (CRP), serving as the redox probe. While existing literature comprehensively establishes the strong affinity between PcA-containing compounds and CRP, it is noteworthy that the application of this specific molecule for the electrochemical detection of CRP has not been documented in scientific literature before.

3.5 Interference Studies and Percent of Recoveries

The cross-reactive interference studies performed for all the three analytes, Total Hb, HbA1c, and CRP is depicted in Figure 3- 6. The studies were performed using the original methods pertaining to the manufacturing and detection protocol of the analytes stated. In this case, the cut-off value of the three analytes were chosen to be submitted to the presence of high concentrations of a possible cross-reactive species.

A volume of 10 µL of CRP (0.05 mg/mL) was added to the Total Hb (70 mg/mL) and HbA1c (9.7 mg/mL) detection samples, and 10 µL of Total Hb (100 mg/mL) was added to the CRP detection sample (0.03 mg/mL) to induce cross interferences. Comparing the AUC values for the IF samples with the original samples retrieved previously (Figure 3- 3(a),Figure 3- 4(a),Figure 3- 5(a)), the results demonstrate similar AUC values and hence imply the presence of insignificant interferences. This result suggests that the electrochemical systems present herein could quantify total Hb, HbA1c, and CRP in mixed samples containing such analytes.

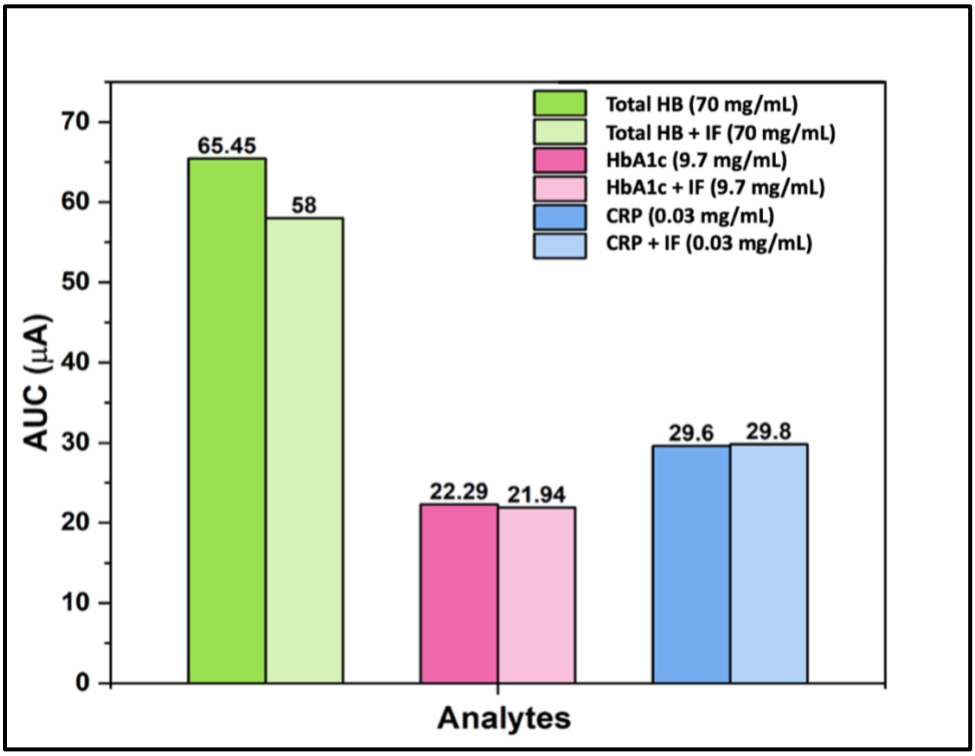

Figure 3- 6: Comparison of interference samples.

The percent recovery analysis for all the three label-free EC biosensors was performed by adding 10 µL of Chicken Red Blood Cells Packed 5% to the detection sample for each analyte. The Total Hb, HbA1c, and CRP concentrations were quantified for each addition, as depicted in Table 3- 1 below. The practical applicability of the biosensors were measured by determining the recovery of the known concentrations added for each analyte. The corresponding recovered values for Total Hb were between 94.4 – 98.3%, 96 – 103% for HbA1c, and 90 – 95% for CRP. The satisfactory recoveries for all clinical ranges corresponding to the Total Hb, HbA1c, and CRP indicate that such a method has good specificity and applies to quantifying such analytes in complex biological samples.

Table 3- 1: Percent Recovery Analysis for all the three analytes.

Sample no.	Total Hb added (mg/mL)	Total Hb measured (mg/mL)	% Recovery
1	70	68	97.0
2	120	116	98.3
3	170	164	96.4

Sample no.	HbA1c added (mg/mL)	HbA1c measured (mg/mL)	% Recovery
1	9.7	10.0	103
2	15.0	15.5	103
3	30.0	29.0	96

Sample no.	CRP added (mg/mL)	CRP measured (mg/mL)	% Recovery
1	0.10	0.095	95
2	0.30	0.27	90
3	0.50	0.45	90

4 Conclusions

The elevated inflammatory state induced by heightened C-reactive protein (CRP) levels plays a pivotal role in delineating the pathogenesis of Type 2 Diabetes Mellitus (T2DM), thereby substantiating the strong correlation between diabetes and Coronary Heart Disease (CHD). This study presents a novel label-free biosensing platform, enabling researchers to potentially conduct the concurrent detection of %HbA1c and CRP, in order to assess the risk of developing CHD.

The calibration curves attained demonstrate a notable level of sensitivity and selectivity through the utilization of redox probes tailored to each biomarker. Notably, the redox probe PcA-NO2, which contains phosphorylcholine (PcA), was employed for the assessment of C-reactive protein (CRP). It is noteworthy that this specific application of PcA-NO2 as a redox probe for CRP is a novel approach, unreported in literature studies. The study reports a LOD of 5 mg/mL and 6 mg/mL in PBS (8) FeCN (II) and SB for the detection of HbA1c respectively. In addition, a LOD

of 0.007 mg/mL and 0.008 mg/mL for measurement of CRP in PBS (7.4) PcA-NO_2 and SB respectively is reported.

To broaden the scope of this study, the incorporation of dual working screen-printed carbon electrodes (DWSPCEs) can be considered to enhance sensitivity. Furthermore, the integration of electrochemical sensors with artificial intelligence (AI) is promising in advancing both diabetes prevention strategies and the efficacy of daily physical health assessments pertaining to the development of CHD.

5 References

[1] Schramm, T. K., Gislason, G. H., Køber, L., Rasmussen, S., Rasmussen, J. N., Abildstrøm, S. Z., Hansen, M. L., Folke, F., Buch, P., Madsen, M., Vaag, A., & Torp-Pedersen, C. (2008). Diabetes patients requiring glucose-lowering therapy and nondiabetics with a prior myocardial infarction carry the same cardiovascular risk. *Circulation*, *117*(15), 1945–1954. https://doi.org/10.1161/circulationaha.107.720847

[2] Spencer, E. A., Pirie, K. L., Stevens, R. J., Beral, V., Brown, A., Liu, B., Green, J., & Reeves, G. K. (2008). Diabetes and modifiable risk factors for cardiovascular disease: The Prospective Million Women Study. *European Journal of Epidemiology*, *23*(12), 793–799. https://doi.org/10.1007/s10654-008-9298-3

[3] Khaw, K.-T., Wareham, N., Bingham, S., Luben, R., Welch, A., & Day, N. (2004). Association of hemoglobin a1c with cardiovascular disease and mortality in adults: The European Prospective Investigation into cancer in Norfolk. *Annals of Internal Medicine*, *141*(6), 413. https://doi.org/10.7326/0003-4819-141-6-200409210-00006

[4] The Emerging Risk Factors Collaboration. (2010). Diabetes mellitus, fasting blood glucose concentration, and risk of vascular disease: A collaborative meta-analysis of 102 prospective studies. *The Lancet*, *375*(9733), 2215–2222. https://doi.org/10.1016/s0140-6736(10)60484-9

[5] Sherwani, S. I., Khan, H. A., Ekhzaimy, A., Masood, A., & Sakharkar, M. K. (2016). Significance of hba1c test in diagnosis and prognosis of diabetic patients. *Biomarker Insights*, *11*. https://doi.org/10.4137/bmi.s38440

[6] American Diabetes Association. (2010). Diagnosis and classification of diabetes mellitus. *Diabetes Care*, *33*(Supplement_1), S62–S69. https://doi.org/10.2337/dc10-s062

[7] Moriarity, D. P., Horn, S. R., Kautz, M. M., Haslbeck, J. M. B., & Alloy, L. B. (2021). How handling extreme C-reactive protein (CRP) values and regularization influences CRP and Depression Criteria Associations in network analyses. *Brain, Behavior, and Immunity*, *91*, 393–403. https://doi.org/10.1016/j.bbi.2020.10.020

[8] Ridker, P. M. (2014). Inflammation, C-reactive protein, and cardiovascular disease. *Circulation Research*, *114*(4), 594–595. https://doi.org/10.1161/circresaha.114.303215

[9] Gabay, C., & Kushner, I. (1999). Acute-phase proteins and other systemic responses to inflammation. *New England Journal of Medicine*, *340*(6), 448–454. https://doi.org/10.1056/nejm199902113400607

[10] Stanimirovic, J., Radovanovic, J., Banjac, K., Obradovic, M., Essack, M., Zafirovic, S., Gluvic, Z., Gojobori, T., & Isenovic, E. R. (2022). Role of C-reactive protein in diabetic inflammation. *Mediators of Inflammation*, *2022*, 1–15. https://doi.org/10.1155/2022/3706508

[11] Kanmani, S., Kwon, M., Shin, M.-K., & Kim, M. K. (2019). Association of C-reactive protein with risk of developing type 2 diabetes mellitus, and role of obesity and hypertension: A large population-based Korean cohort study. *Scientific Reports*, *9*(1). https://doi.org/10.1038/s41598-019-40987-8

[12] Lee, C. C., Adler, A. I., Sandhu, M. S., Sharp, S. J., Forouhi, N. G., Erqou, S., Luben, R., Bingham, S., Khaw, K. T., & Wareham, N. J. (2009). Association of C-reactive protein with type 2 diabetes: Prospective Analysis and meta-analysis. *Diabetologia*, *52*(6), 1040–1047. https://doi.org/10.1007/s00125-009-1338-3

[13] Mugabo, Y., Li, L., & Renier, G. (2010). The connection between C-reactive protein (CRP) and Diabetic Vasculopathy. focus on preclinical findings. *Current Diabetes Reviews*, *6*(1), 27–34. https://doi.org/10.2174/157339910790442628

[14] American Diabetes Association. (2022). National Diabetes Statistics Report. *Centers for Disease Control and Prevention*. https://www.cdc.gov/diabetes/data/statistics-report/index.html

[15] Stanimirovic, J., Radovanovic, J., Banjac, K., Obradovic, M., Essack, M., Zafirovic, S., Gluvic, Z., Gojobori, T., & Isenovic, E. R. (2022a). Role of C-reactive protein in diabetic inflammation. *Mediators of Inflammation*, *2022*, 1–15. https://doi.org/10.1155/2022/3706508

[16] Adesina, A., & Mashazi, P. (2021). Oriented antibody covalent immobilization for label-free impedimetric detection of C-reactive protein via direct and sandwich immunoassays. *Frontiers in Chemistry*, *9*. https://doi.org/10.3389/fchem.2021.587142

[17] Yuan, Y., Zhou, X., Gao, L., Ren, Q., & Ji, L. (2020). Silent hemoglobin variant during capillary electrophoresis: A case report. *Journal of Diabetes Investigation*, *11*(4), 1014–1017. https://doi.org/10.1111/jdi.13222

[18] Mallya, M., Shenoy, R., Kodyalamoole, G., Biswas, M., Karumathil, J., & Kamath, S. (2013). Absorption spectroscopy for the estimation of glycated hemoglobin (hba1c) for the diagnosis and management of diabetes mellitus: A pilot study. *Photomedicine and Laser Surgery*, *31*(5), 219–224. https://doi.org/10.1089/pho.2012.3421

[19] Zhang, P., Bao, Y., Draz, M., Lu, H., Liu, C., & Han, H. (2015). Rapid and quantitative detection of C-reactive protein based on quantum dots and immunofiltration assay. *International Journal of Nanomedicine*, *10*, 6161. https://doi.org/10.2147/ijn.s89307

[20] Davis, J. E., Mcdonald, J. M., & Jarett, L. (1978). A high-performance liquid chromatography method for hemoglobin A1C. *Diabetes*, *27*(2), 102–107. https://doi.org/10.2337/diab.27.2.102

[21] Agrawal, A., Xu, Y., Ansardi, D., Macon, K. J., & Volanakis, J. E. (1992). Probing the

phosphocholine-binding site of human C-reactive protein by site-directed mutagenesis. *Journal of Biological Chemistry*, *267*(35), 25352–25358. https://doi.org/10.1016/s0021-9258(19)74047-2

[22] Ivaska, A., & Bobacka, J. (2005). Process analysis | electroanalytical techniques. *Encyclopedia of Analytical Science*, 309–316. https://doi.org/10.1016/b0-12-369397-7/00487-8

[23] Gomez Cardoso, A., Rahin Ahmed, S., Keshavarz-Motamed, Z., Srinivasan, S., & Reza Rajabzadeh, A. (2023). Recent advancements of nanomodified electrodes – towards point-of-care detection of cardiac biomarkers. *Bioelectrochemistry*, *152*, 108440. https://doi.org/10.1016/j.bioelechem.2023.108440

[24] Campuzano, S., Pedrero, M., Yáñez-Sedeño, P., & Pingarrón, J. M. (2021). New challenges in point of care electrochemical detection of clinical biomarkers. *Sensors and Actuators B: Chemical*, *345*, 130349. https://doi.org/10.1016/j.snb.2021.130349

[25] Young, S. L., Kellon, J. E., & Hutchison, J. E. (2016). Small gold nanoparticles interfaced to electrodes through molecular linkers: A platform to enhance electron transfer and increase electrochemically active surface area. *Journal of the American Chemical Society*, *138*(42), 13975–13984. https://doi.org/10.1021/jacs.6b07674

[26] Billett, H. H. (1990). Hemoglobin and Hematocrit. In H.K. Walker, W.D. Hall, & J.W. Hurst (Eds.), Clinical Methods: The History, Physical, and Laboratory Examinations (3rd ed., Chapter 151). Boston: Butterworths.

[27] Eissa, S., Almusharraf, A. Y., & Zourob, M. (2019). A comparison of the performance of Voltammetric Aptasensors for glycated haemoglobin on different carbon nanomaterials-modified screen printed electrodes. *Materials Science and Engineering: C*, *101*, 423–430. https://doi.org/10.1016/j.msec.2019.04.001

[28] Postnikova, G. B., & Shekhovtsova, E. A. (2016). Hemoglobin and myoglobin as

reducing agents in biological systems. redox reactions of globins with copper and iron salts and complexes. *Biochemistry (Moscow)*, *81*(13), 1735–1753. https://doi.org/10.1134/s0006297916130101

[29] Dybas, J., Bokamper, M. J., Marzec, K. M., & Mak, P. J. (2020). Probing the structure-function relationship of hemoglobin in living human red blood cells. *Spectrochimica Acta Part A: Molecular and Biomolecular Spectroscopy*, *239*, 118530. https://doi.org/10.1016/j.saa.2020.118530

[30] García Armada, M. P., Losada, J., López-Villanueva, F. J., Frey, H., Alonso, B., & Casado, C. M. (2008). Electrochemical and bioelectrocatalytical properties of novel block-copolymers containing interacting ferrocenyl units. *Journal of Organometallic Chemistry*, *693*(16), 2803–2811. https://doi.org/10.1016/j.jorganchem.2008.05.038

[31] Liu, S., Wollenberger, U., Katterle, M., & Scheller, F. W. (2006). Ferroceneboronic acid-based amperometric biosensor for glycated hemoglobin. *Sensors and Actuators B: Chemical*, *113*(2), 623–629. https://doi.org/10.1016/j.snb.2005.07.011

[32] Eissa, S., & Zourob, M. (2017). Aptamer- based label-free electrochemical biosensor array for the detection of total and glycated hemoglobin in human whole blood. *Scientific Reports*, *7*(1). https://doi.org/10.1038/s41598-017-01226-0

[33] Lin, H., & Yi, J. (2017). Current status of HbA1c biosensors. *Sensors*, *17*(8), 1798. https://doi.org/10.3390/s17081798

[34] Shajaripour Jaberi, S. Y., Ghaffarinejad, A., & Omidinia, E. (2019). An electrochemical paper based nano-genosensor modified with reduced graphene oxide-gold nanostructure for determination of glycated hemoglobin in blood. *Analytica Chimica Acta*, *1078*, 42–52. https://doi.org/10.1016/j.aca.2019.06.018

[35] Kanno, K., Wu, M. K., Scapa, E. F., Roderick, S. L., & Cohen, D. E. (2007). Structure and function of phosphatidylcholine transfer protein (PC-TP)/STARD2. *Biochimica et Biophysica Acta (BBA) - Molecular and Cell Biology of Lipids*, *1771*(6), 654–662. https://doi.org/10.1016/j.bbalip.2007.04.003

[36] Thompson, D., Pepys, M. B., & Wood, S. P. (1999). The physiological structure of human C-reactive protein and its complex with phosphocholine. *Structure*, *7*(2), 169–177. https://doi.org/10.1016/s0969-2126(99)80023-9

[37] Qian, S., Zhang, S., Chen, D., Wang, J., Wu, W., Zhang, S., Geng, Z., He, Y., & Zhu, B. (2023). Phosphorylcholine-functionalized pedot-gated organic electrochemical transistor devices for ultra-specific and sensitive C-reactive protein detection. *Polymers*, *15*(18), 3739. https://doi.org/10.3390/polym15183739

[38] Lee, R. T., Takagahara, I., & Lee, Y. C. (2002). Mapping the binding areas of human C-reactive protein for phosphorylcholine and polycationic compounds. *Journal of Biological Chemistry*, *277*(1), 225–232. https://doi.org/10.1074/jbc.m106039200

[39] Wu, J.-G., Wei, S.-C., Chen, Y., Chen, J.-H., & Luo, S.-C. (2017). Critical study of the recognition between C-reactive protein and surface-immobilized phosphorylcholine by quartz crystal microbalance with dissipation. *Langmuir*, *34*(3), 943–951. https://doi.org/10.1021/acs.langmuir.7b02724

[40] Pinyorospathum, C., Chaiyo, S., Sae-ung, P., Hoven, V. P., Damsongsang, P., Siangproh, W., & Chailapakul, O. (2019). Disposable paper-based electrochemical sensor using thiol-terminated poly(2-methacryloyloxyethyl phosphorylcholine) for the label-free detection of C-reactive protein. *Microchimica Acta*, *186*(7). https://doi.org/10.1007/s00604-019-3559-6

[41] Xing, Y., Gao, Q., Zhang, Y., Ma, L., Loh, K. Y., Peng, M., Chen, C., & Cui, Y. (2017).

The improved sensitive detection of C-reactive protein based on the chemiluminescence immunoassay by employing monodispersed PAA-au/fe3O4 nanoparticles and zwitterionic glycerophosphoryl choline. *Journal of Materials Chemistry B*, *5*(21), 3919–3926. https://doi.org/10.1039/c7tb00637c

[42] Pomowski, A., Baricham, C., Rapp, B. E., Matern, A., & Lange, K. (2015). Acoustic biosensors coated with phosphorylcholine groups for label-free detection of human C-reactive protein in serum. *IEEE Sensors Journal*, *15*(8), 4388–4392. https://doi.org/10.1109/jsen.2015.2419278

[43] Chen, Y., Han, H., Tong, H., Chen, T., Wang, H., Ji, J., & Jin, Q. (2016). Zwitterionic phosphorylcholine–TPE conjugate for PH-responsive drug delivery and aie active imaging. *ACS Applied Materials and Interfaces*, *8*(33), 21185–21192. https://doi.org/10.1021/acsami.6b06071

Chapter 4 : Examining the Stability of Screen-Printed Carbon Electrodes – Challenges & Perspective

4.1 Preface

This chapter begins by outlining the challenges associated with biomolecule-free sensing devices and extends to explicitly examining the chemical instability of such a sensing approach for the roadside detection of THC [45], devised by the members of the same laboratory research group. The publishable manuscript presented in Section 4.3 stems from the research above and identifies optimal storage conditions to promote the long-term stability of the proposed device. The contributors of the manuscript include:

1. *Ms. Rehmat Grewal*
2. *Dr. Greter A. Ortega* – division 2.4, and parts of 3.2.3 and 3.3 (under the scope of section 4.3 in this chapter).
3. *Dr. Herlys Viltres* – divisions 2.5 and 3.2.1.1 (under the scope of section 4.3 in this chapter).

4.2 Introduction to the Challenges Associated with the Stability of a Biomolecule-Free Electrochemical Sensor

The term “biomolecule-free” refers to the development of a biosensor without the use of specific biomolecules including nucleic acids, enzymes, antibodies for the detection of the target analyte. Although biomolecule-free sensing approaches for drug detection eliminate the need for extensive pre-treatment, analyte adsorption, complex procedures, longer processing times and are cost-effective [45], challenges pertaining with this method must be addressed before the implementation of this sensing approach.

Due to the lack of specific antibodies and enzymes, biomolecule-free sensing devices often struggle with achieving high sensitivity and selectivity. Consequently, the absence of signal

amplification mechanisms provided by enzymes can result in the inability to detect and differentiate between low concentrations of the target analyte. Other major challenges associated with a biomolecule-free sensor include the lack of stability and the reproducibility in the resultant EC signals over time. Furthermore, preserving the long-term stability without degradation of the sensor components whilst maintaining its performance is crucial for continuous biosensing applications.

The instability of biomolecule-free sensors in drug detection applications can be a result of: chemical instability caused by environmental factors such as temperature, humidity, and pH, sensor surface instability due to the degradation of the functionalized surfaces, electrode surface instability, or sample matrix effects as a result of interfering substances present in biological fluids [25]. Opposingly, challenges associated with the reproducibility could be due to the batch-to-batch inconsistency during the fabrication of the sensor, and lack of the antibody-antigen specific interactions. The subsequent section provides an in-depth analysis on the chemical instability of a biomolecule-free EC sensing device for the detection of THC [45] and provides optimal storage conditions to tackle this aberration.

4.3 Determining Optimal Storage Conditions to Enhance the Stability of Δ9-tetrahydrocannabinol (THC)-Modified Screen-Printed Carbon Electrodes (SPCEs)

THC (Δ9-tetrahydrocannabinol) is the major psychoactive constituent of cannabis, accountable for instigating euphoric effects in individuals. With the imperative need for a roadside testing device for the detection of THC, this study aims to overcome the challenges associated with the Stability of a biomolecule-free sensor capable of detecting ultra-low concentrations of THC. Since THC is highly susceptible to oxidation, this study explores different avenues to create optimal storage conditions to minimize the oxidation of THC prior to detection. Hence, all experiments were conducted by controlling the principal factors contributing to the oxidation of THC: temperature,

humidity, airflow and light, to extend the shelf-life of the manufactured electrodes and engender stable electrochemical signals. It was concluded that frozen storage conditions and a second acidic pH modification were ideal in improving the stability of the modified electrodes from day one, upto a period of six months.

1. Introduction

Δ9-tetrahydrocannabinol (THC) is a common natural component of the plant *Cannabis sativa* [1]. It is the chief psychoactive product of marijuana (cannabis) and is responsible for exhibiting euphoric effects in individuals. The legalization of medical and recreational marijuana in Canada has increased the number of drug-impaired drivers and the associated number of accidents. [2-5]. Epidemiologic data shows that the danger of being involved in a motor vehicle accident (MVA) increases 2-fold after cannabis consumption [3]. Hence, regulatory authorities require the development of roadside testing devices for the detection of THC to reduce cannabis-impaired driving.

In order to be viable for the roadside testing of THC, the sensing device must be easy-to-use, portable, economical, operable under ambient environmental conditions, and administer results preferably in less than 5 minutes. However, the current sensing devices available are either enzyme or biomolecule based [6] and therefore are obligated to undergo complex procedures for the adsorption of the analyte [7], resulting in the whole process being extremely time-consuming.

Ortega and colleagues [8] introduced a biomolecule-free electrochemical sensing approach for the detection of ultra-low concentrations of THC in phosphate buffer (PBS), real saliva, and simulated saliva. Their sensing device uses the approach of depositing THC molecules (THCi) onto the working electrode (WE) of the screen-printed carbon electrode (SPCE) prior to detection (Figure 4-1). In this case, the THCi on the WE improves the interaction with the THC analytes by

covalent binding and physical interactions. The final electrochemical detection is associated with the irreversible oxidation of the phenol group of THC. The design proposed is also successful in meeting the desired criteria listed above, for the device is easily operable, portable, cost-effective, and possesses a testing time of only 38 seconds.

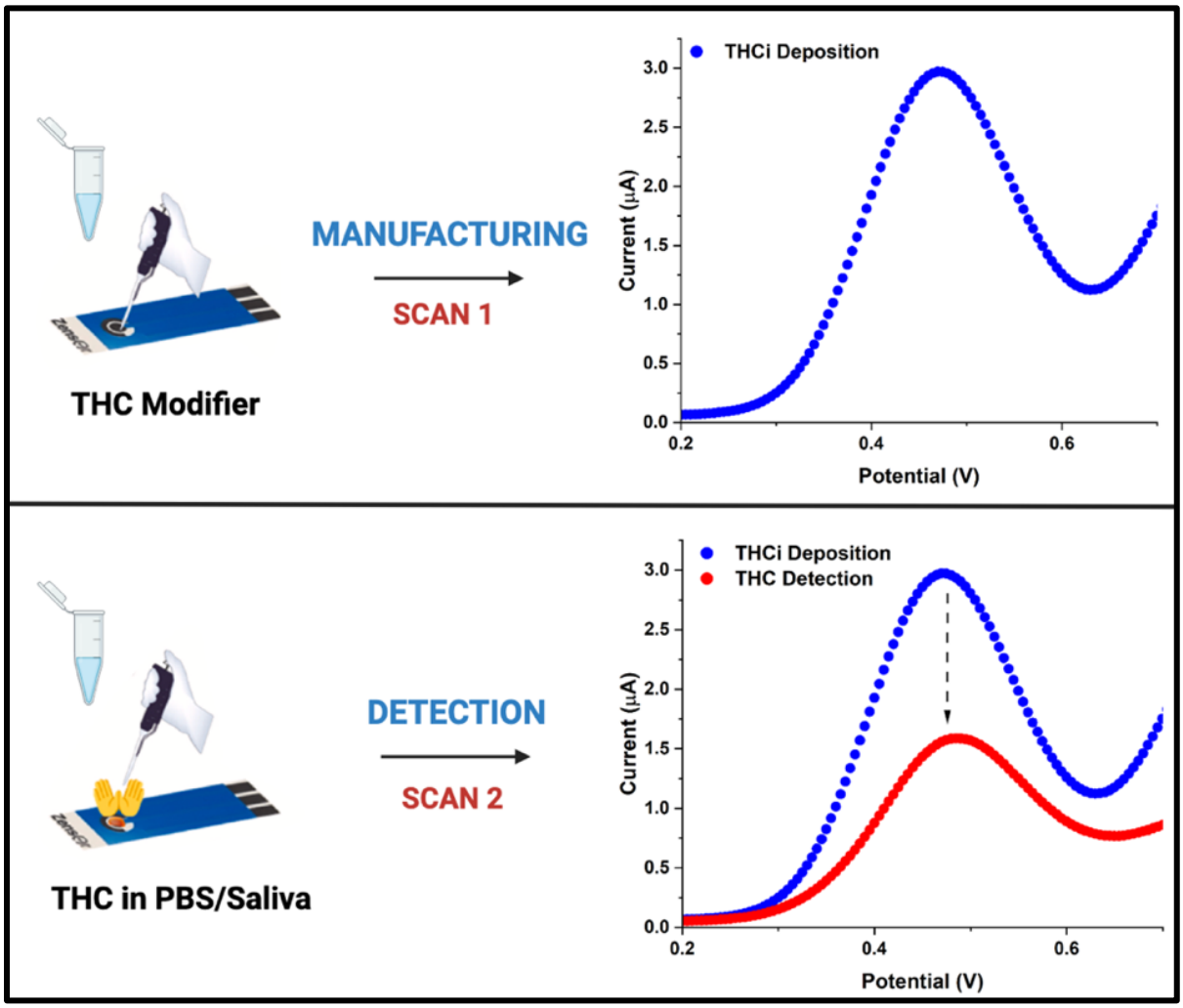

Figure 4- 1: An overview of the manufacturing and detection process proposed by Ortega et al. [8], created using BioRender.com.

Although this approach [8] has resulted in creating an extremely efficient testing system for the detection of THC, it presents a major challenge. After the working electrode of the sensor is manufactured with an initial THCi electrodeposition, the intensity of the current is observed to be proportional to the amount of THC deposited when subjected to the electrochemical method of

square wave voltammetry (SWV). The decrease in the intensity of the signals from the manufacturing (SCAN 1) to the detection scan (SCAN 2) is a result of the partial oxidation of THCi plus the contribution of the THC analyte (Figure 4-1). However, with THCi being highly susceptible to oxidation, the intensity of the current decreases significantly with a lack of reproducibility when testing the modified electrode for sample detection via SWV.

With the ability of THC to oxidize so easily, this makes the pre-treatment process very difficult, impacting the test process and the corresponding test results negatively. Thus, this research paper stems from the study above [8] and aims to explore different avenues to create an ambient environment which can potentially minimize the oxidation of THC prior to detection. Characteristics pertaining to the shelf-life of biosensors are extremely crucial for their overall performance and yet are often not reported in literature studies.

The stability of the biosensor strongly dictates its commercial viability. All biological products, including biosensors are prone to ageing, directly influencing the functionality of the sensor. The ageing of a biosensor can be defined as a decrease in its sensitivity over the course of time. A study conducted by Panjan and colleagues [9] provides insight about the ageing of biosensors to be linearly dependent on temperature conditions. The study concludes that irrespective of their application, all electrochemical biosensors degraded faster at higher temperatures. Additionally, the study proposes a novel method to examine the characteristics for rapid ageing by using Arrhenius and linear models.

Consequently, temperature, humidity, airflow & light are the four principal factors which contribute to the oxidation of THC. Controlling these factors can result in extending the shelf-life of the manufactured electrodes and provide stable intensity signals during the detection of THC. Therefore, the main objective of this research is to explore different storage conditions suitable for

preserving THC by minimizing the oxidation of THC during manufacturing. Finally, the sensor performance will be evaluated after applying the optimized storage conditions.

2. Materials and Methods

2.1 Materials

TE-100 SPCE's purchased from Zensor R&D were used for the purposes of this research. The deposition of the analyte onto the working electrode (WE) of the Zensor electrodes was performed using the machine-driven dispensing technology, the BioDot. The Glove Box 2700 Series and a multifunctional food vacuum sealer were purchased from Cleatech LLC and Hogance respectively, to store the electrodes in a low-pressure and an inert environment. Metallic mylar Ziploc bags lined with aluminum foil were used to impede the exposure of the THC-modified electrodes to light. Additionally, oxygen scavenger sachets were used to reduce the oxygen levels to less than or equal to 0.1%. The electrochemical detection was carried out using a PalmSens4 potentiostat, driven by the PSTrace 5-Palm-Sens software. Lastly, Δ^9-tetrahydrocannabinol solution (1.0 mg/mL) in methanol was purchased from Sigma-Aldrich.

2.2 Methods

2.2.1 Electrode cleaning

The TE-100 Zensor pristine electrodes were washed using milli Q water and then dried using hot airflow in the fume hood.

2.2.2 Electrode modification

The washed electrodes were modified with 130 ng of the Δ^9-THC solution (THCi) prepared onto the WE using the BioDot, and then dried in the fume hood using warm airflow. The dried electrodes were then inserted into the multi-potentiostat and scanned (SCAN 1) with PBS (pH 7.4) using the following conditions for SWV: a precondition potential of 0.05 V for 0 s, an equilibration

time of 3 s, a voltametric potential scan from 0 to 0.8 V, a frequency of 15 Hz, an amplitude of 0.025 V and a step potential of 0.005 V.

2.2.3 Additional modifiers

The THCi modified electrodes were also used in conjunction with a second modification of an additional modifier to further minimize oxidation. Hence, this modification was performed upon the completion of Section 2.2.2. The additional modifiers include PBS (pH 4), 13 ng of Ascorbic Acid (AA), 13 ng of Citric Acid (CA), and 5.2 ng of butylated hydroxytoluene (BHT) in conjunction with diethylene glycol monoethyl ether (Transcutol).

2.2.4 Alternative modifiers

Modifiers with similar electrochemical behaviour to that of THC were pre-deposited onto the WE as an alternative to THCi deposition. In this case, the modification stated in Section 2.2.2 was performed using the following modifiers instead of THC: 130 ng of tetrahydrocannabinolic acid (THCA), 130 ng of Δ^9-Tetrahydrocannabinol Acetate (THC-OAc), 100 ng of dopamine (DA), and 100 ng and 130 ng of cannabidiol (CBD).

2.2.5 Electrode Storage

Electrodes prepared in Sections 2.2.2, 2.2.4, and 2.2.3 were vacuum sealed using oxygen absorber sachets in mylar Ziploc bags and then stored at different temperature conditions.

2.2.5.1 Optimizing temperature

It has been reported that THC is highly unstable at room temperature [10] and exhibits favourable stability condition at lower temperatures [11-13]. Hence, the electrochemical sensors were stored at room temperature (RT), 4°C, and -20°C for the purposes of shelf-life studies.

2.2.5.2 Controlling atmospheric oxidation

Oxygen absorbers function via the occurrence of a chemical reaction; they are comprised of powdered iron, which reacts with the oxygen in the atmosphere to form iron oxide, resulting in the rusting of the iron powder. Upon the oxidization of the iron powder, the O_2 absorbers are loaded, and hence, the absorbing mechanism comes to an end. Subsequently, they are known to help reduce oxygen levels to less than or equal to 0.1%. Air oxidation plays a crucial role in contributing to the oxidation of THC [14, 15].

2.2.5.3 Eliminating exposure to light

Mylar is a clear material made from polyester resin which possesses numerous desirable properties for long-term storage, such as gas and moisture resistance, chemical stability, and high tensile strength. Mylar bags offer an extremely low Oxygen Transmission Rate (OTR) due to their thick foil laminate layer and hence, are impermeable to gases. They help in providing a thick layer of protection from moisture, light, and odour. The oxidative degradation of THC to CBN is known to have been accelerated when exposed to light [16, 17].

2.2.5.4 Minimizing airflow

Lastly, to minimize airflow, two different vacuum systems were implemented. In the first system, the vacuum pump was used in conjunction with a glove box purged with nitrogen (N_2) gas and for the second vacuum system, the electrodes and the desiccants were vacuum sealed using a simple food vacuum sealer. Vacuum packing diminishes the amount of oxygen exposure and airflow, protects the contents from dust and moisture, and shields the electrodes from any physical damage. Literature has previously recommended storing THC under nitrogen gas whilst in the dark [18-20].

2.2.6 Graphical procedural overview

The comprehensive graphical procedural overview is depicted in Figure 4- 2 below, delineating the essential stages from electrode manufacturing, subsequent storage under varied temperature conditions, culminating in the detection process employing PBS/saliva via the electrochemical technique of SWV.

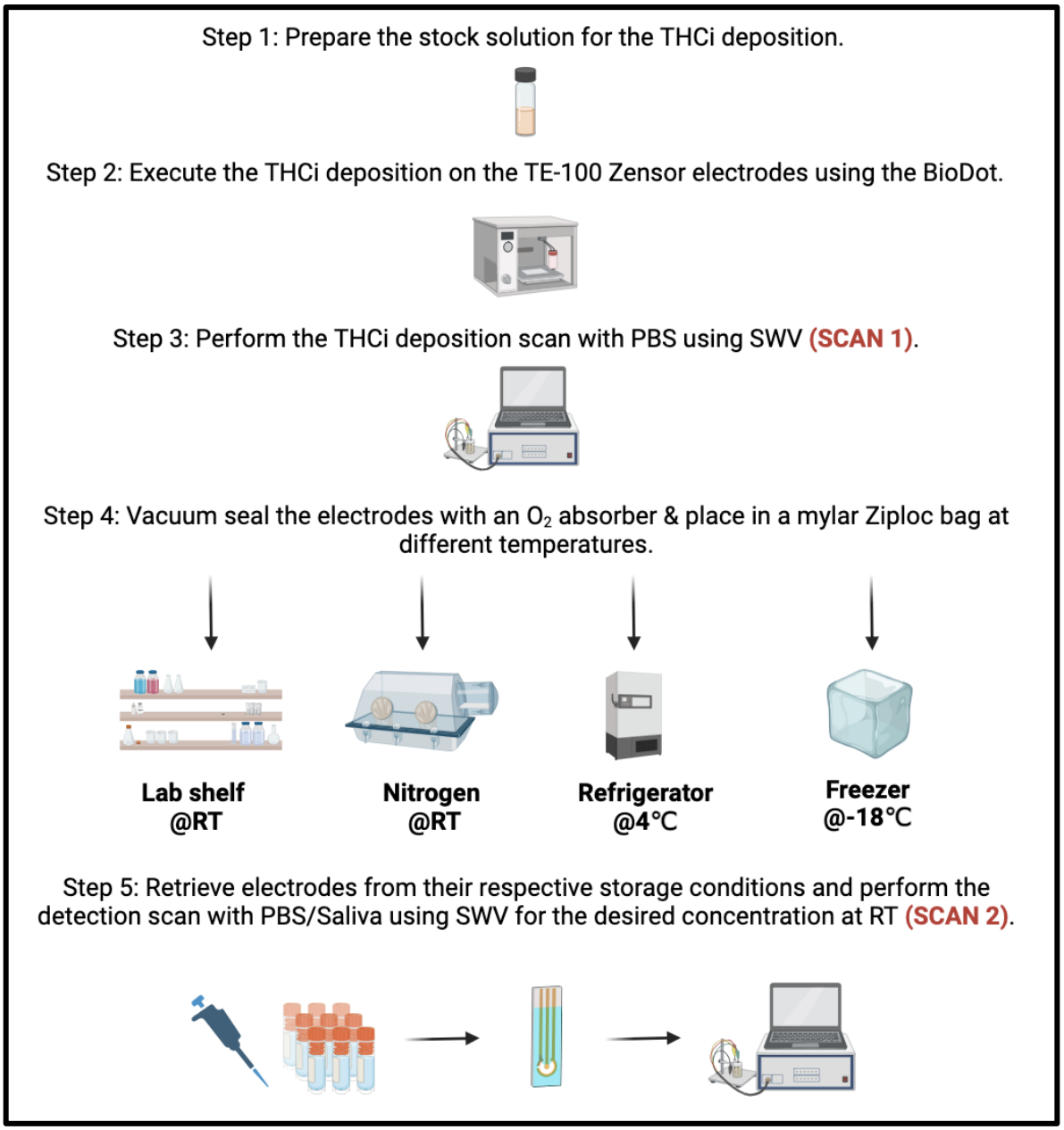

Figure 4- 2: A graphical representation of the procedural overview of the storage conditions during the manufacturing process, created using BioRender.com.

2.3 Detection

The electrodes were retrieved from their respective storage conditions after the specified time (Table 4- 1). and subjected to SWV for the final reproducibility scan (SCAN 2) post-storage. All of the electrodes were tested at RT using PBS using the following SWV conditions: a precondition potential of 0.05 V for 30 s, an equilibration time of 3 s, a voltametric potential scan from 0 to 0.8 V, a frequency of 15 Hz, an amplitude of 0.025 V and a step potential of 0.005 V.

2.4 Sensor performance after optimization of the storage conditions

The TE-100 Zensor electrodes were modified with 100 ng of THCi deposited onto the WE using the BioDot, vacuum sealed with oxygen absorbers and then stored in the freezer at -18°C for one week. The electrodes were then retrieved from their respective storage conditions after days 5, 6 and 7, and then tested (after reaching RT upon thawing) with THC samples in PBS (pH 7.4) with concentrations 0, 5, 10, 25, 50, 100, 300 and 1000 ng/mL. The electrodes were tested using the following SWV conditions: a precondition potential of 0.05 V for 30 s, an equilibration time of 3 s, a voltametric potential scan from 0 to 0.8 V, a frequency of 15 Hz, an amplitude of 0.025 V and a step potential of 0.005 V.

2.5 Characterization

X-ray photoelectron spectroscopy (XPS) was performed for the purposes of examining the best temperature condition for the storage of the THCi-modified electrodes. The THCi-modified electrodes were stored at RT, 4°C, and -18°C for a period of one week for XPS analysis. The XPS assessments were conducted utilizing a PHI Quantera II Scanning XPS Microprobe spectrometer. Survey scans encompassed an analysis area of 300 × 700 μm with a pass energy of 224 eV. High-resolution investigations were performed using a pass energy of 20 eV. To rectify the spectra, adjustments were made to align them with the main line of the carbon 1s spectrum (representing

organic carbon) set at 285 eV. CasaXPS software (version 2.3.14) was employed for spectrum analysis.

3 Results & Discussion

3.1 Electrode degradation

The THCi-modified electrodes vacuum sealed with O_2 absorbers and stored at RT for a period of one week (Figure 4- 3) is detrimental in showcasing the instability of the modified electrodes, as a result of the oxidation of THC. Additionally, as portrayed in (Figure 4-1), the decrease in the peak values of the THCi-modified electrodes from the manufacturing (SCAN 1) to the detection scan (SCAN 2), also performed at RT, further validates the instability of the electrodes.

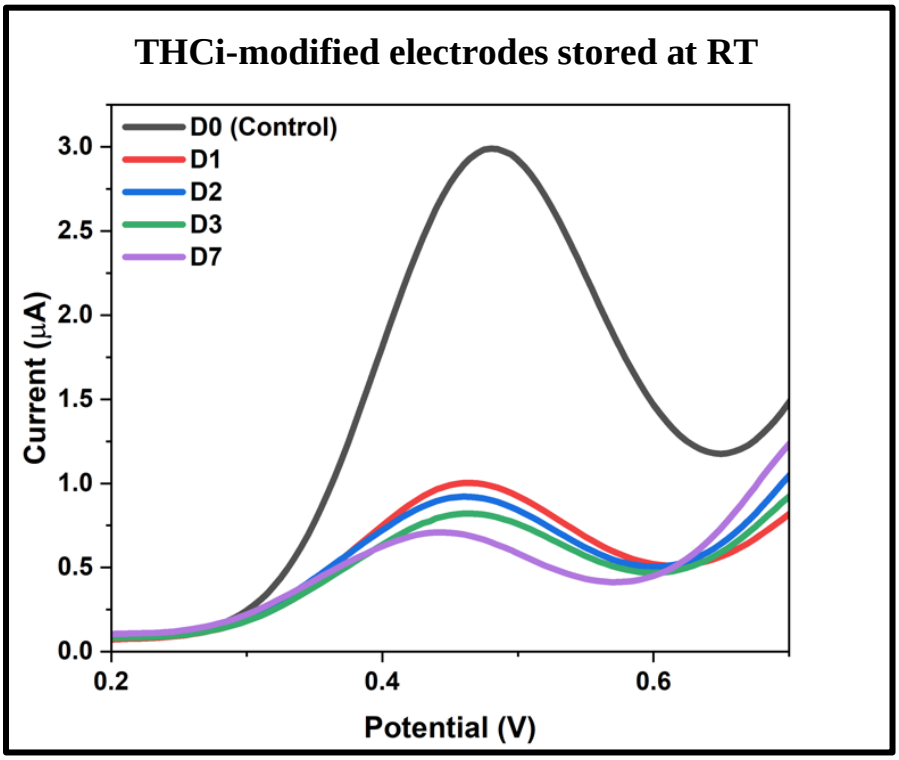

Figure 4- 3: THCi modified electrodes (130 ng) vacuum sealed with oxygen absorbers at RT for a period of one week, where D = day.

It has been well established in the literature that cannabis-based products tend to lose their potency during storage due to a loss in the amount of Δ^9-tetrahydrocannabinol (Δ^9-THC) [21]. The

Stability of different cannabinoids is directly dependent on their storage conditions [22]. Prior to extraction, both THC and CBD exist in their acidic forms i.e., as THCA and CBDA in the corporeal plant. The neutral cannabinoids, THC and CBD are known to be stable for a period of two weeks at room temperature when stored in darkness. However, exposure to light can result in the deterioration of these compounds. Opposingly, the acidic cannabinoids are capable of decarboxylating into their neutral forms in the daylight, as well as in the dark. The oxidation is known to be a process which is highly reliant on temperature [14, 23].

THC is a highly unstable compound which is easily oxidized to its nonenzymatic oxidation by-product cannabinol (CBN) under improper and prolonged storage conditions (Figure 4- 4). CBN consists of 1/4th the potency of THC, and hence, it is considered to be the less psychoactive compound. CBN is also the final product of the oxidation process, which seems to be dependent predominantly on heat and light [21]. Studies [11-13] validate the effect of heat and light on cannabinoid stability by presenting that the Δ^9-THC content was found to be higher in samples stored at 4°C and -18°C in the dark, as opposed to samples stored at room temperature with exposure to light.

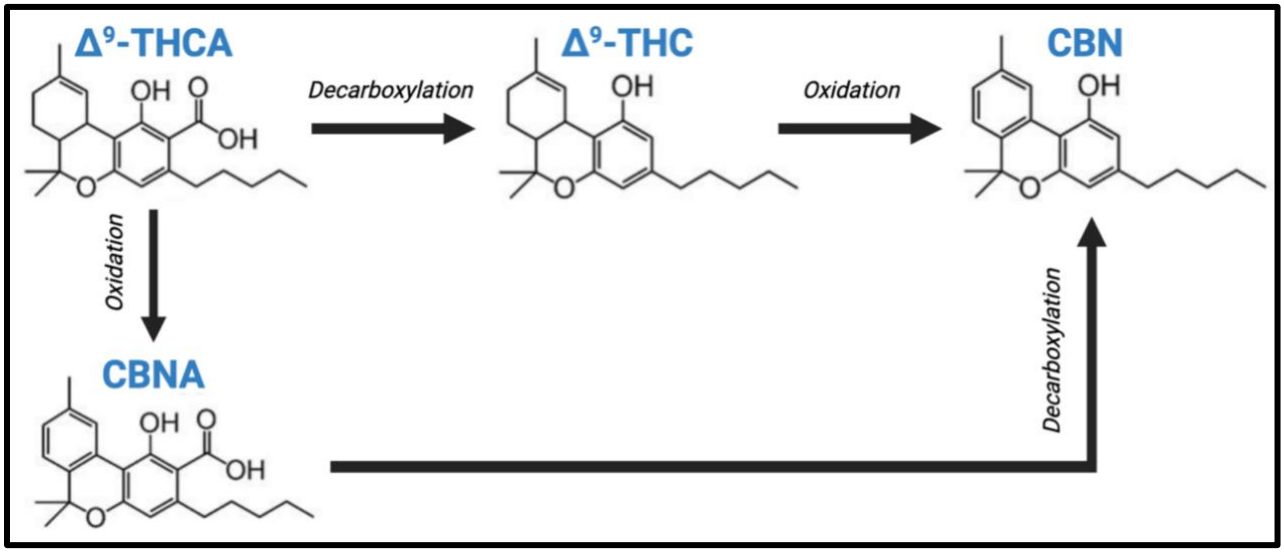

Figure 4- 4: The decarboxylation and oxidation of Δ^9-THC, created using BioRender.com.

Both cannabinoids, THC and CBD are highly electroactive species due to the presence of their respective hydroxyl groups [24]. Subsequently, the hydroxyl groups become deprotonated during oxidation and result in the formation of active phenoxy radicals [26]. This can lead to the prospective irreversible dimerization of both the cannabinoids at low potentials, resulting in the generation of an insulating layer on the surface of the WE after the first run [30].

Jaidee and colleagues [13] conducted a study to examine the kinetics of Δ^9-THC degradation in cannabis resin at different temperatures and pH conditions. Their study exhibits first-order and pseudo-first-order degradation kinetics for CBD and THC, respectively. Additionally, minimal transformation of THC was achieved with low temperature, and moderately acidic pH values in conjunction with shorter processing times. Another study [15] showed that THC samples stored at lower humidity levels (0% and 13% relative humidity) were deemed more stable with respect to degradation, as opposed to those stored at higher humidity levels. Additionally, it was found that air oxidation is another major factor contributing to the loss of Δ^9-THC during cannabis storage [14].

3.2 Electrode stability

3.2.1 Electrode storage

The THCi modified TE-100 Zensor electrodes vacuum sealed with O_2 absorbers and stored on the lab bench at RT, under N_2 gas in the glove box at RT, in the refrigerator at 4°C and, in the freezer at -18 °C for a span of one week are illustrated below in Figure 4- 5. The corresponding electrochemical signals obtained via SWV indicate that the set of electrodes stored at RT, irrespective of the storage condition, demonstrate instability as a result of the decrease in the peak intensity values of the electrodes over time. The electrochemical signals for electrodes stored at 4°C present a decrease in the intensity after day one, after which the electrodes maintained their

stability. Irrevocably, the electrodes stored at -18°C presented a consistent stability over the entire span of one week and hence, this condition was further used to examine the long-term stability of the electrodes.

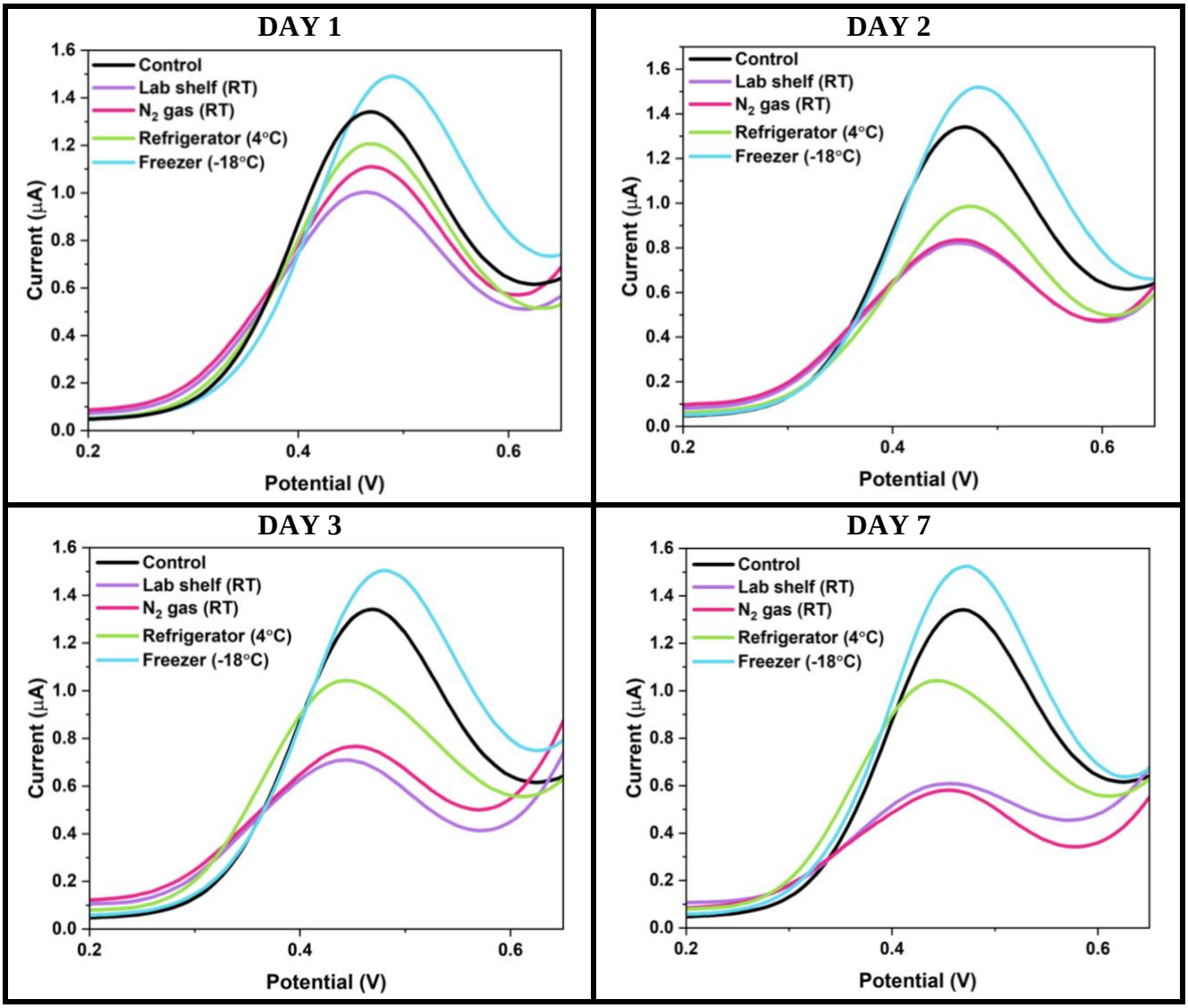

Figure 4- 5: THCi modified electrodes (130 ng) vacuum sealed with oxygen absorbers at different temperature conditions.

The THCi modified TE-100 Zensor electrodes vacuum sealed with O_2 absorbers and stored in the freezer at -18°C for a period of six months is depicted in Figure 4- 6. The electrodes were tested after 15-20 minutes (i.e., the time consumed to reach RT upon thawing) with PBS (pH 7.4)

using SWV. The electrodes are stable over the entire span of the 6-month storage period at -18°C, supported by the low variability presented over time in the corresponding column graph.

The practical significance of using these storage conditions for the long-term stability of the modified electrodes was further validated using statistical analyses (S2, section I). Specifically, a one-way analysis of variance (ANOVA) test was conducted to provide statistical evidence associated with the best storage conditions presented in conjunction with the Levene's test for determining the homogeneity of variance, and the Tukey-Kramer test to compare multiple group means for each of the time periods.

The corresponding coefficient of variation (CV) obtained for Figure 4- 6 (S2, Table S2-2) of 4.28% indicates a relatively low level of variability in dataset, when compared with the mean. The results from the Tukey test showcased that the group means for the pairs M2-D7, and M5-M4 comprised of insignificant differences, statistically. With these time periods crucial in serving as the beginning and the end of the shelf-life study, the practical significance of storing the THCi-modified electrodes at -18°C for a period of 6 months is validated. Additionally, the data also implies that although the error bars present higher variability amongst the electrodes during the first month of storage, this variability begins to decrease from the first month till the sixth.

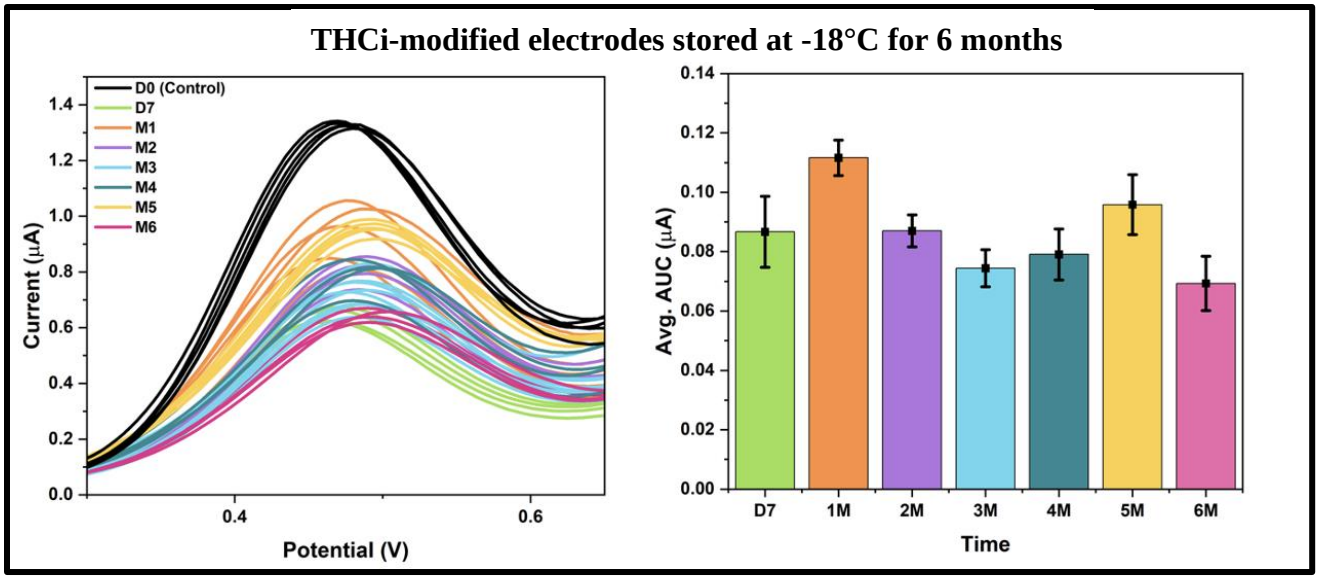

Figure 4- 6: THCi-modified electrodes (130 ng) at -18°C over the span of 6 months (tested at RT).

The results are in compliance with literature studies, which state that the oxidation of THC is arrested at temperatures as low as -18°C. Repka et al., [27] fabricated an HPC polymeric film comprised of THC to examine THC content and the extent of its degradation to CBN at fixed temperatures and time intervals. Their study concludes that the degradation of THC was insignificant for up to 15 months when stored at -18°C, with nearly 70% of the THC content still preserved. The study also reports that the percentage of CBN formation was maximum at 25°C, as opposed to lower temperatures such as 4°C and -18°C. Another study [28] articulates that the concentrations of THC-glucuronide in urine samples were stable for a period of one year at -20°C after which, the occurrence of adsorption, protein binding, or molecular degradation is probable. Additionally, the decarboxylation of THC has been proven to be occurring moderately when stored in the dark at -25°C [29].

3.2.1.1 XPS Characterization

The XPS characterization of the modified electrodes before and after being stored at different conditions (Room Temperature (RT), fridge at 4 ^{0}C **(**4CT), and freezer at -18 ^{0}C (-18CT)) was

carried out to understand the effect of each condition on the working electrode modification better. Carbon, oxygen, nitrogen, chlorine, silicon, and iron are the principal elements present in the working electrode of the screen-printed electrode employed in this study. After the electrode modification, an increase in the atomic percent of the Carbon and Oxygen elements is evidenced on the surface of the working electrode due to the incorporation of THC molecules (S2, Table S2-13).

The C 1s high-resolution signal for the pristine screen-printed electrode (P-Z) was deconvoluted into four peaks at 284.4, 285.0, 286.5, and 289.0 eV attributed to C=C (aromatic), C-C/C-CH, C-OH/C-O-C/C-Cl, and O-C=O, respectively [30] After the electrode modification, an increase in the atomic percent of the second and third contributions and a decrease in the second peak are verified, which corroborates the incorporation of THC on the surface of the working electrode (Figure 4- 7, S2, Table S2-14). In the case of O 1s high-resolution signal for P-Z electrodes, two contributions were employed for this signal fit, which were related to C=O (532.5 eV) and O-(C=O)-C/C-O (aromatic) (533.5 eV) [30].

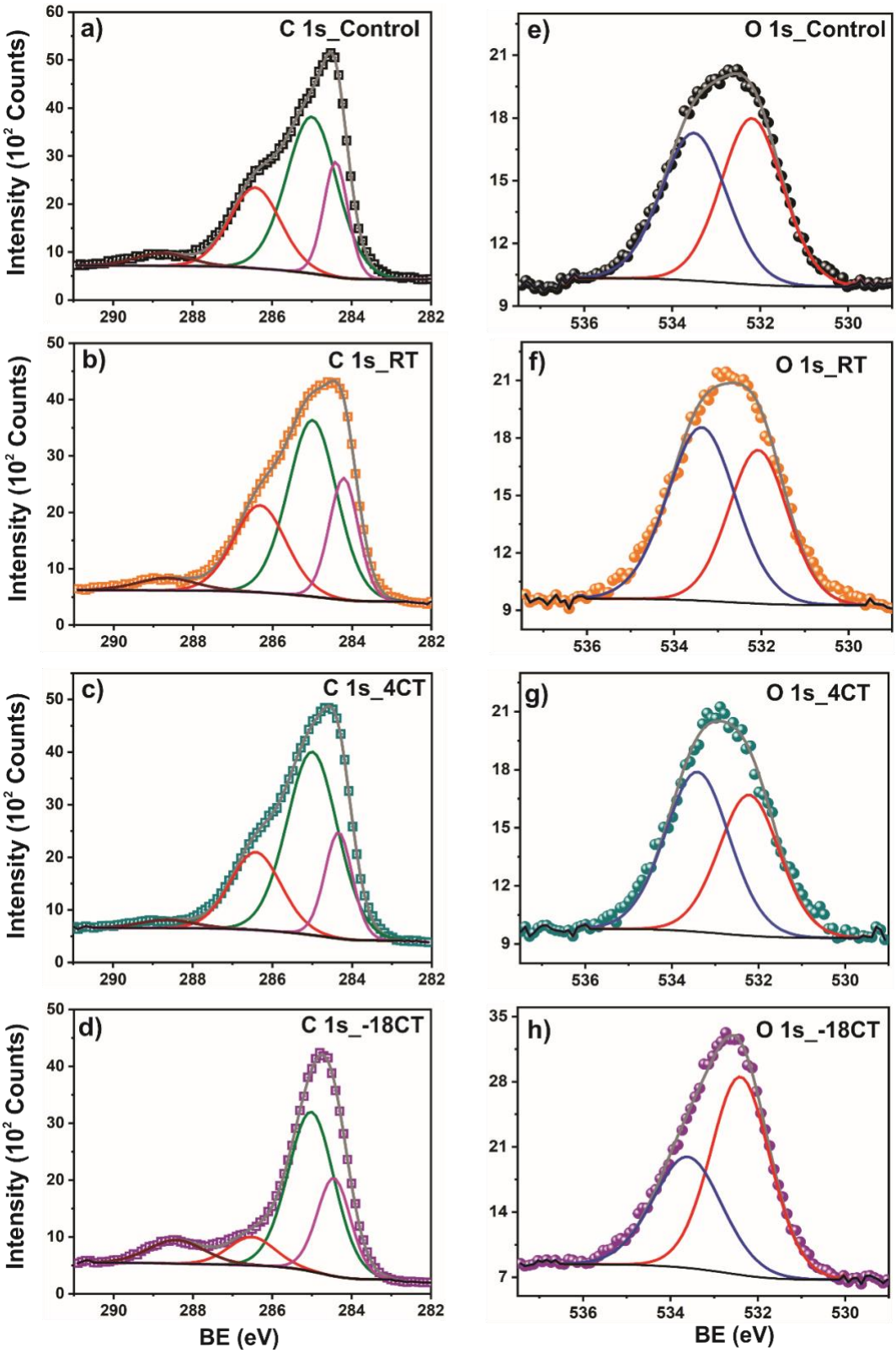

Figure 4- 7: C 1s and O1s high resolution for THCi-modified electrodes after working electrode modification, (a) and (e) Control, and after being stored at different conditions, (b) and (f) Room Temperature (RT), (c) and (g) fridge at 4 0C (4CT), and (d) and (h) freezer -18 0C (-18CT).

Once the THCi-modified electrodes are prepared, a decrease and an increase in the atomic percent in the first (68.3% to 51.5%) and second contributions (31.7% to 48.5), respectively, is observed (Figure 4- 7, S2, Table S2-15). These results are attributed to the incorporation of the THC molecules on the working electrode surface and the oxidation of the quinones groups of THC structure, which appear at 532.2 eV (C=O, first contribution).

After the preparation of THCi-modified electrodes, different conditions for the modified electrode storage were studied to find the best requirements that allow the extension of the modified electrodes' usability for long periods. Figure 4- 7 shows the results of C 1s and O 1s high-resolution signals before and after storing the modified electrodes for one week at Room Temperature (RT), fridge at 4 ^{0}C **(**4CT), and freezer at -18 ^{0}C (-18CT) (Figure 4- 7(b), (c), (e), and (f)). As evidenced in the figure, the signals for both regions (C 1s and O1s) are wider when the electrodes are kept at room temperature (Figure 4- 7(b), (f)) and 4 ^{0}C (fridge) (Figure 4- 7(c), (g)). However, when the electrodes are stored in the freezer (-18 ^{0}C), the signals are less noisy and narrow (Figure 4- 7(d), (h)).

The principal changes in the C 1s high-resolution signals are observed in the three first contributions for RT and 4CT storage conditions when they are compared to the control signal (electrode analyzed after its preparation) (Figure 4- 7(b), (c)). These three peaks are assigned to C=C (aromatic), C-C/C-CH, and C-OH/C-O-C/C-Cl; for these storage conditions, there is no proper control of the OH functional groups oxidation in the THC molecules and the following formation of quinone, adducts or more complex structures [8].

In the case of the -18 ^{0}C storage condition, the main changes are observed in the C=C (aromatic), C-OH/C-O-C/C-Cl, and O-C=O (Figure 4- 7(d)), where an increase in the atomic percent is evidenced for the last contribution related to the quinone formation, this result suggests

that under this temperature there is better control of the THC molecules oxidation and stability of the electrodes during the storage process. On the other hand, more evident changes are observed in the O 1s peaks after storing the electrodes at the three different conditions.

In the case of RT and 4CT storage conditions, the main changes in the atomic percent observed were a decrease in the first contribution (C=O, 532.5 eV) and an increase in the second contribution (O-(C=O)-C/C-O (aromatic), 533.5 eV) (Figure 4- 7(f) and (g)). This result suggests that other processes are occurring in the THC molecules simultaneously as the OH oxidation, such as adducts or more complex structures.

In the case of the -18CT condition, an increase in the first contribution (C=O, from 51.5% to 60.0%) and a decrease in the second contribution (O-(C=O)-C/C-O, from 48.5% to 39.4%) (Figure 4- 7(h)) can be observed when these results are compared to the control (Figure 4-7e). This is related to the possibility that during the application of a potential to create C=O due to the OH groups oxidation in the THC molecules, the formation of quinones is more suitable than other adducts or more complex molecules when the modified electrodes are stored at this temperature, which give the THCi-modified electrode the possibility to be storage for more extended periods of time under this condition. Overall, it was evidenced that Oxygen plays the primary role during the working electrode modification and that the best condition for the storage of the THCi-modified electrodes is -18 ^{0}C.

3.2.2 Additional modifiers

The THCi 130 ng modified electrodes were used in conjunction with a second modification of PBS (pH 4), 13 ng AA, 13 ng CA, and 5.2 ng BHT. The results demonstrate that the THCi modified TE-100 Zensor electrodes with a second modification of PBS (pH 4) vacuum sealed with O_2 absorbers and stored at -18°C were found to be stable for six months, when tested at RT with PBS

(pH 7.4) (Figure 4- 8) (See statistical analysis in S2, section II(b)). Comparing these results with those depicted in Figure 4- 6, the electrodes with a second modification of PBS (pH 4) resulted in an increase in the intensity of the electrochemical peak values of the electrodes due to the increase in conductivity caused by the acidic pH value.

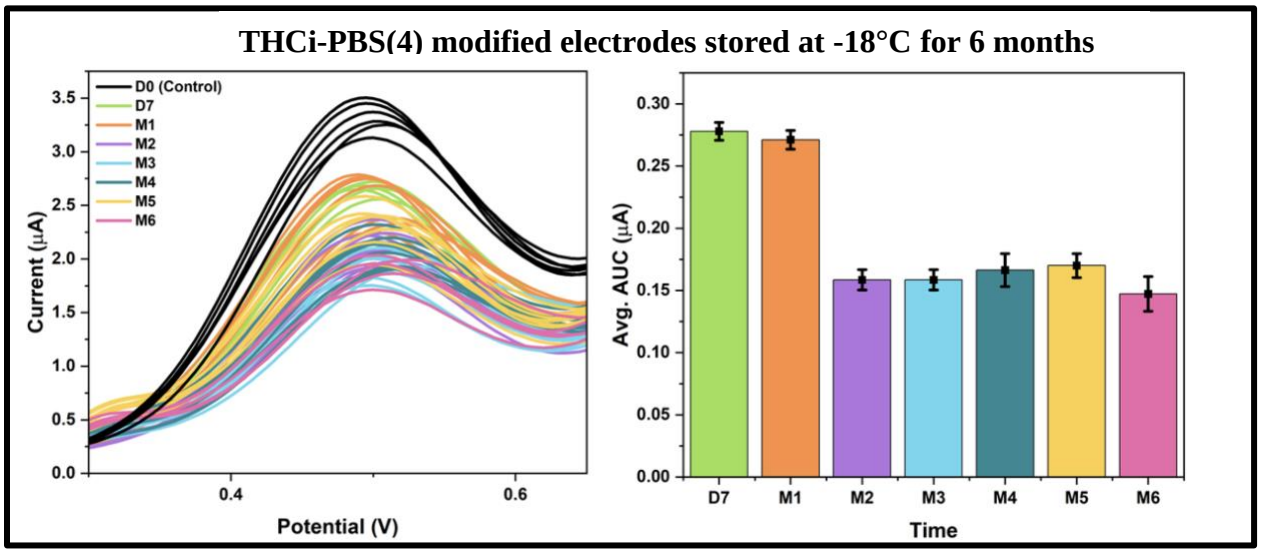

Figure 4- 8: THCi-modified electrodes (130 ng) with a second modification of PBS (pH 4) at -18°C over the span of 6 months (tested at RT).

When tested using the same conditions at 4°C, the THCi modified electrodes with a second modification of PBS (pH 4) were stable for a period of three months (Figure 4- 9). Upon the completion of three months in storage, the THC is perceived to be fully oxidized, as depicted by the flat electrochemical signal observed from 4 – 6 months. The associated Levene's test for absolute deviations concluded that with $0.05 > \alpha$ for both, Figure 4- 8 and Figure 4- 9, the variances in the AUC values of the electrodes were found to be statistically insignificant over time (S2, sections II(b) and (c)). Interpreting Tukey's test, multiple group means exhibited insignificant differences in the AUC values for the modified electrodes in Figure 4- 8 and Figure 4- 9 at the 0.05 significance level, crucial for quality control and the stability of the electrode.

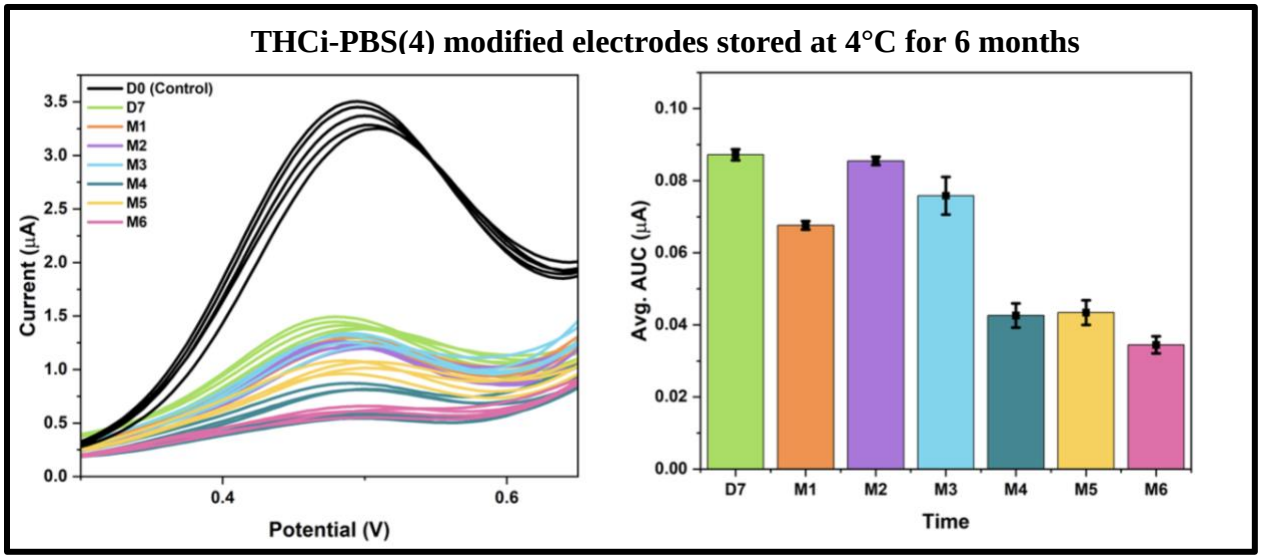

Figure 4- 9: THCi-modified electrodes (130 ng) with a second modification of PBS (pH 4) at 4°C over the span of 6 months (tested at RT).

As observed by Zanfrognini and colleagues [31], all cases of a modified electrode resulted in increasing the intensity of the peak current as a result of the local conductivity increment by coating the electrode with PBS salt. The surface acidic pH undermines the phenol oxidation of THC and results in improving electrode stabilization. The second modification of PBS was adjusted to pH 4 to facilitate restoring the ideal surface pH of the electrode to 7.4 for the purposes of THC detection.

As previously stated, Repka's study [27] reports the difference between THC degradation occurring at -18°C versus 4°C. The study demonstrates that although THC degradation was insignificant at -18°C with 70% THC content still preserved after 15 months, the degradation continued to occur at 4°C but at a significantly slower rate i.e., with 45% THC content preserved for the same time. Therefore, the electrodes stored at -18°C were able to resist oxidation for a period of 6 months (Figure 4- 8), as opposed to the electrodes stored at 4°C which demonstrated Stability for only 3 months (Figure 4- 9).

Other additional modifiers, including Ascorbic Acid (AA) and Citric Acid (CA) were tested as oxygen scavengers (S2, section III). AA-modified and CA-modified electrodes continued

to cause a shift in the potential of the peak over time and provided low reproducibility of the scans when stored at 4°C (S2, Figure S2-1). Conjointly, electrodes with a second modification of BHT and Transcutol only remained stable for a period of 48 hours at RT, after which a flat signal was observed for the modified electrode (S2, Figure S2-2).

3.2.3 Alternative modifiers

In this provision, derivates of THC or molecules with a similar chemistry and electrochemical performance were used to mimic the THCi function and to obtain better Stability. In doing so, electrodes were modified with tetrahydrocannabinolic acid (THCA), Δ^9-Tetrahydrocannabinol Acetate (THC-OAc), dopamine (DA), and cannabidiol (CBD) molecules by using the same electrodeposition protocol (S2, section IV).

Electrodes modified with THCA resulted in displaying an additional second peak during detection (SCAN 2), implying partial decomposition of the compound into THC (S2, Figure S2-3). Opposingly, the DA-modified electrodes displayed an extremely broad electrochemical signal and were unable to detect the oxidation of THC (S2, Figure S2-4). With the limit of detection being as low as 2 ng/mL for THC, the oxidation of phenolic compounds to quinones was expected to cause interferences in the electrochemical signal.

The electrochemical signals obtained for electrodes modified with 100 ng and 130 ng of CBD were similar to that of THC i.e., illustrated by an electrochemical oxidation peak observed at 0.48 V (S2, Figure S2-5). Both THC and CBD are known to undergo the course of oxidation at the same potential values due to their analogous redox active moieties [31]. Nevertheless, for both species, the products of the electrochemical reaction present fouling on the surface of the electrode, which causes a drastic decay in the subsequent scans.

Lastly, an acetate-protected THC (THC-OAc), a synthetic cannabinoid with a higher stability than THC to oxidation, was also tested as an alternative modifier. This cannabinoid resisted unaltered electrochemical oxidation under the established SWV condition, serving as a perfect candidate to improve electrode stability (S2, Figure S2-6). However, aggressive chemical conditions are necessary to hydrolyze the acetate group to obtain the oxidation signal that mimics the THCi function during the THC detection. Therefore, THC-OAc resulted in being impractical for our sensor approach.

3.2.4 Experimental summary

An overview of the stability experiments conducted using different temperature conditions is presented below in Table 4- 1. The temperature conditions which ministered the best stability for the electrodes include storage at 4°C and -18°C. Although storing the electrodes at 4°C was able to render short-term stability using a majority of the modifiers tested, storing the electrodes at -18°C provided superlative long-term stability for the THCi-modified electrodes. Conjointly, the THCi-modified electrodes with a second modification of PBS (pH 4) stored at -18°C were also successful in extending the long-term stability of the electrode to a period of 6 months.

Table 4- 1: A summary of all the stability experiments conducted using different temperature conditions.

	Vacuum (RT)					Nitrogen (RT)					Refrigerator (4℃)							Freezer (-18℃)						
	D1	D2	D3	D7	1M	D1	D2	D3	D7	1M	D1	D2	D3	D7	1M	3M	6M	D1	D2	D3	D7	1M	3M	6M
THC	✓	↓	↓	↓	-	✓	↓	↓	↓	-	✓	✓	✓	↓	↓	↓	↓	✓	✓	✓	✓	✓	✓	✓
THCA	✓	✓	✓	✓	-	-	-	-	-	-	✓	✓	✓	✓	-	-	-	-	-	-	-	-	-	-
CBD	✓	↓	↓	↓	-	✓	↓	↓	↓	-	✓	✓	✓	↓	↓	-	-	-	-	-	-	-	-	-
pH4	✓	↓	↓	↓	-	-	-	-	-	-	✓	✓	✓	✓	✓	✓	↓	✓	✓	✓	✓	✓	✓	✓
AA	-	-	-	-	-	-	-	-	-	-	✓	✓	✓	↓	-	-	-	-	-	-	-	-	-	-
CA	-	-	-	-	-	-	-	-	-	-	✓	✓	✓	↓	-	-	-	-	-	-	-	-	-	-
BHT	✓	✓	↓	↓	↓	-	-	-	-	-	-	-	-	-	-	-	-	-	-	-	-	-	-	-

✓ = Signal remained consistent.
↓ = Signal changed in comparison to the previous day.

3.3 Sensor performance using the best storage conditions for the modified electrodes

The calibration curves associated with THCi 100 ng modified electrodes vacuum sealed with oxygen absorbers and stored in the freezer at -18°C for one week, tested using 0, 5, 10, 25, 50, 100, 300, and 1000 ng/mL of THC in PBS (pH 7.4) are illustrated in Figure 4- 10. The electrodes were tested using different concentrations of THC on days 5, 6 and 7 to examine the stability of modified electrodes during detection.

With the limit of detection (LOD) and sensitivity proven to be dependent on the temperature of the substrate [32], storing the THCi modified electrodes at -18°C was able to influence these parameters positively. The corresponding results demonstrate better linearity, an improved LOD, and maintaining sensitivity over time. This suggests that the signal stability of the modified electrodes enhanced with increasing time, implying that the electrodes required a span of 7 days after storage before attaining stability.

A biosensor must be stored at its reference conditions to examine the time period at which saturation occurs (exponential progression). The time period cannot be defined until saturation transpires, with the process being directly dependent on the application of the biosensor [33, 34]. The long-term shelf life of a thermally accelerated aging biosensor is known to be established typically after 4 days [9]. In this case, the 7-day time period allowed for the electrodes to acclimatize to the temperature and the physical storage environment before suspending the natural phenomena of aging.

With biosensor aging defined as a decrease in the electrochemical signal over time, the 7-day time period was adequate in stabilizing the electrochemical signals of the sensor prior to detection. Electrodes often require a period of stabilization for the purposes of conditioning,

removal of contaminants, equilibration, minimizing drift, and optimizing performance associated with consistency and reproducibility [35].

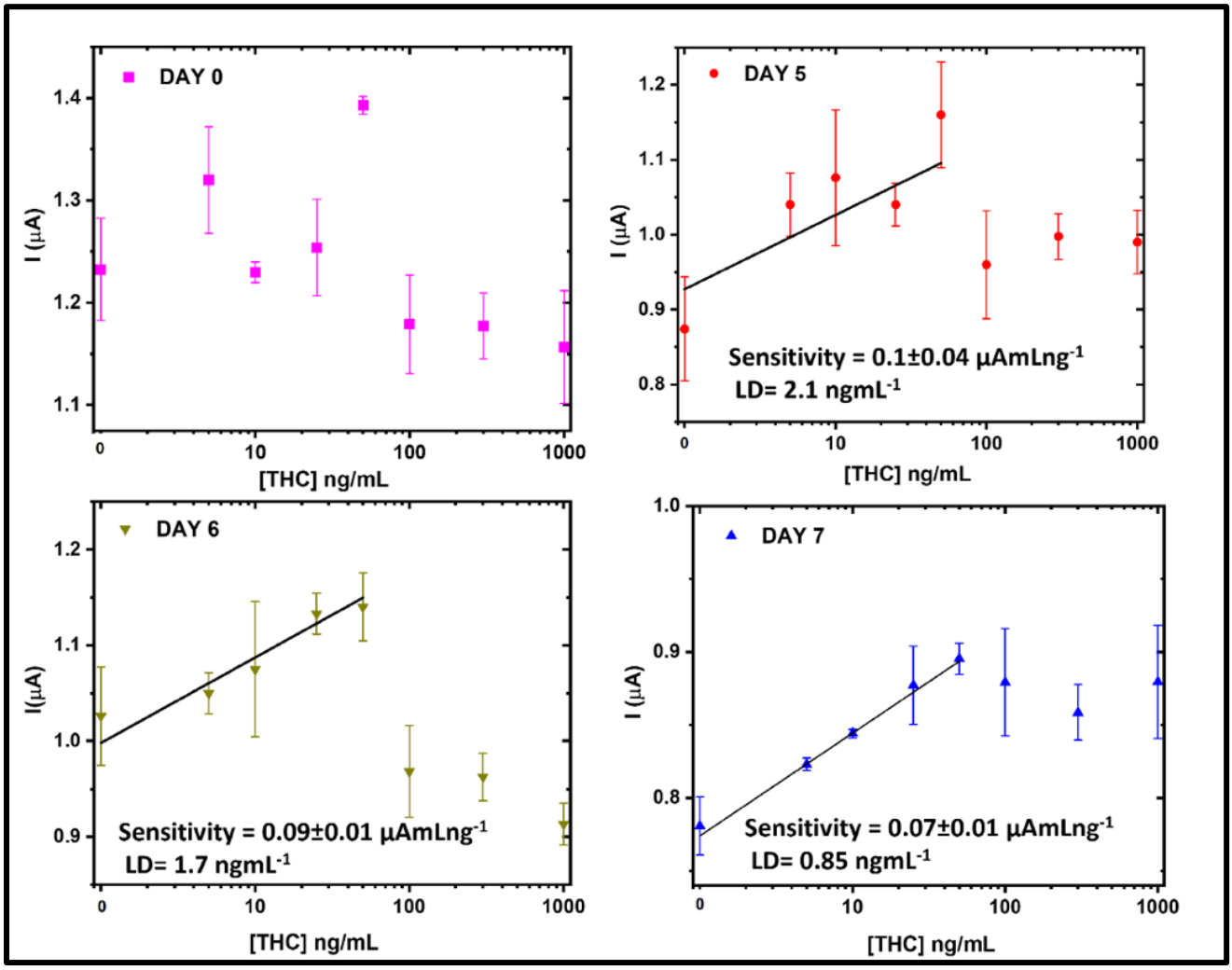

Figure 4- 10: Calibration curves obtained for THCi-modified electrodes (100 ng) stored at -18°C for a span of one week.

4 Conclusions

The results obtained during this study substantiate that the frozen storage of the THCi-modified electrodes provided optimal THC stability. Although the results illustrate that the degradation of THC impedes at 4°C, the oxidation of THC was found to be arrested at -18°C. While the storage of the THCi-modified electrodes vacuum sealed with oxygen absorbers in the absence of light at 4°C demonstrated stability for about 3 months, the same electrodes stored at -18°C exhibited an

extended stability for about 6 months. Hence, temperatures as low as -18°C, and even lower possess the ability to arrest THC degradation and are ideal for the long-term stability of the sensor.

Additional conditions implemented including the use of different oxygen scavenger additives, THC derivatives, and pH control deemed unsuccessful in improving the stability of the electrode. Finally, modified electrodes stored under optimal conditions were interrogated with different THC samples, delivering improved calibration curves after an aging period of one week. Although further studies must be conducted to apply this lab-scale discovery to real-life roadside testing applications, the optimal storage conditions identified in this study can help regulation authorities detect the toxicity of THC rapidly, accurately, and effortlessly via the use of stable biosensors.

5 References

[1] Cristino, L., Bisogno, T., & Di Marzo, V. (2019). Cannabinoids and the expanded endocannabinoid system in neurological disorders. *Nature Reviews Neurology*, *16*(1), 9–29. https://doi.org/10.1038/s41582-019-0284-z

[2] Lenné, M. G., Dietze, P. M., Triggs, T. J., Walmsley, S., Murphy, B., & Redman, J. R. (2010). The effects of cannabis and alcohol on simulated arterial driving: Influences of driving experience and task demand. *Accident Analysis and Prevention*, *42*(3), 859–866. https://doi.org/10.1016/j.aap.2009.04.021

[3] Hartman, R. L., & Huestis, M. A. (2013). Cannabis effects on driving skills. *Clinical Chemistry*, *59*(3), 478–492. https://doi.org/10.1373/clinchem.2012.194381

[4] Hartman, R. L., Brown, T. L., Milavetz, G., Spurgin, A., Pierce, R. S., Gorelick, D. A., Gaffney, G., & Huestis, M. A. (2015). Cannabis effects on driving lateral control with and without alcohol. *Drug and Alcohol Dependence*, *154*, 25–37. https://doi.org/10.1016/j.drugalcdep.2015.06.015

[5] Pearlson, G. D., Stevens, M. C., & D'Souza, D. C. (2021). Cannabis and driving. *Frontiers in Psychiatry*, *12*. https://doi.org/10.3389/fpsyt.2021.689444

[6] Gunasekaran, S. (2022). *Nanozymes: Advances and applications* (1st ed.). CRC Press.

[7] Chand, R., Mittal, N., Srinivasan, S., & Rajabzadeh, A. R. (2021). Upconverting nanoparticle clustering based rapid quantitative detection of tetrahydrocannabinol (THC) on lateral-flow immunoassay. *The Analyst*, *146*(2), 574–580. https://doi.org/10.1039/d0an01850c

[8] Ortega, G. A., Ahmed, S. R., Tuteja, S. K., Srinivasan, S., & Rajabzadeh, A. R. (2022). A biomolecule-free electrochemical sensing approach based on a novel electrode modification technique: Detection of ultra-low concentration of Δ9-tetrahydrocannabinol in saliva by turning a

sample analyte into a sensor analyte. *Talanta*, *236*, 122863. https://doi.org/10.1016/j.talanta.2021.122863

[9] Panjan, P., Virtanen, V., & Sesay, A. M. (2017). Determination of stability characteristics for electrochemical biosensors via thermally accelerated ageing. *Talanta*, *170*, 331–336. https://doi.org/10.1016/j.talanta.2017.04.011

[10] Harvey, D. J. (1990). Stability of cannabinoids in dried samples of cannabis dating from around 1896–1905. *Journal of Ethnopharmacology*, *28*(1), 117–128. https://doi.org/10.1016/0378-8741(90)90068-5

[11] Sannikova, N. (2020). *The effects of storage conditions on cannabinoid stability*. The Effects of Storage Conditions on Cannabinoid Stability. https://ascensionsciences.com/newsroom/technical-articles/effects-of-storage-conditions-on-cannabinoid conditions/#:~:text=The%20CBN%20content%20increases%20during,darkness%20and%20at%20lower%20temperatures.

[12] Trofin, I. G., Dabija, G., Vaireanu, D.-I., & Laurentiu, F. (2012). The Influence of Long-term Storage Conditions on the Stability of Cannabinoids derived from Cannabis Resin. *Revista de Chimie*, *63*(4), 422–427.

[13] Jaidee, W., Siridechakorn, I., Nessopa, S., Wisuitiprot, V., Chaiwangrach, N., Ingkaninan, K., & Waranuch, N. (2022). Kinetics of CBD, Δ9-thc degradation and cannabinol formation in cannabis resin at various temperature and ph conditions. *Cannabis and Cannabinoid Research*, *7*(4), 537–547. https://doi.org/10.1089/can.2021.0004

[14] Fairbairn, J. W., Liebmann, J. A., & Rowan, M. G. (1976). The stability of cannabis and its preparations on storage. *Journal of Pharmacy and Pharmacology*, *28*(1), 1–7.

https://doi.org/10.1111/j.2042-7158.1976.tb04014.x

[15] Thumma, S., Majumdar, S., ElSohly, M. A., Gul, W., & Repka, M. A. (2008). Preformulation studies of a prodrug of Δ9-tetrahydrocannabinol. *AAPS PharmSciTech*, *9*(3), 982–990. https://doi.org/10.1208/s12249-008-9136-7

[16] Smith, R. N., & Vaughan, C. G. (1977). The decomposition of acidic and neutral cannabinoids in organic solvents. *Journal of Pharmacy and Pharmacology*, *29*(1), 286–290. https://doi.org/10.1111/j.2042-7158.1977.tb11313.x

[17] Ross, S. A., & Elsohly, M. A. (1997). CBN and D9-THC concentration ratio as an indicator of the age of stored marijuana samples. *Bulletin on Narcotics* , *50*(1–2), 139–147. https://www.unodc.org/unodc/en/data-and-analysis/bulletin/bulletin_1997-01-01_1_page008.html

[18] Mechoulam, R. (1970). Marihuana chemistry. *Science*, *168*(3936), 1159–1166. https://doi.org/10.1126/science.168.3936.1159

[19] Turk, R. F., Manno, J. E., Jain, N. C., & Forney, R. B. (1971). The identification, isolation, and preservation of Δ9-tetrahydrocannabinol (Δ9-THC). *Journal of Pharmacy and Pharmacology*, *23*(3), 190–195. https://doi.org/10.1111/j.2042-7158.1971.tb08640.x

[20] Garrett, E. R., & Tsau, J. (1974). Stability of Tetrahydrocannabinols I. *Journal of Pharmaceutical Sciences*, *63*(10), 1563–1574. https://doi.org/10.1002/jps.2600631016

[21] Carbone, M., Castelluccio, F., Daniele, A., Sutton, A., Ligresti, A., Di Marzo, V., & Gavagnin, M. (2010). Chemical characterisation of oxidative degradation products of Δ9-THC. *Tetrahedron*, *66*(49), 9497–9501. https://doi.org/10.1016/j.tet.2010.10.025

[22] Lindholst, C. (2010). Long term stability of cannabis resin and cannabis extracts. *Australian Journal of Forensic Sciences*, *42*(3), 181–190.

https://doi.org/10.1080/00450610903258144

[23] Smith, R. N., & Vaughan, C. G. (1977a). The decomposition of acidic and neutral cannabinoids in organic solvents. *Journal of Pharmacy and Pharmacology*, *29*(1), 286–290. https://doi.org/10.1111/j.2042-7158.1977.tb11313.x

[24] Zanfrognini, B., Pigani, L., & Zanardi, C. (2020). Recent advances in the direct electrochemical detection of drugs of abuse. *Journal of Solid State Electrochemistry*, *24*(11–12), 2603–2616. https://doi.org/10.1007/s10008-020-04686-z

[25] Klimuntowski, M., Alam, M. M., Singh, G., & Howlader, M. M. (2020). Electrochemical sensing of cannabinoids in Biofluids: A noninvasive tool for drug detection. *ACS Sensors*, *5*(3), 620–636. https://doi.org/10.1021/acssensors.9b02390

[26] Tanasescu, R., & Constantinescu, C. S. (2013). Pharmacokinetic evaluation of Nabiximols for the treatment of multiple sclerosis pain. *Expert Opinion on Drug Metabolism and Toxicology*, *9*(9), 1219–1228. https://doi.org/10.1517/17425255.2013.795542

[27] Repka, M. A., Munjal, M., ElSohly, M. A., & Ross, S. A. (2006). Temperature stability and bioadhesive properties of Δ9-tetrahydrocannabinol incorporated hydroxypropylcellulose polymer matrix systems. *Drug Development and Industrial Pharmacy*, *32*(1), 21–32. https://doi.org/10.1080/03639040500387914

[28] Desrosiers, N. A., Lee, D., Scheidweiler, K. B., Concheiro-Guisan, M., Gorelick, D. A., & Huestis, M. A. (2013). In vitro stability of free and glucuronidated cannabinoids in urine following controlled smoked cannabis. *Analytical and Bioanalytical Chemistry*, *406*(3), 785–792. https://doi.org/10.1007/s00216-013-7524-7

[29] Taschwer, M., & Schmid, M. G. (2015). Determination of the relative percentage distribution of THCA and Δ9-THC in herbal cannabis seized in Austria – impact of different storage temperatures on stability. *Forensic Science International*, *254*, 167–171. https://doi.org/10.1016/j.forsciint.2015.07.019

[30] Viltres, H., Odio, O. F., Biesinger, Mark. C., Montiel, G., Borja, R., & Reguera, E. (2020). Preparation of amine- and disulfide-containing pamam-based dendrons for the functionalization of hydroxylated surfaces: XPS as structural sensor. *ChemistrySelect*, *5*(16), 4875–4884. https://doi.org/10.1002/slct.202000432

[31] Zanfrognini, B., Monari, A., Foca, G., Ulrici, A., Pigani, L., & Zanardi, C. (2022). Preliminary evaluation of the use of a disposable electrochemical sensor for selective identification of Δ9-tetrahydrocannabinol and cannabidiol by multivariate analysis. *Microchemical Journal*, *183*, 108108. https://doi.org/10.1016/j.microc.2022.108108

[32] Zhang, D., Chen, A., Chen, Y., Wang, Q., Li, S., Jiang, Y., & Jin, M. (2021). Influence of substrate temperature on the detection sensitivity of surface-enhanced libs for analysis of heavy metal elements in water. *Journal of Analytical Atomic Spectrometry*, *36*(6), 1280–1286. https://doi.org/10.1039/d1ja00003a

[33] Bhalla, N., Jolly, P., Formisano, N., & Estrela, P. (2016). Introduction to biosensors. *Essays in Biochemistry*, *60*(1), 1–8. https://doi.org/10.1042/ebc20150001

[34] Rocchitta, G., Spanu, A., Babudieri, S., Latte, G., Madeddu, G., Galleri, G., Nuvoli, S., Bagella, P., Demartis, M., Fiore, V., Manetti, R., & Serra, P. (2016). Enzyme biosensors for biomedical applications: Strategies for safeguarding analytical performances in biological fluids. *Sensors*, *16*(6), 780. https://doi.org/10.3390/s16060780

[35] Maganzini, N., Thompson, I., Wilson, B., & Soh, H. T. (2022). Pre-equilibrium

biosensors as an approach towards rapid and continuous molecular measurements. *Nature Communications*, *13*(1). https://doi.org/10.1038/s41467-022-34778-5

Chapter 5 : Conclusions

5.1 Thesis Summary

This thesis presents a comprehensive review on the significance of employing electrochemical (EC) biosensing devices, characterized by their rapid response time, user-friendly operation, and precision in clinical diagnosis. Furthermore, the thesis investigates several challenges pertaining to EC biosensors, notable their susceptibility to chemical instability, lack of reproducibility, and the inability to detect low analyte concentrations. As a result, this research delves into identifying solutions to these problems in-depth, ultimately enhancing the performance and the associated functionality of the biosensor.

5.2 Key Findings

5.2.1 The Label-Free Electrochemical Detection of Glycated Hemoglobin (HbA1c) and C-Reactive Protein (CRP) as a Potential Maturation of Coronary Heart Disease (CHD) due to Diabetes

The development of a label-free electrochemical sensor for the detection of HbA1c and CRP in Chapter 3 involved a series of optimization experiments. These experiments were specifically focused on the exploration of various redox probes, the evaluation of different electrochemical techniques and their associated parameters, as well as the manipulation of factors such as pH, concentrations, and incubation times. Particularly, the heightened sensitivity of this device arises from using tailored redox probes with a strong affinity for both biomarkers used. Specific key findings include:

→ The utilization of PcA-NO_2 as a redox probe which presented a notable affinity for CRP, which has not been reported in literature before.

→ The employment of PCA-NO_2 as a redox probe enabled the detection of ultra-low concentrations of CRP (hs-CRP).

→ The calibration curve for HbA1c yielded a LOD of 5 mg/mL in PBS (pH 8) FeCN (II) and 6 mg/mL in simulated blood (SB) for a linear range of 0 – 30 mg/mL.

→ The calibration curve for CRP demonstrated a LOD of 0.007 mg/mL in PBS (pH 7.4) PcA-NO_2 and 0.008 mg/mL for measurement in SB for a linear range of 0 – 0.05 mg/mL.

→ The recovered values for HbA1c and CRP were between the range 96 – 103%, and 90 – 95%, respectively, validating the specificity and the practical applicability of this approach.

5.2.2 Determining Optimal Storage Conditions to Enhance the Stability of Δ9-tetrahydrocannabinol (THC)-Modified Screen-Printed Carbon Electrodes (SPCEs)

To address the challenges of chemical instability and the resulting impact on reproducibility in the previously reported sensor [45], Chapter 4 focused on identifying ideal storage conditions for the THC-modified, biomolecule-free electrodes. This was achieved through a series of optimization studies targeting the control of temperature, humidity, airflow, and light conditions.

→ The frozen storage of THCi-modified electrodes ensured the optimal long-term stability of THC for a period of six months.

→ While the results demonstrated that the degradation of THC slowed at 4°C, it was observed that THC oxidation arrested at -18°C.

→ The calibration curves associated with the detection of different concentrations of THC depicted that the electrodes needed a 7-day storage period to achieve optimal stability.

5.3 Field Contributions

5.3.1 The Label-Free Electrochemical Detection of Glycated Hemoglobin (HbA1c) and C-Reactive Protein (CRP) as a Potential Maturation of Coronary Heart Disease (CHD) due to Diabetes

→ Highlighting the robust correlation between diabetes and CHD, with only a limited number of studies reported regarding both, the association and the electrochemical detection of both.

→ The development of a label-free electrochemical biosensor for the detection of CRP using a novel redox probe.

→ All three calibration curves enable diagnosis within the clinical range, thereby facilitating the early-stage detection of CHD.

→ Designing a platform for the label-free "dual detection" of HbA1c and CRP in the future.

5.3.2 Determining Optimal Storage Conditions to Enhance the Stability of Δ9-tetrahydrocannabinol (THC)-Modified Screen-Printed Carbon Electrodes (SPCEs)

→ Identifying ambient environmental storage conditions for the long-term stability of the THC-modified electrodes.

→ Extending the shelf-life of the manufactured electrodes by engendering stable electrochemical signals.

→ Assisting regulatory authorities in detecting the toxicity of THC through the utilization of stable biosensors.

Bibliography

[1] Lowe, C. R. (1984). Biosensors. *Trends in Biotechnology*, *2*(3), 59–65. https://doi.org/10.1016/0167-7799(84)90011-8

[2] Kumar, A. M., & Kachhawa, K. (2023). Biomedical applications of bioelectrochemical sensors. *Multifaceted Bio-Sensing Technology*, *4*, 239–260. https://doi.org/10.1016/b978-0-323-90807-8.00014-2

[3] Grieshaber, D., MacKenzie, R., Vörös, J., & Reimhult, E. (2008). Electrochemical biosensors - sensor principles and Architectures. *Sensors*, *8*(3), 1400–1458. https://doi.org/10.3390/s80314000

[4] Eggins, B. R. (2002). Analytical Techniques in the Sciences. *Chemical Sensors and Biosensors*. https://doi.org/10.1002/9780470511305

[5] Chaubey, A., & Malhotra, B. D. (2002). Mediated biosensors. *Biosensors and Bioelectronics*, *17*(6–7), 441–456. https://doi.org/10.1016/s0956-5663(01)00313-x

[6] Tvorynska, S., Barek, J., & Josypčuk, B. (2021). Flow amperometric uric acid biosensors based on different enzymatic mini-reactors: A comparative study of uricase immobilization. *Sensors and Actuators B: Chemical*, *344*, 130252. https://doi.org/10.1016/j.snb.2021.130252

[7] Mahato, K., & Wang, J. (2021). Electrochemical sensors: From the bench to the skin. *Sensors and Actuators B: Chemical*, *344*, 130178. https://doi.org/10.1016/j.snb.2021.130178

[8] Renedo, O. D., Alonso-Lomillo, M. A., & Martínez, M. J. A. (2007). Recent developments in the field of screen-printed electrodes and their related applications. *Talanta*, *73*(2), 202–219. https://doi.org/10.1016/j.talanta.2007.03.050

[9] Silva, R. M., da Silva, A. D., Camargo, J. R., de Castro, B. S., Meireles, L. M., Silva, P. S., Janegitz, B. C., & Silva, T. A. (2023). Carbon nanomaterials-based screen-printed electrodes for

sensing applications. *Biosensors*, *13*(4), 453. https://doi.org/10.3390/bios13040453

[10] Shi, J.-X., Lei, X.-W., & Natsuki, T. (2021). Review on carbon nanomaterials-based nano-mass and nano-force sensors by theoretical analysis of vibration behavior. *Sensors*, *21*(5), 1907. https://doi.org/10.3390/s21051907

[11] Luppa, P. B., Sokoll, L. J., & Chan, D. W. (2001). Immunosensors—principles and applications to clinical chemistry. *Clinica Chimica Acta*, *314*(1–2), 1–26. https://doi.org/10.1016/s0009-8981(01)00629-5

[12] Wang, J. (2006). Electrochemical biosensors: Towards Point-of-Care Cancer Diagnostics. *Biosensors and Bioelectronics*, *21*(10), 1887–1892. https://doi.org/10.1016/j.bios.2005.10.027

[13] Bakker, E., & Pretsch, E. (2005). Potentiometric sensors for Trace-level analysis. *TrAC Trends in Analytical Chemistry*, *24*(3), 199–207. https://doi.org/10.1016/j.trac.2005.01.003

[14] Koncki, R. (2007). Recent developments in potentiometric biosensors for biomedical analysis. *Analytica Chimica Acta*, *599*(1), 7–15. https://doi.org/10.1016/j.aca.2007.08.003

[15] Caras, Steve., & Janata, Jiri. (1980). Field effect transistor sensitive to penicillin. *Analytical Chemistry*, *52*(12), 1935–1937. https://doi.org/10.1021/ac50062a035

[16] D'Orazio, P. (2003). Biosensors in clinical chemistry. *Clinica Chimica Acta*, *334*(1–2), 41–69. https://doi.org/10.1016/s0009-8981(03)00241-9

[17] Thévenot, D. R., Toth, K., Durst, R. A., & Wilson, G. S. (2001). Electrochemical biosensors: Recommended definitions and classification1international union of Pure and Applied Chemistry: Physical Chemistry Division, Commission I.7 (Biophysical Chemistry); Analytical Chemistry Division, commission v.5 (Electroanalytical Chemistry).1. *Biosensors and Bioelectronics*, *16*(1–2), 121–131. https://doi.org/10.1016/s0956-5663(01)00115-4

[18] Cullen, D. C., Sethi, R. S., & Lowe, C. R. (1990). Multi-analyte miniature conductance

biosensor. *Analytica Chimica Acta*, *231*, 33–40. https://doi.org/10.1016/s0003-2670(00)86394-1

[19] Patolsky, F., Zheng, G., & Lieber, C. M. (2006). Nanowire-based biosensors. *Analytical Chemistry*, *78*(13), 4260–4269. https://doi.org/10.1021/ac069419j

[20] Yagiuda, K., Hemmi, A., Ito, S., Asano, Y., Fushinuki, Y., Chen, C.-Y., & Karube, I. (1996). Development of a conductivity-based immunosensor for sensitive detection of methamphetamine (stimulant drug) in human urine. *Biosensors and Bioelectronics*, *11*(8), 703–707. https://doi.org/10.1016/0956-5663(96)85920-3

[21] Chouteau, C., Dzyadevych, S., Chovelon, J.-M., & Durrieu, C. (2004). Development of novel conductometric biosensors based on immobilised whole Cell Chlorella vulgaris microalgae. *Biosensors and Bioelectronics*, *19*(9), 1089–1096. https://doi.org/10.1016/j.bios.2003.10.012

[22] Gutkin, D. W., Metes, D., & Shurin, M. R. (2005). Handling sera and obtaining fluid from different compartments: Practical considerations. *Measuring Immunity*, 121–130. https://doi.org/10.1016/b978-012455900-4/50271-3

[23] Kasemo, B. (2002). Biological surface science. *Surface Science*, *500*(1–3), 656–677. https://doi.org/10.1016/s0039-6028(01)01809-x

[24] Elmongy, H., & Abdel-Rehim, M. (2016). Saliva as an alternative specimen to plasma for Drug Bioanalysis: A Review. *TrAC Trends in Analytical Chemistry*, *83*, 70–79. https://doi.org/10.1016/j.trac.2016.07.010

[25] Cardoso, A. G., Viltres, H., Ortega, G. A., Phung, V., Grewal, R., Mozaffari, H., Ahmed, S. R., Rajabzadeh, A. R., & Srinivasan, S. (2023). Electrochemical sensing of analytes in Saliva: Challenges, progress, and Perspectives. *TrAC Trends in Analytical Chemistry*, *160*, 116965. https://doi.org/10.1016/j.trac.2023.116965

[26] Kim, J. H., Suh, Y. J., Park, D., Yim, H., Kim, H., Kim, H. J., Yoon, D. S., & Hwang, K. S. (2021). Technological advances in electrochemical biosensors for the detection of disease biomarkers. *Biomedical Engineering Letters*, *11*(4), 309–334. https://doi.org/10.1007/s13534-021-00204-w

[27] *Biomarkers in risk assessment: Validity and validation*. Biomarkers In Risk Assessment: Validity And Validation (EHC 222, 2001). (n.d.). https://www.inchem.org/documents/ehc/ehc/ehc222.htm

[28] Bodaghi, A., Fattahi, N., & Ramazani, A. (2023). Biomarkers: Promising and valuable tools towards diagnosis, prognosis and treatment of COVID-19 and other diseases. *Heliyon*, *9*(2). https://doi.org/10.1016/j.heliyon.2023.e13323

[29] Henry, B. M., & Lippi, G. (2020). Chronic kidney disease is associated with severe coronavirus disease 2019 (COVID-19) infection. *International Urology and Nephrology*, *52*(6), 1193–1194. https://doi.org/10.1007/s11255-020-02451-9

[30] Yip, T. T. C. (2004). Protein chip array profiling analysis in patients with severe acute respiratory syndrome identified serum amyloid a protein as a biomarker potentially useful in monitoring the extent of pneumonia. *Clinical Chemistry*, *51*(1), 47–55. https://doi.org/10.1373/clinchem.2004.031229

[31] Han, Y., Zhang, H., Mu, S., Wei, W., Jin, C., Tong, C., Song, Z., Zha, Y., Xue, Y., & Gu, G. (2020). Lactate dehydrogenase, an independent risk factor of severe COVID-19 patients: A retrospective and Observational Study. *Aging*, *12*(12), 11245–11258. https://doi.org/10.18632/aging.103372

[32] Ji, W., Bishnu, G., Cai, Z., & Shen, X. (2020). Analysis clinical features of COVID-19 infection in secondary epidemic area and report potential biomarkers in evaluation. *International*

Journal of Biological Macromolecules, *193*. https://doi.org/10.1101/2020.03.10.20033613

[33] Li, W., Luo, W., Li, M., Chen, L., Chen, L., Guan, H., & Yu, M. (2021). The impact of recent developments in electrochemical POC sensor for Blood Sugar Care. *Frontiers in Chemistry*, *9*. https://doi.org/10.3389/fchem.2021.723186

[34] Thapa, M., & Heo, Y. S. (2023). Label-free electrochemical detection of glucose and glycated hemoglobin (hba1c). *Biosensors and Bioelectronics*, *221*, 114907. https://doi.org/10.1016/j.bios.2022.114907

[35] Zhan, Z., Li, Y., Zhao, Y., Zhang, H., Wang, Z., Fu, B., & Li, W. J. (2022). A review of electrochemical sensors for the detection of glycated hemoglobin. *Biosensors*, *12*(4), 221. https://doi.org/10.3390/bios12040221

[36] Wu, H., Fang, F., Wang, C., Hong, X., Chen, D., & Huang, X. (2021). Selective molecular recognition of low density lipoprotein based on β-cyclodextrin coated electrochemical biosensor. *Biosensors*, *11*(7), 216. https://doi.org/10.3390/bios11070216

[37] Balayan, S., Chauhan, N., Rosario, W., & Jain, U. (2022). Biosensor development for C-Reactive Protein Detection: A Review. *Applied Surface Science Advances*, *12*, 100343. https://doi.org/10.1016/j.apsadv.2022.100343

[38] Boralessa, H., De Beer, F. C., Manchie, A., Whitam, J. G., & Pepys, M. B. (1986). C-reactive protein in patients undergoing cardiac surgery. *Anaesthesia*, *41*(1), 11–15. https://doi.org/10.1111/j.1365-2044.1986.tb12696.x

[39] Spencer, E. A., Pirie, K. L., Stevens, R. J., Beral, V., Brown, A., Liu, B., Green, J., & Reeves, G. K. (2008). Diabetes and modifiable risk factors for cardiovascular disease: The Prospective Million Women Study. *European Journal of Epidemiology*, *23*(12), 793–799. https://doi.org/10.1007/s10654-008-9298-3

[40] Akbari jonous, Z., Shayeh, J. S., Yazdian, F., Yadegari, A., Hashemi, M., & Omidi, M. (2019). An electrochemical biosensor for prostate cancer biomarker detection using graphene oxide–gold nanostructures. *Engineering in Life Sciences*, *19*(3), 206–216. https://doi.org/10.1002/elsc.201800093

[41] Supraja, P., Sudarshan, V., Tripathy, S., Agrawal, A., & Singh, S. G. (2019). Label free electrochemical detection of cardiac biomarker troponin T using znsno3 perovskite nanomaterials. *Analytical Methods*, *11*(6), 744–751. https://doi.org/10.1039/c8ay02617c

[42] Grabowska, I., Sharma, N., Vasilescu, A., Iancu, M., Badea, G., Boukherroub, R., Ogale, S., & Szunerits, S. (2018). Electrochemical aptamer-based biosensors for the detection of cardiac biomarkers. *ACS Omega*, *3*(9), 12010–12018. https://doi.org/10.1021/acsomega.8b01558

[43] Asav E. (2021). Development of a functional impedimetric immunosensor for accurate detection of thyroid-stimulating hormone. *Turkish journal of chemistry*, *45*(3), 819–834. https://doi.org/10.3906/kim-2012-69

[44] Singh, N. K., Chung, S., Sveiven, M., & Hall, D. A. (2021). Cortisol Detection in Undiluted Human Serum Using a Sensitive Electrochemical Structure-Switching Aptamer over an Antifouling Nanocomposite Layer. *ACS omega*, *6*(42), 27888–27897. https://doi.org/10.1021/acsomega.1c03552

[45] Ortega, G. A., Ahmed, S. R., Tuteja, S. K., Srinivasan, S., & Rajabzadeh, A. R. (2022). A biomolecule-free electrochemical sensing approach based on a novel electrode modification technique: Detection of ultra-low concentration of Δ9-tetrahydrocannabinol in saliva by turning a sample analyte into a sensor analyte. *Talanta*, *236*, 122863. https://doi.org/10.1016/j.talanta.2021.122863

[46] Florea, A., Cowen, T., Piletsky, S., & De Wael, K. (2019). Electrochemical sensing of

cocaine in real samples based on electrodeposited biomimetic affinity ligands. *The Analyst*, *144*(15), 4639–4646. https://doi.org/10.1039/c9an00618d

[47] Costa, N. G., Antunes, J. C., Paleo, A. J., & Rocha, A. M. (2022). A review on flexible electrochemical biosensors to monitor alcohol in sweat. *Biosensors*, *12*(4), 252. https://doi.org/10.3390/bios12040252

[48] Riu, J., & Giussani, B. (2020). Electrochemical biosensors for the detection of pathogenic bacteria in food. *TrAC Trends in Analytical Chemistry*, *126*, 115863. https://doi.org/10.1016/j.trac.2020.115863

[49] Ali, H., Mukhopadhyay, S., & Jana, N. R. (2019). Selective electrochemical detection of bisphenol A using a molecularly imprinted polymer nanocomposite. *New Journal of Chemistry*, *43*(3), 1536–1543. https://doi.org/10.1039/c8nj05883k

[50] Noori, J. S., Mortensen, J., & Geto, A. (2020). Recent development on the electrochemical detection of selected pesticides: A focused review. *Sensors*, *20*(8), 2221. https://doi.org/10.3390/s20082221

[51] Cross, E. S., Williams, L. R., Lewis, D. K., Magoon, G. R., Onasch, T. B., Kaminsky, M. L., Worsnop, D. R., & Jayne, J. T. (2017). Use of electrochemical sensors for measurement of Air Pollution: Correcting interference response and validating measurements. *Atmospheric Measurement Techniques*, *10*(9), 3575–3588. https://doi.org/10.5194/amt-10-3575-2017

[52] Rainbow, J., Sedlackova, E., Jiang, S., Maxted, G., Moschou, D., Richtera, L., & Estrela, P. (2020). Integrated electrochemical biosensors for detection of waterborne pathogens in low-resource settings. *Biosensors*, *10*(4), 36. https://doi.org/10.3390/bios10040036

[53] Sang, S., Wang, Y., Feng, Q., Wei, Y., Ji, J., & Zhang, W. (2016). Progress of new label-free techniques for biosensors: a review. *Critical reviews in biotechnology*, *36*(3), 465–481.

https://doi.org/10.3109/07388551.2014.991270

[54] Andryukov, B. G., Besednova, N. N., Romashko, R. V., Zaporozhets, T. S., & Efimov, T. A. (2020). Label-Free Biosensors for Laboratory-Based Diagnostics of Infections: Current Achievements and New Trends. *Biosensors*, *10*(2), 11. https://doi.org/10.3390/bios10020011

Appendices

S1. Supplementary Information (pertaining to Chapter 3)

I. Existent commercial devices for the binary detection of HbA1c and CRP

Table S1- 1: Current commercial devices available for the binary detection of HbA1c & CRP.

Device Name	**Method of Detection**	**Testing Matrix**		**Range of Detection**		**Time for Analysis (minutes)**		**Ref**
		HbA1c	*CRP*	*HbA1c*	*CRP*	*HbA1c*	*CRP*	
Cobas b 101	Immunoassay	Capillary or venous whole blood with anticoagulant (EDTA or heparin)	Capillary or venous whole blood, or plasma with anticoagulant (EDTA)	20-130 mmol/mol (IFCC) or 4-14 % (DCCT)	0.30-40.0 mg/dL	6	4	[1]
Skyla Hi Analyzer	Immunoassay	Whole blood	Whole blood, plasma, or serum	70 – 110 mg/dL	CRP > 40 mg/dL	6	6	[2]
InnovaStar	Photometric/ Turbidimetric	Whole blood	Whole blood or plasma	9-130 mmol/mol (IFCC) or 3-14% (DCCT)	5-400 mg/L (whole blood) and 2-160 mg/L (plasma)	5	8	[3]
Spinit	Advanced microfluidics with surface plasmon resonance	Whole blood-venous or capillary blood	Whole blood, plasma, or serum	N/A	2-300 mg/mL	6	4	[4]
B-analyst	Biochips/micro fluidics	Whole blood	Whole blood, plasma, or serum	3.3-12.6% (DCCT)	0.1-20 mg/dL (CRP), 0.1 – 4 mg/dL (hsCRP)	7’30	7’30	[5]

II. AuNP Characterization

The corresponding Figure S1-1 supports Figure 3- 2(e) in Chapter 3 by validating the presence of gold nanoparticles (AuNPs) 5mM arrested onto the screen-printed carbon electrode via cyclic voltammetry, with an atomic weight composition of 54%.

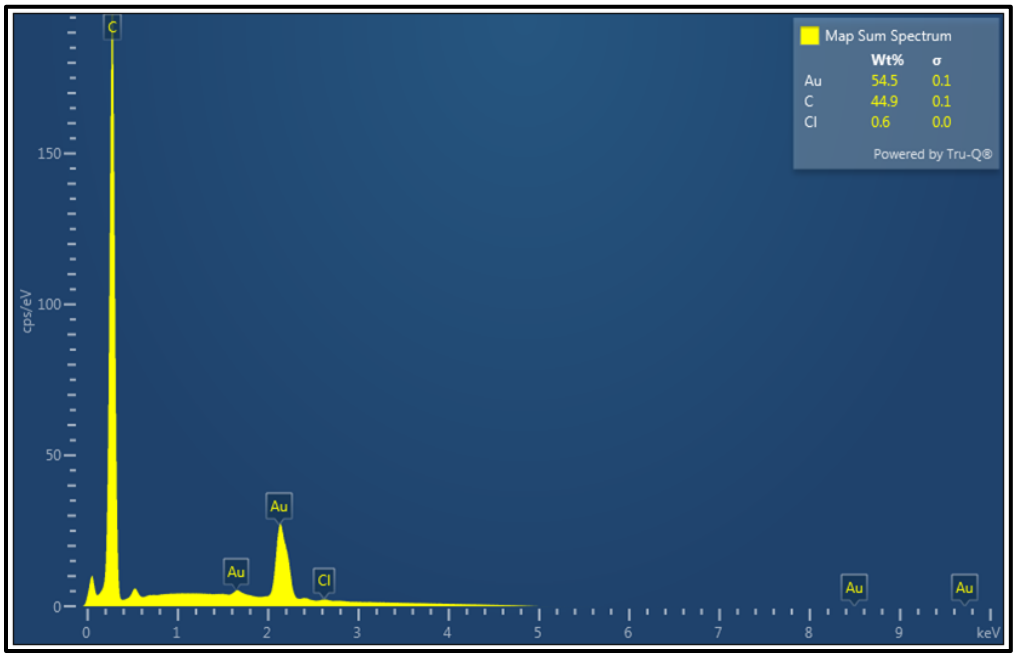

Figure S1- 1: The Map Sum Spectrum retrieved using Aztec Live Smart Mapping to indicate the presence of AuNPs deposited onto the electrode.

III. FeCN (II) Optimization

The optimization studies for FeCN (II) were conducted through a systematic exploration of varying FeCN (II) concentrations, specifically 1 mM and 10 mM (Figure S1-2) and employing diverse electrochemical techniques including Square Wave Voltammetry (SWV), Cyclic Voltammetry (CV), and Differential Pulse Voltammetry (DPV).

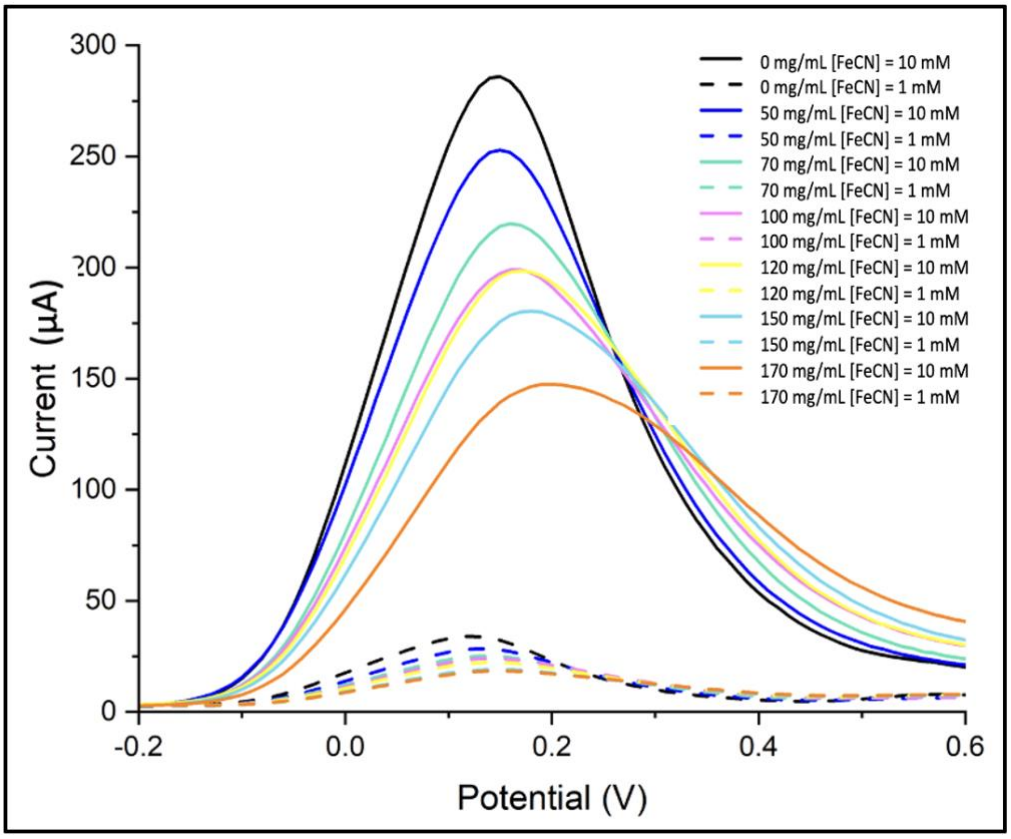

Figure S1- 2: The comparison between the detection of total Hb in [FeCN (II)] = 1 mM and 10 mM using DPV after one minute.

These methods were coupled with differential incubation times, namely 1 minute and 5 minutes, in order to determine the optimal conditions for the precise detection of Hemoglobin (Hb) (Figure S1-3). Ultimately, the electrochemical signal detection was performed using settled using 10 mM of FeCN(II) in PBS (pH 8) and using DPV, after an incubation time of one minute.

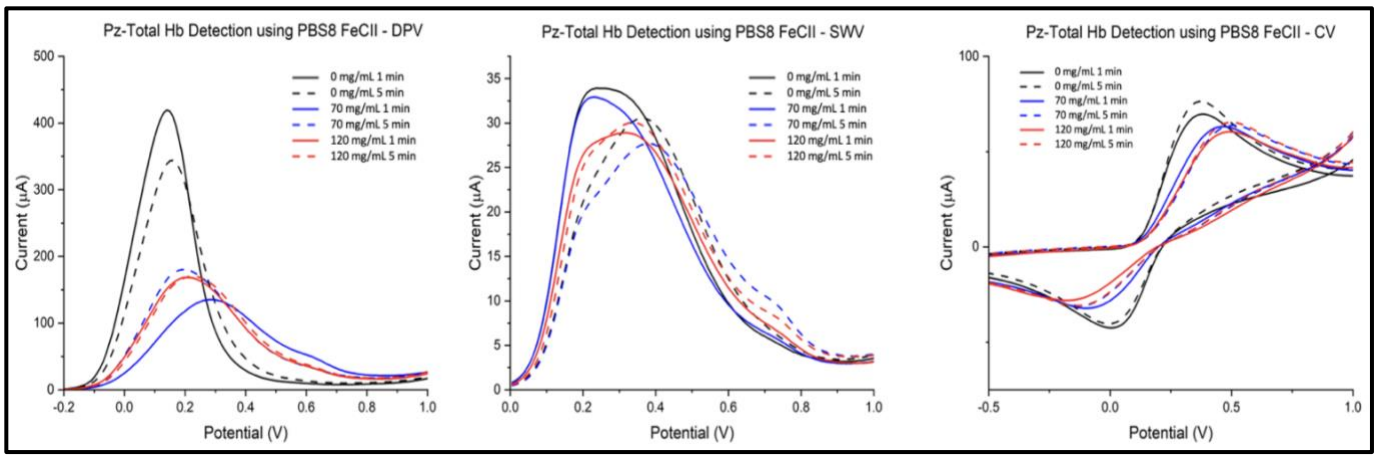

Figure S1- 3:The comparison between the detection of total Hb in 10 mM of FeCN (II) using different voltammetric techniques (DPV, SWV, and CV) and different incubation times (1 min and 5 mins).

Additionally, to have a better understanding about the interaction between Hb and FeCN (II), the UV-Vis spectrum obtained using 30 mg/mL of Hb and 10 mM of FeCN (II) in PBS (pH 8) is depicted below in Figure S1-4.

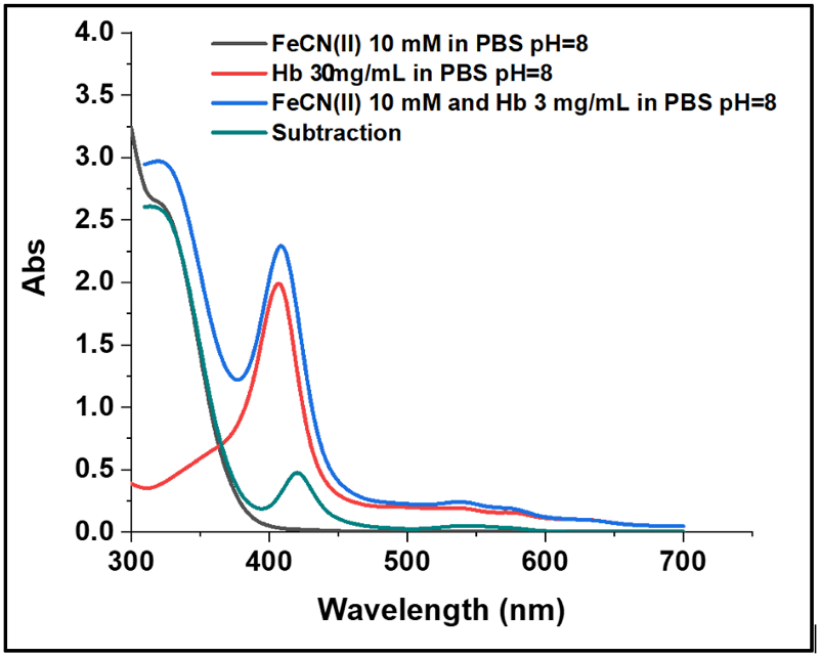

Figure S1- 4: The UV-Vis spectrum for Hb and FeCN (II).

IV. Existent electrochemical biosensors for the detection of HbA1c

Table S1- 2: Electrochemical biosensors reported for the detection of HbA1c.

Modified electrode	Electrochemical Technique	Linear Range	LOD/Sensitivity	Ref
GOX/GNF/C-Ab/**DWSPCE**	CV	0.02 – 35 mM (glucose) and 0.01 – 1 mg/mL (HbA1c)	0.5 $\mu Amm^{-2}mM^{-1}$ (glucose) and 0.09 μAmm^{-2} $\mu g^{-1}ml$ (HbA1c)	[6]
AuNPs/**SPE**	EIS/DPV/CV	20 – 200 $\mu g\ mL^{-1}$	15.5 $\mu g\ mL^{-1}$/ 0.0938 $\mu A/\mu gmL^{-1}$	[7]
Fe_3O_4NPs/MIP/**SPE**	EIS	1 pM - 0.1 µM	1 pM	[8]
pTBA/MWCNT/**SPCE**	CV	0.006-0.74 µM	3.7 nM	[9]
4-MPBA/AuNFs/**SPCE**	CV	5-1000 $\mu g\ mL^{-1}$	0.65%	[10]
APBA/pTTBA/Au NPs/**SPCE**	AMP	0.1 to 1.5%	0.052 ± 0.02%.	[11]
CS/TEOS/**RVC**	CV/AMP	0.2–12.0 mg mL^{-1}	89 $\mu g\ mL^{-1}$	[12]
Dend-FPBA/BA/GOX/**GE**	CV	2.5–15%.	2.5%	[13]

V. The deconvolution of HbA1c peak values

The electrochemical detection of HbA1c in PBS (pH 8) FeCN (II) resulted in displayed two distinct peaks, as visually represented in the accompanying figure S1-5. Consequently, the peaks were subjected deconvolution, with the area under the curve values serving as the basis for the construction of calibration curves for this analyte.

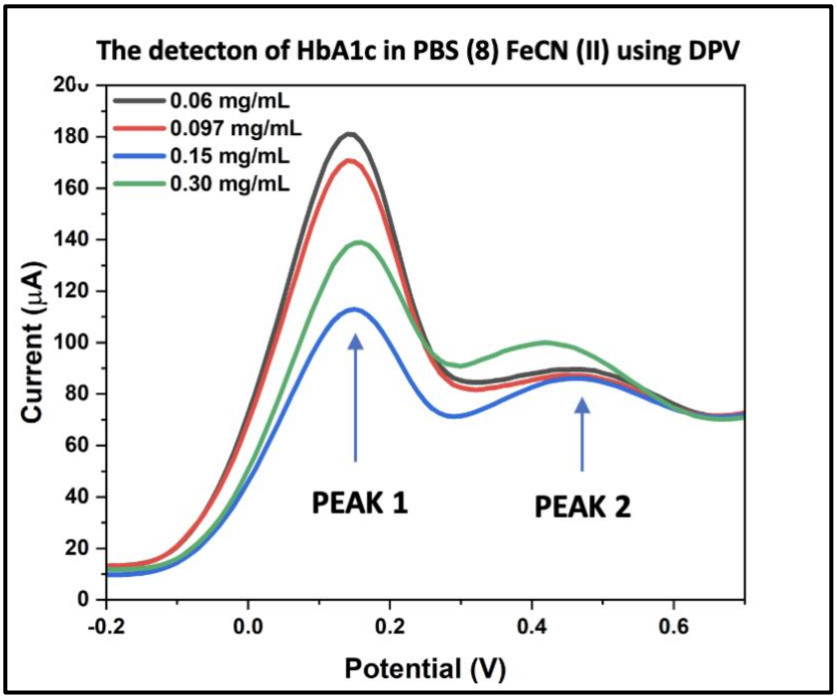

Figure S1- 5: Depiction of the two distinct peaks generated by the electrochemical detection of HbA1c in PBS (8) FeCN (II) using DPV (post-dilution of HbA1c concentrations by a factor of 10 x)

VI. Determining the biosensing analyte for CRP

Although ferrocyanide FeCN (II) was also employed as the redox probe for the detection of C-reactive protein (CRP), mirroring the approach utilized for HbA1c detection to ensure procedural uniformity, the corresponding results were unfavorable. FeCN (II) lacked the ability to differentiate between varying CRP concentrations, as illustrated in Figure S1-6, retrieved using CV. This limitation could be associated with the necessity for a more specific molecular interaction between the analyte and the redox probe to effectively detect low analyte concentrations.

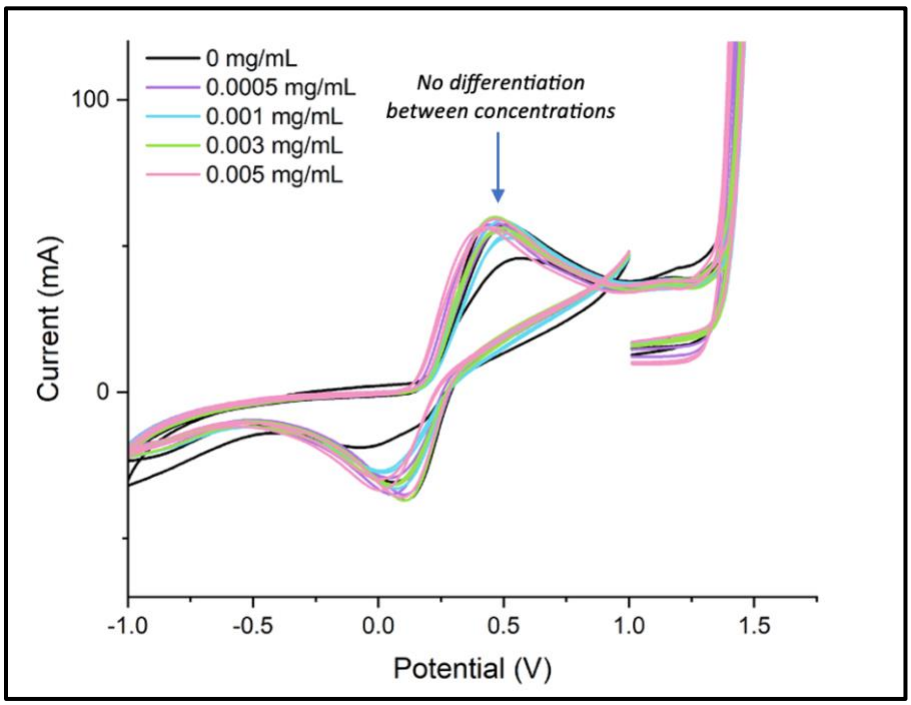

Figure S1- 6: The detection of CRP in FeCN (II) PBS (pH 8) using CV, post-dilution by a factor of 10x.

As a result, PcA-NO2 in PBS (pH 7.4) was used as the redox probe for the detection of CRP due to its specific affinity for the target analyte (Figure S1-7).

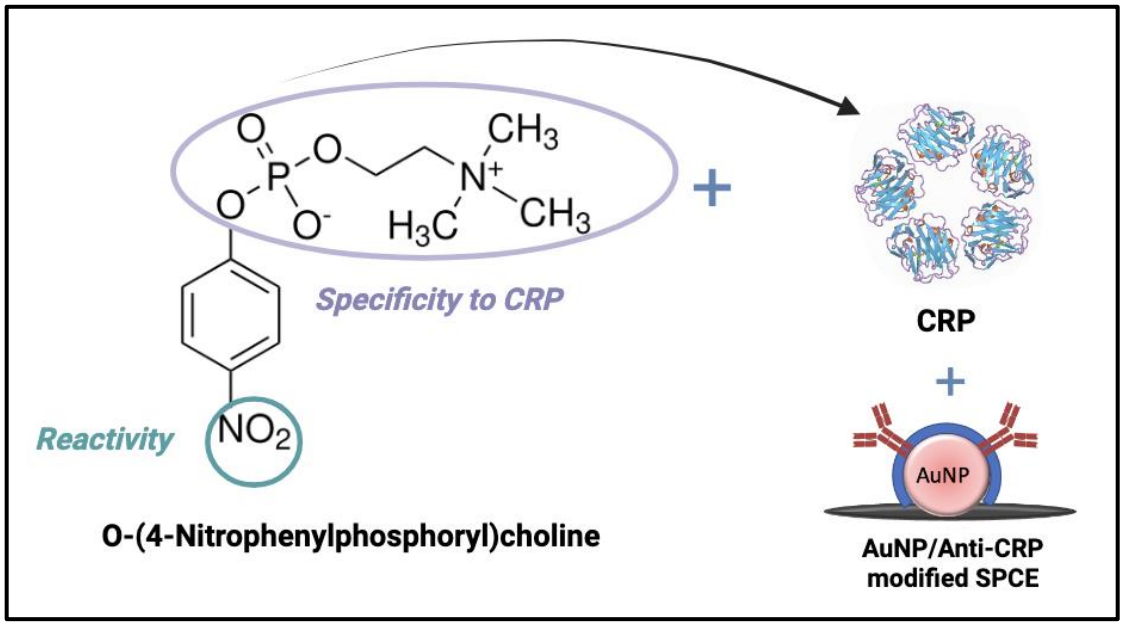

Figure S1- 7: The specific interaction between PcA-NO_2 and CRP mediated by the AuNP/Anti-CRP modified electrodes, created via BioRender.com.

Notably, the conversion of the nitro (NO2) group in PcA-NO2 to the amine (NH2) group involves a two-step reduction process: PcA-NO2 → PcA-NH-OH (SCAN 1) → PcA-NH2 (SCAN 2) (Figure S1-8).

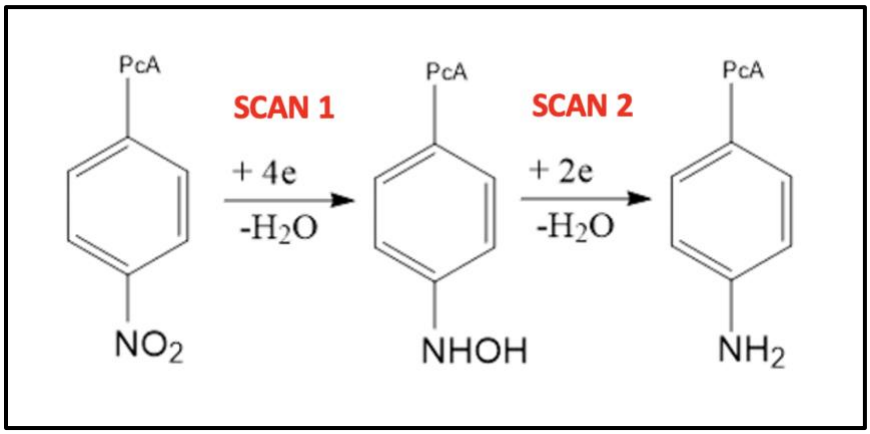

Figure S1- 8: The two-step reduction process associated with the amine group of phosphorylcholine.

Hence, due to the reason stated above, resultant DPV signals for the calibration curves were retrieved after performing a second scan (SCAN 2) for CRP in PcA-NO_2 (Figure S1-9).

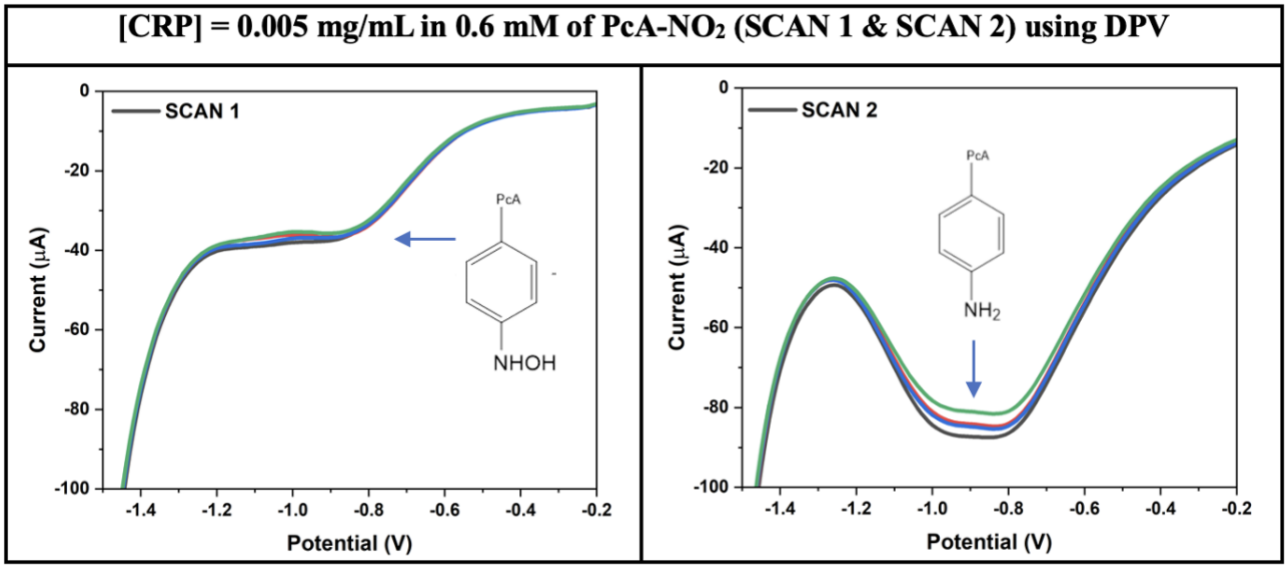

Figure S1- 9: The depiction of the two-scan process for the detection of CRP in PcA-NO_2 using DPV, post-dilution by a factor of 10x.

VII. Existent electrochemical biosensors for the detection of CRP

Table S1- 3: Electrochemical biosensors reported for the detection of CRP.

Modified electrode	**Electrochemical Technique**	**Linear Range**	**LOD/Sensitivity**	**Ref**
GO-COOH/AuNPs/MGAs/**SPE**	DPV	0.001 – 100 ng mL^{-1}	0.001 ng mL^{-1}	[14]
GDQs/anti-CRP/**SPCEs**	AMP	0.5 – 10 ng mL^{-1}	0.036 ng mL^{-1}/ 12.45 µA ng^{-1} mL^{-1} cm^{-2}	[15]
AuNPs/SAM/anti-CRP/**SPE**	AMP	0.047 – 23.6 µg mL^{-1}	17 ng mL^{-1}/90.7 nA nM^{-1}	[16]
AuNPs-IL-MoS_2/GO-DN/anti-CRP/**GCE**	AMP	0.01 – 100 ng mL^{-1}	3.3 pg mL^{-1}	[17]
PMPC-SH/AuNPs/**SPCE**	DPV	5 – 5000 ng mL^{-1}	1.55 ng mL-1	[18]
AuNPs/anti-CRP/**GCE**	DPV	1 fg mL^{-1} – 100 ng mL^{-1}	0.33 fg mL^{-1}	[19]

VIII. References

[1] *Cobas B 101 system*. Roche Diagnostics. (2019). https://diagnostics.roche.com/global/en/products/instruments/cobas-b-101-ins-2892.html

[2] Skyla. (n.d.). *Skyla Hi Immunoassay Analyzer*. Immunoassay analyzer. http://www.skyla.com/page/about/index.aspx?kind=82

[3] DiaSys Diagnostic Systems GmbH. (2014). *InnovaStar*®. https://www.diasys-diagnostics.com/products/poct-systems/innovastar/

[4] Seara.com. (n.d.). *Spinit*. biosurfit. https://www.biosurfit.com/en/spinit/.

[5] NAGASE Group. (n.d.). *Laboratory*. B-analyst S1 µTAS drop analyzer (HBA1C, CRP, HSCRP). https://www.medicalexpo.com/medical-manufacturer/glycated-hemoglobin-analyzer-600.html

[6] Thapa, M., & Heo, Y. S. (2023). Label-free electrochemical detection of glucose and glycated hemoglobin (hba1c). *Biosensors and Bioelectronics*, *221*, 114907. https://doi.org/10.1016/j.bios.2022.114907

[7] Zhao, Y., Zhang, H., Li, Y., Wang, X., Zhao, L., Xu, J., Zhan, Z., Zhang, G., & Li, W. J. (2022). Glycated hemoglobin electrochemical immunosensor based on screen-printed electrode. *Biosensors*, *12*(10), 902. https://doi.org/10.3390/bios12100902

[8] Mahobiya, S. (2022). Developing a sensing platform based on molecular imprinting of hba1c on FE3O4 nanoparticle modified screen-printed electrode. *Biointerface Research in Applied Chemistry*, *13*(3), 228. https://doi.org/10.33263/briac133.228

[9] Moon, J.-M., Kim, D.-M., Kim, M. H., Han, J.-Y., Jung, D.-K., & Shim, Y.-B. (2017). A disposable amperometric dual-sensor for the detection of hemoglobin and glycated hemoglobin in a finger prick blood sample. *Biosensors and Bioelectronics*, *91*, 128–135.

https://doi.org/10.1016/j.bios.2016.12.038

[10] Wang, X., Su, J., Zeng, D., Liu, G., Liu, L., Xu, Y., Wang, C., Liu, X., Wang, L., & Mi, (2019). Gold Nano-Flowers (AU NFS) modified screen-printed carbon electrode electrochemical biosensor for label-free and quantitative detection of glycated hemoglobin. *Talanta*, *201*, 119–125. https://doi.org/10.1016/j.talanta.2019.03.100

[11] Kim, D.-M., & Shim, Y.-B. (2013). Disposable amperometric glycated hemoglobin sensor for the finger prick blood test. *Analytical Chemistry*, *85*(13), 6536–6543. https://doi.org/10.1021/ac401411y

[12] Liu, A., Xu, S., Deng, H., & Wang, X. (2016). A new electrochemical hba1c biosensor based on flow injection and screen-printed electrode. *International Journal of Electrochemical Science*, *11*(4), 3086–3094. https://doi.org/10.1016/s1452-3981(23)16166-9

[13] Song, S. Y., & Yoon, H. C. (2009). Boronic acid-modified thin film interface for specific binding of glycated hemoglobin (hba1c) and electrochemical biosensing. *Sensors and Actuators B: Chemical*, *140*(1), 233–239. https://doi.org/10.1016/j.snb.2009.04.057

[14] Gao, H., Bai, Y., He, B., & Tan, C. S. (2022). A simple label-free aptamer-based electrochemical biosensor for the sensitive detection of C-reactive proteins. *Biosensors*, *12*(12), 1180. https://doi.org/10.3390/bios12121180

[15] Lakshmanakumar, M., Nesakumar, N., Sethuraman, S., S, R. K., Krishnan, U. M., & Rayappan, J. B. (2021). Fabrication of GQD-electrodeposited screen-printed carbon electrodes for the detection of the CRP Biomarker. *ACS Omega*, *6*(48), 32528–32536. https://doi.org/10.1021/acsomega.1c04043

[16] Thangamuthu, M., Santschi, C., & J. F. Martin, O. (2018). Label-free electrochemical immunoassay for C-reactive protein. *Biosensors*, *8*(2), 34. https://doi.org/10.3390/bios8020034

[17] Ma, Y., Yang, J., Yang, T., Deng, Y., Gu, M., Wang, M., Hu, R., & Yang, Y. (2020). Electrochemical detection of C-reactive protein using functionalized iridium nanoparticles/graphene oxide as a tag. *RSC Advances*, *10*(16), 9723–9729. https://doi.org/10.1039/c9ra10386d

[18] Pinyorospathum, C., Chaiyo, S., Sae-ung, P., Hoven, V. P., Damsongsang, P., Siangproh, W., & Chailapakul, O. (2019). Disposable paper-based electrochemical sensor using thiol-terminated poly(2-methacryloyloxyethyl phosphorylcholine) for the label-free detection of C-reactive protein. *Microchimica Acta*, *186*(7). https://doi.org/10.1007/s00604-019-3559-6

[19] Zhang, J., Zhang, W., Guo, J., Wang, J., & Zhang, Y. (2017). Electrochemical detection of C-reactive protein using copper nanoparticles and hybridization chain reaction amplifying signal. *Analytical Biochemistry*, *539*, 1–7. https://doi.org/10.1016/j.ab.2017.09.017

S2. Supplementary Information (pertaining to Chapter 4)

I. Statistical Analysis (ANOVA)

The one-way analysis of variance (ANOVA) was conducted to provide statistical evidence associated with the best storage conditions presented in Figures 5-7 in the manuscript.

a. THCi-modified electrodes (130 ng) at -18°C over the span of 6 months

The associated ANOVA analysis (Table S2-1) was performed using a significance level (α) of 0.05. With the resultant p-value < α, the null hypothesis is rejected, implying that the mean AUC values for the modified electrodes are significantly different over time when stored at -18°C.

Table S2- 1: Overall ANOVA analysis performed for the THCi-modified electrodes stored at -18°C for 6 months.

	DF	Sum of Squares	Mean Square	F Value	Prob>F
Model	6	0.01121	0.00187	250.95651	4.77321E-17
Error	19	1.41506E-4	7.4477E-6		
Total	25	0.01136			

The corresponding percentage of variation (R^2) of 98% (Table S2-2) signifies a highly robust model and indicates a strong relationship between the storage conditions and the stability of the electrodes. A coefficient of variation (CV) of 4.28% suggests a relatively low level of variability in the dataset compared to the mean. Hence, there is a high degree of consistency in the AUC values for the modified electrodes stored at -18°C over time. Analyzing Levene's Test (Table S2-3) for determining the homogeneity of variance, the population variances are significantly different at the 0.05 significance level with the p-value < α.

Table S2- 2: Fit Statistics performed for the THCi-modified electrodes stored at -18°C for 6 months.

	R-Square	Coeff Var	Root MSE	Data Mean
	0.98754	0.04283	0.00273	0.06371

Table S2- 3: Levene's Test performed for the THCi-modified electrodes stored at -18°C for 6 months.

	DF	Sum of Squares	Mean Square	F Value	Prob>F
Model	6	2.79177E-5	4.65294E-6	5.2807	0.00237
Error	19	1.67413E-5	8.81122E-7		

Lastly, the Tukey-Kramer test (Table S2-4) was conducted to compare multiple group means for each of the time periods, where Sig = 1 indicates that the difference of means is significant AND Sig = 0 indicates that the difference of means is insignificant at the 0.05 level. The results obtained demonstrate that pairs M2-D7, and M5-M4 consist of statistically insignificant differences with respect to their means. Since these are crucial time periods which mark the beginning and the end of the shelf-life study, the practical significance of using these storage conditions for the long-term stability of the modified electrodes is validated.

Table S2- 4: The Tukey Test performed for the THCi-modified electrodes stored at -18°C for 6 months.

	MeanDiff	SEM	q Value	Prob	Alpha	Sig	LCL	UCL
M1 D7	-0.01953	0.00223	12.39726	7.19733E-7	0.05	1	-0.02685	-0.01221
M2 D7	-0.00101	0.00193	0.73896	0.99815	0.05	0	-0.00735	0.00533
M2 M1	0.01853	0.00193	13.57616	2.13855E-7	0.05	1	0.01219	0.02486
M3 D7	-0.01136	0.00223	7.20776	0.00105	0.05	1	-0.01868	-0.00404
M3 M1	0.00818	0.00223	5.1895	0.02267	0.05	1	8.5798E-4	0.0155
M3 M2	-0.01035	0.00193	7.58384	5.94763E-4	0.05	1	-0.01669	-0.00401
M4 D7	-0.04372	0.00223	27.74998	0	0.05	1	-0.05104	-0.0364
M4 M1	-0.02419	0.00223	15.35272	5.99538E-8	0.05	1	-0.03151	-0.01687
M4 M2	-0.04272	0.00193	31.30395	0	0.05	1	-0.04905	-0.03638
M4 M3	-0.03237	0.00223	20.54222	6.65008E-8	0.05	1	-0.03969	-0.02505
M5 D7	-0.04288	0.00208	29.09491	0	0.05	1	-0.04973	-0.03604
M5 M1	-0.02335	0.00208	15.84168	5.05698E-8	0.05	1	-0.03019	-0.0165
M5 M2	-0.04187	0.00176	33.61607	0	0.05	1	-0.04766	-0.03609
M5 M3	-0.03153	0.00208	21.38949	1.27438E-7	0.05	1	-0.03837	-0.02468
M5 M4	8.41667E-4	0.00208	0.57106	0.99957	0.05	0	-0.006	0.00769
M6 D7	-0.05224	0.00208	35.44221	0	0.05	1	-0.05908	-0.04539
M6 M1	-0.0327	0.00208	22.18898	1.30518E-7	0.05	1	-0.03955	-0.02586
M6 M2	-0.05123	0.00176	41.1263	0	0.05	1	-0.05701	-0.04544
M6 M3	-0.04088	0.00208	27.73679	0	0.05	1	-0.04773	-0.03403
M6 M4	-0.00851	0.00208	5.77624	0.00939	0.05	1	-0.01536	-0.00167
M6 M5	-0.00935	0.00193	6.85587	0.0018	0.05	1	-0.01569	-0.00302

b. THCi-modified electrodes (130 ng) with a second modification of PBS (pH 4) at -18°C over the span of 6 months

The overall ANOVA analysis for the THCi-modified electrodes with PBS(4) at -18°C for 6 months is depicted in Table S2-5. The p-value < α infers that the mean AUC values for the electrodes are significantly different over time at the 0.05 significance level. The corresponding R^2 value (Table S2-6) of 96% implies a solid correlation between the storage conditions and the stability of the electrode at those conditions.

Table S2- 5: Overall ANOVA analysis performed for the THCi-modified electrodes with PBS(4) stored at -18°C for 6 months.

	DF	Sum of Squares	Mean Square	F Value	Prob>F
Model	6	0.07607	0.01268	118.03968	1.36871E-15
Error	22	0.00236	1.07409E-4		
Total	28	0.07843			

Table S2- 6:Fit Statistics performed for the THCi-modified electrodes with PBS(4) stored at -18°C for 6 months.

	R-Square	Coeff Var	Root MSE	Data Mean
	0.96987	0.05397	0.01036	0.19203

Examining the Levene's Test for the electrodes in Table S2-7 with the p-value > α, this corroborates that the population variances are not significantly different at the 0.05 level. Hence, the corresponding electrodes demonstrated exceptional stability using the storage conditions described.

Table S2- 7: Levene's Test performed for the THCi-modified electrodes with PBS(4) stored at -18°C for 6 months.

	DF	Sum of Squares	Mean Square	F Value	Prob>F
Model	6	1.39851E-4	2.33085E-5	0.94961	0.48077
Error	22	5.39998E-4	2.45454E-5		

Analyzing the resultant Tukey Test for the associated electrodes in Table S2-8, multiple pairs of time periods consisted of insignificant differences between their means at the 0.05 significance level. These pairs comprised of M1-D7, M3-M2, M4-M2, M4-M3, M5-M2, M5-M3, M5-M4, M6-M2, M6-M3,M6-M4, and M6-M5. Therefore, these specific groups do not exhibit statistically significant variation in shelf life, valuable for quality control and the product stability.

Table S2- 8: The Tukey Test performed for the THCi-modified electrodes with PBS(4) stored at -18°C for 6 months.

	MeanDiff	SEM	q Value	Prob	Alpha	Sig	LCL	UCL
M1 D7	-0.00683	0.00733	1.31708	0.96315	0.05	0	-0.03054	0.01689
M2 D7	-0.11813	0.00733	22.79559	8.56344E-8	0.05	1	-0.14184	-0.09441
M2 M1	-0.1113	0.00733	21.47851	8.39501E-8	0.05	1	-0.13502	-0.08758
M3 D7	-0.11903	0.00695	24.21173	1.39416E-7	0.05	1	-0.14152	-0.09653
M3 M1	-0.1122	0.00695	22.82341	8.5667E-8	0.05	1	-0.1347	-0.0897
M3 M2	-9E-4	0.00695	0.18308	1	0.05	0	-0.0234	0.0216
M4 D7	-0.11154	0.00669	23.57961	1.33739E-7	0.05	1	-0.13319	-0.08989
M4 M1	-0.10472	0.00669	22.13683	8.48275E-8	0.05	1	-0.12637	-0.08307
M4 M2	0.00658	0.00669	1.3917	0.95229	0.05	0	-0.01507	0.02823
M4 M3	0.00748	0.00628	1.68637	0.88964	0.05	0	-0.01283	0.02779
M5 D7	-0.10803	0.00898	17.0211	5.53563E-8	0.05	1	-0.13707	-0.07898
M5 M1	-0.1012	0.00898	15.94571	6.40884E-8	0.05	1	-0.13025	-0.07215
M5 M2	0.0101	0.00898	1.59142	0.91338	0.05	0	-0.01895	0.03915
M5 M3	0.011	0.00867	1.79406	0.85869	0.05	0	-0.01706	0.03906
M5 M4	0.00352	0.00846	0.58772	0.99951	0.05	0	-0.02387	0.0309
M6 D7	-0.12768	0.00733	24.63853	1.43138E-7	0.05	1	-0.15139	-0.10396
M6 M1	-0.12085	0.00733	23.32145	8.62292E-8	0.05	1	-0.14457	-0.09713
M6 M2	-0.00955	0.00733	1.84294	0.84329	0.05	0	-0.03327	0.01417
M6 M3	-0.00865	0.00695	1.75956	0.86906	0.05	0	-0.03115	0.01385
M6 M4	-0.01613	0.00669	3.41054	0.24027	0.05	0	-0.03778	0.00552
M6 M5	-0.01965	0.00898	3.09618	0.34012	0.05	0	-0.0487	0.0094

c. THCi-modified electrodes (130 ng) with a second modification of PBS (pH 4) at 4°C over the span of 6 months

The overall ANOVA analysis for the affiliated electrodes is presented in Table S2-9. As per the p-value < α, the AUC means for the modified electrodes are significantly different at the 0.05 level. Approximately 76% of the total variation (Table S2-10) associated with the stability of the electrodes can be accounted for by the storage conditions used, specifically, the storage at 4°C in this case. Interpreting the Levene's Test of Absolute Deviations (Table S2-11) with the p-value > α, it can be concluded that the variances in the AUC values of the electrodes are insignificant over time at the 0.05 significance level.

Table S2- 9: Overall ANOVA analysis performed for the THCi-modified electrodes with PBS(4) stored at 4°C for 6 months.

	DF	Sum of Squares	Mean Square	F Value	Prob>F
Model	6	0.00555	9.25594E-4	15.01965	1.28803E-7
Error	28	0.00173	6.16255E-5		
Total	34	0.00728			

Table S2- 10: Fit Statistics performed for the THCi-modified electrodes with PBS(4) stored at 4°C for 6 months.

	R-Square	Coeff Var	Root MSE	Data Mean
	0.76295	0.09157	0.00785	0.08573

Table S2- 11: Levene's Test (Absolute Deviations) performed for the THCi-modified electrodes with PBS(4) stored at 4°C for 6 months.

	DF	Sum of Squares	Mean Square	F Value	Prob>F
Model	6	1.48209E-4	2.47014E-5	1.55813	0.19634
Error	28	4.43892E-4	1.58533E-5		

Examining Tukey's Test for multiple groups means in Table S2-12, numerous pairs of groups exhibited insignificant differences among the means at the 0.05 significance level. The pairs consist of M2-D7, M3-D7, M3-M2, M4-D7, M4-M2, M4-M3, M5-D7, M5-M2, M5-M4, M6-D7, M6-M3, and M6-M4. Hence, the Tukey Test supports the storage conditions tested for its contribution to extending the stability of the modified electrodes.

Table S2- 12: The Tukey Test performed for the THCi-modified electrodes with PBS(4) stored at 4°C for 6 months.

	MeanDiff	SEM	q Value	Prob	Alpha	Sig	LCL	UCL
M1 D7	0.03081	0.00496	8.77657	2.00334E-5	0.05	1	0.01506	0.04656
M2 D7	0.0078	0.00496	2.22234	0.70059	0.05	0	-0.00795	0.02355
M2 M1	-0.02301	0.00496	6.55423	0.00131	0.05	1	-0.03876	-0.00726
M3 D7	-0.00624	0.00496	1.77628	0.8656	0.05	0	-0.02199	0.00951
M3 M1	-0.03705	0.00496	10.55284	8.09407E-7	0.05	1	-0.0528	-0.0213
M3 M2	-0.01404	0.00496	3.99862	0.10491	0.05	0	-0.02979	0.00171
M4 D7	-0.00165	0.00496	0.46885	0.99987	0.05	0	-0.0174	0.0141
M4 M1	-0.03246	0.00496	9.24542	8.38147E-6	0.05	1	-0.04821	-0.01671
M4 M2	-0.00945	0.00496	2.69119	0.49498	0.05	0	-0.0252	0.0063
M4 M3	0.00459	0.00496	1.30743	0.96531	0.05	0	-0.01116	0.02034
M5 D7	0.0122	0.00496	3.47394	0.21361	0.05	0	-0.00355	0.02795
M5 M1	-0.01862	0.00496	5.30263	0.01275	0.05	1	-0.03437	-0.00287
M5 M2	0.00439	0.00496	1.2516	0.97193	0.05	0	-0.01136	0.02014
M5 M3	0.01843	0.00496	5.25022	0.01397	0.05	1	0.00268	0.03418
M5 M4	0.01384	0.00496	3.94279	0.11368	0.05	0	-0.00191	0.02959
M6 D7	-0.00877	0.00496	2.49693	0.58047	0.05	0	-0.02452	0.00698
M6 M1	-0.03958	0.00496	11.2735	2.49058E-7	0.05	1	-0.05533	-0.02383
M6 M2	-0.01657	0.00496	4.71927	0.03431	0.05	1	-0.03232	-8.18687E-4
M6 M3	-0.00253	0.00496	0.72065	0.9985	0.05	0	-0.01828	0.01322
M6 M4	-0.00712	0.00496	2.02808	0.77914	0.05	0	-0.02287	0.00863
M6 M5	-0.02096	0.00496	5.97087	0.00386	0.05	1	-0.03671	-0.00521

II. XPS Characterization

Table S2- 13: XPS survey data (atomic percentage) for the most concentrated elements in the materials.

Samples	**Elements (At. %)**					
	C 1s	**O 1s**	**N 1s**	**Cl 2p**	**Si 2p**	**Fe 2p**
P-Z*	82.2	8.7	0.4	7.9	0.9	0.3
Control	77.4	9.1	2.2	10.1	1.0	0.2
RT	81.1	9.5	1.4	7.4	0.4	0.2
4CT	82.2	10.2	1.5	5.9	-	0.2
-18CT	73.6	21.4	0.7	-	2.8	1.4

*P-Z: Pristine TE-100 Zensor electrode

Table S2- 14: The peak-fitting results of C1s high-resolution signal of materials.

Samples	Assignment	E_B (eV)	FWHM (eV)	At. %
P-Z	**C1s** C=C aromatic	284.4	0.6	16.2
	C1s C-C, C-H	285.0	1.3	57.6
	C1s C-OH, C-O-C, C-Cl	286.5	1.3	22.0
	C1s O-C=O	289.0	1.3	4.2
Control	**C1s** C=C aromatic	284.4	0.7	18.2
	C1s C-C, C-H	285.0	1.5	51.1
	C1s C-OH, C-O-C, C-Cl	286.4	1.5	26.3
	C1s O-C=O	288.8	1.6	4.4
RT	**C1s** C=C aromatic	284.2	0.9	20.4
	C1s C-C, C-H	285.0	1.4	49.4
	C1s C-OH, C-O-C, C-Cl	286.3	1.5	26.0
	C1s O-C=O	288.7	1.7	4.2
4CT	**C1s** C=C aromatic	284.3	0.8	17.7
	C1s C-C, C-H	285.0	1.5	55.9
	C1s C-OH, C-O-C, C-Cl	286.4	1.5	23.8
	C1s O-C=O	288.7	1.6	2.7
-18CT	**C1s** C=C aromatic	284.4	1.0	24.8
	C1s C-C, C-H	285.0	1.4	55.5
	C1s C-OH, C-O-C, C-Cl	286.5	1.4	9.9
	C1s O-C=O	288.4	1.7	9.8

Table S2- 15: The peak-fitting results of O1s high-resolution signal of materials.

Samples	Assignment	E_B (eV)	FWHM (eV)	At. %
P-Z	**O1s** C=O	532.5	1.5	68.3
	O1s O*-(C=O)-C, C-O aromatic	533.5	1.6	31.7
Control	**O1s** C=O	532.2	1.6	51.5
	O1s O*-(C=O)-C, C-O aromatic	533.5	1.7	48.5
RT	**O1s** C=O	532.1	1.6	43.4
	O1s O*-(C=O)-C, C-O (aromatic)	533.4	1.8	56.5
4CT	**O1s** C=O	532.2	1.6	45.4
	O1s O*-(C=O)-C, C-O (aromatic)	533.4	1.8	54.6
-18CT	**O1s** C=O	532.4	1.6	60.6
	O1s O*-(C=O)-C, C-O (aromatic)	533.6	1.8	39.4

III. Additional modifiers

Organic compounds, including Ascorbic Acid (AA) and Citric Acid (CA) were used to perform a second modification on the THCi-modified electrodes to perform their role as antioxidants and radical scavengers in controlling the oxidation of THC. Both, AA-modified and CA-modified electrodes were vacuum sealed with O_2 absorbers and stored at 4°C for a period of one week. Although the corresponding results (Figure S2-1) depict similar electrochemical behaviour to THCi-modified electrodes with a second modification of PBS (pH 4), the signals only remained stable for up to day three, after which the intensity of the signal was observed to decrease on day 7. Additionally, electrodes with a second modification of these organic compounds also exhibited significantly low reproducibility.

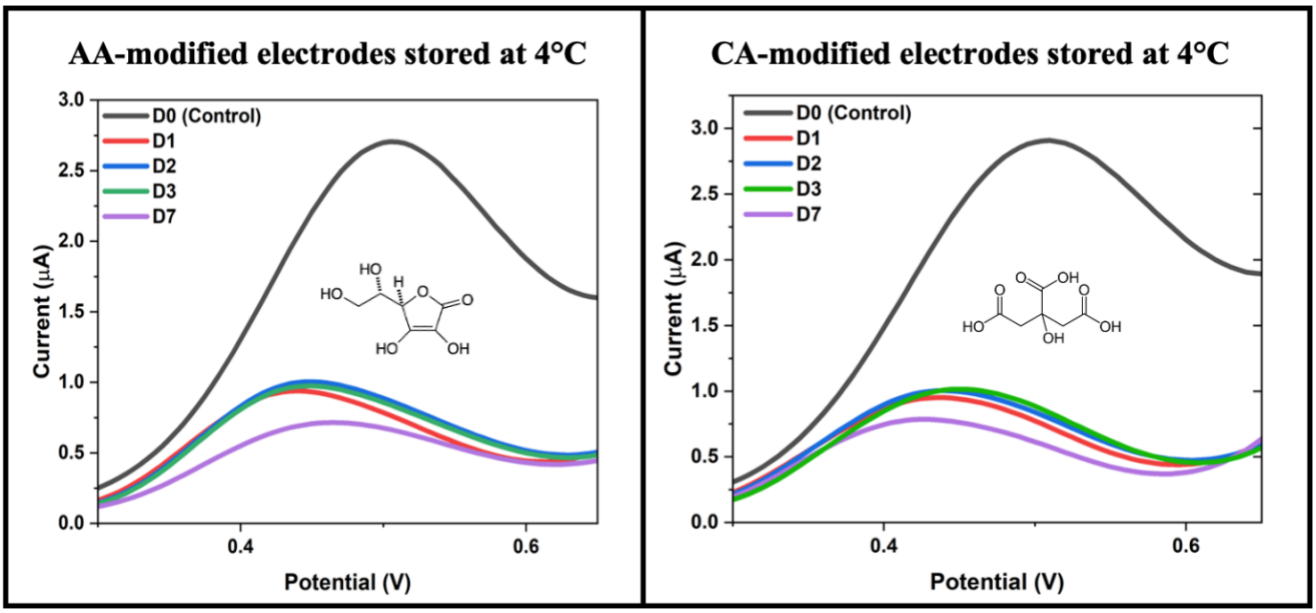

Figure S2- 1: AA-modified electrodes (13 ng) and CA-modified electrodes (13 ng) stored at 4°C for a period of one week.

BHT is yet another organic chemical which functions by blocking the propagation of free radicals, and hence, it was used for its antioxidant properties in this study. The THCi-modified electrodes were modified with a second modification of BHT in conjunction with Transcutol as was previously reported in the literature for THC [1], vacuum sealed with O_2 absorbers and stored on the lab bench at RT for a period of one month. The results showcase (Figure S2-2) that the modified electrodes only remained stable for a period of two days at RT, after which flat signals were observed for the subsequent days.

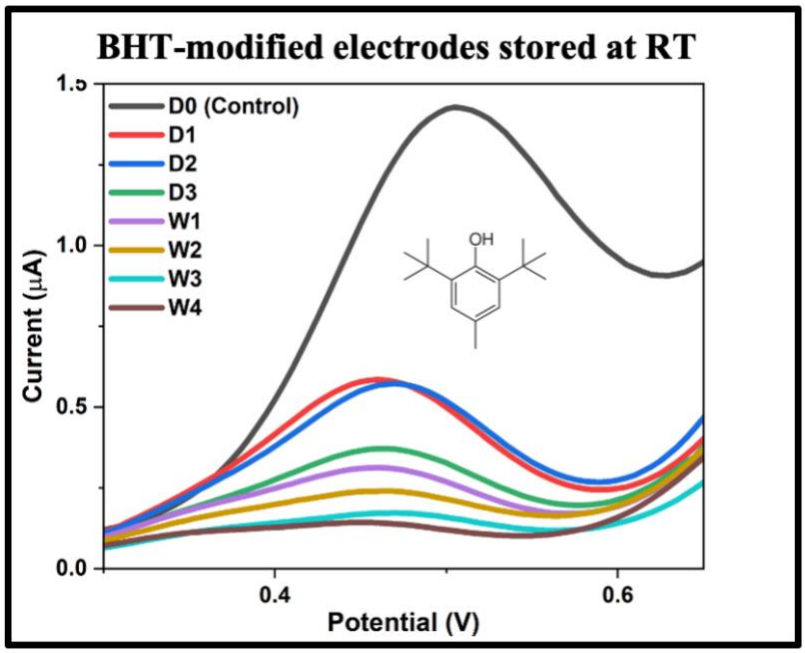

Figure S2- 2: BHT-modified electrodes (5.2 ng) stored at RT for one month.

IV. Alternative modifiers

THCA is the inactive and the more stable precursor of THC due to the presence of an extra carboxylic group. The TE-100 Zensor electrodes were manually modified with 130 ng of THCA, vacuum sealed with O_2 absorbers, placed in a mylar bag and stored on the lab bench at RT and in the refrigerator at 4°C for a period of one week (Figure S2-3). The electrodes were tested using PBS (pH 7.4) via SWV, during which the electrochemical signals displayed an additional second peak during detection (SCAN 2). The presence of the second peak denotes the occurrence of the partial decomposition of THCA into its decarboxylated product, THC.

Comparing the different temperatures for storing the THCA-modified electrodes, storage at both RT and 4°C provided stable electrochemical signals for the entire span of one week. With reproducibility and high intensity values being prime factors in engendering stability, in addition to the second peak observed, the resultant intensities obtained in the graph are too low to be used for the purposes of THC detection.

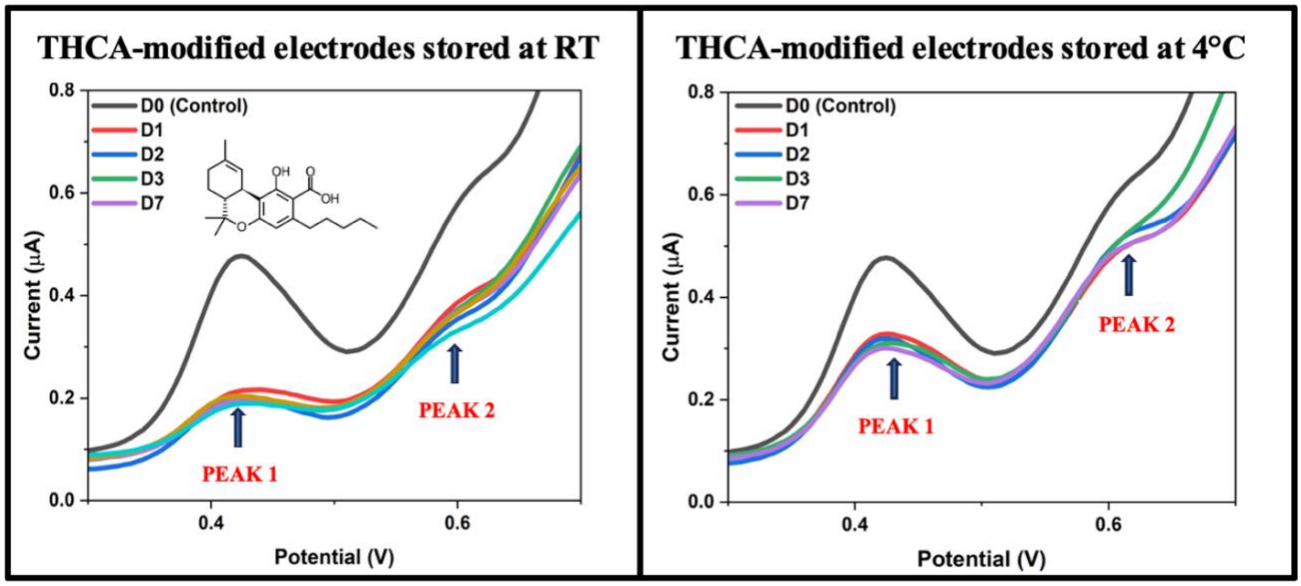

Figure S2- 3: THCA-modified electrodes (130 ng) stored on the lab bench at RT and at 4°C for a period of one week.

Dopamine is a neurotransmitter with a similar electrochemical behaviour to that of THC i.e., with an irreversible oxidation potential at approximately 0.45 V. An amount of 100 ng of DA was manually deposited onto the WE of the pristine electrodes after incubating the deposition sample for 0 minutes and 30 minutes. Irrespective of the sample incubation time tested, the DA-modified electrodes exhibited a broad electrochemical signal comprised of two different oxidation potentials and hence, were unable to detect the oxidation of THC (Figure S2-4). In this case, DA displayed a reversible oxidation peak at 0.25 V, implying electro-oxidation of the molecule. After conducting the first scan, the subsequent four scans for the molecule presented a flat signal via SWV.

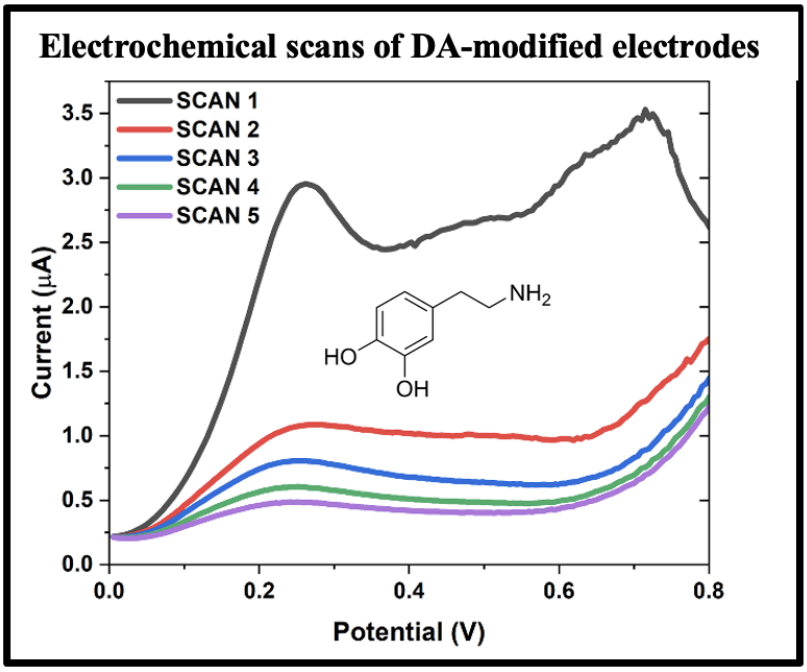

Figure S2- 4: The electrochemical behaviour of DA-modified electrodes (100 ng).

Subsequently, the manual deposition of 130 ng of CBD was performed onto the WE of the TE-100 Zensor electrodes after incubating the deposition sample for 40 minutes. The CBD-modified electrodes were vacuum sealed with O_2 absorbers and stored on the lab bench at RT, and at 4°C for a period of one week. CBD is known to undergo the course of oxidation at the same oxidation potential value as THC (0.48 V) due to the analogous redox active moieties present in both molecules. The resultant graphs (Figure S2-5) obtained in PBS (pH 7.4) via SWV display the same electrochemical behaviour as that of THC at both temperature conditions. The peak current values demonstrate stability at both RT and 4°C until day 3, after which the signal is observed to decrease.

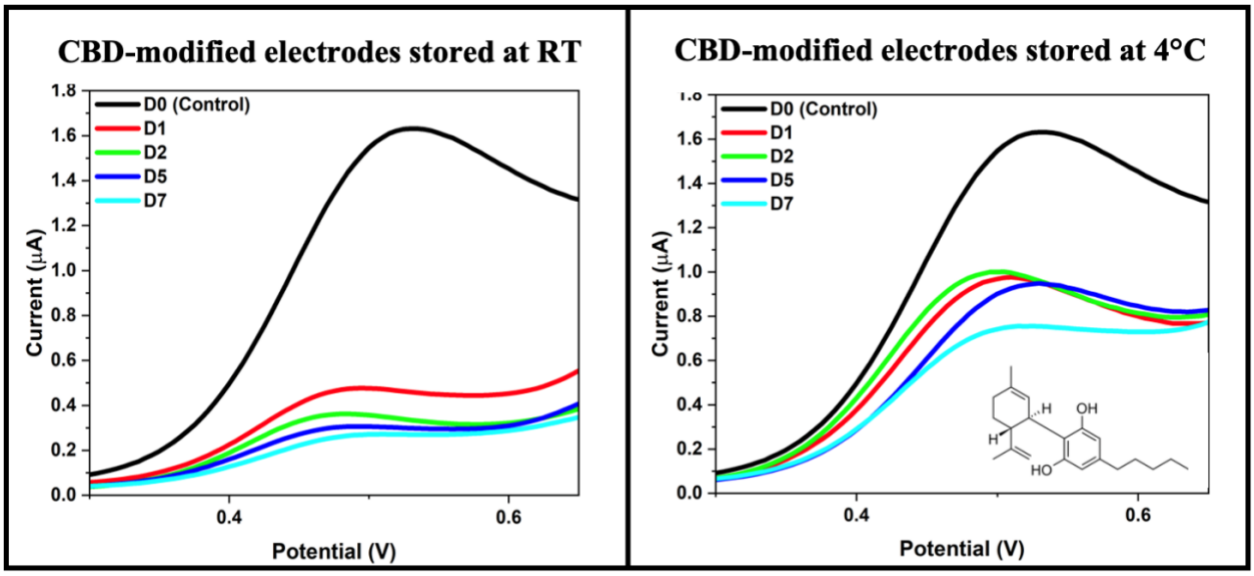

Figure S2- 5: CBD-modified electrodes (130 ng) stored on the lab bench at RT and at 4°C for a period of one week.

Lastly, pristine electrodes were manually modified with THC-OAc (130 ng) and subjected to SCAN 2 using SWV at RT in PBS (pH 10) and PBS (pH 12). The resultant graph (Figure S2-6) demonstrates the lack of signals due to THC oxidation despite a high basic pH, invalidating this modification for sensing purposes. Hence, the flat signals obtained were unfavourable for the purposes of extending stability for our research.

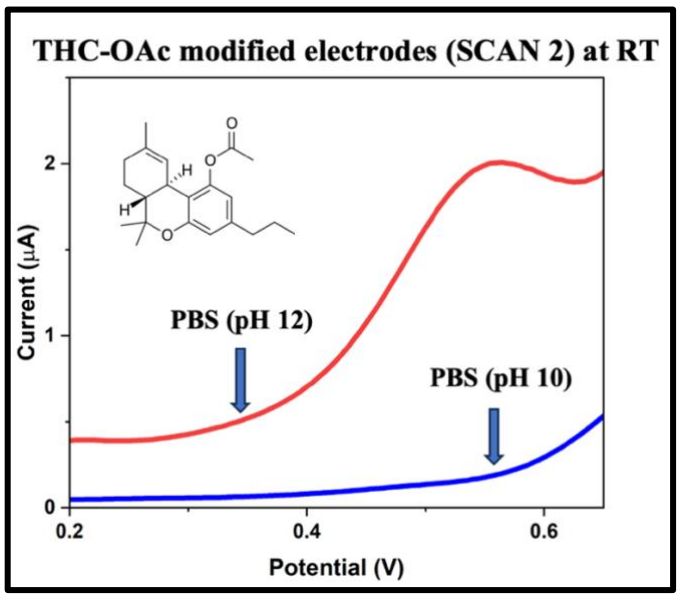

Figure S2- 6: THC-OAc-modified electrodes (130 ng) SCAN 2 performed in PBS(10) and PBS(12) at RT.

V. References

[1] Gonzalez-Cuevas, G., Martin-Fardon, R., Kerr, T. M., Stouffer, D. G., Parsons, L. H., Hammell, D. C., Banks, S. L., Stinchcomb, A. L., & Weiss, F. (2018). Unique treatment potential of cannabidiol for the prevention of relapse to drug use: Preclinical proof of principle. *Neuropsychopharmacology*, *43*(10), 2036–2045. https://doi.org/10.1038/s41386-018-0050-8

.